Master's thesis

NTNU
Norwegian University of Science and Technology
Faculty of Engineering
Department of Ocean Operations and Civil Engineering

Raphaël Kuntz

Bow design for low added resistance in waves

Master's thesis in Naval Architecture
Supervisor: Karl Henning Halse
Co-supervisor: Elisa Solheim Høstmark
June 2023

NTNU
Norwegian University of
Science and Technology

VARD
a Fincantieri company

Raphaël Kuntz

Bow design for low added resistance in waves

Master's thesis in Naval Architecture
Supervisor: Karl Henning Halse
Co-supervisor: Elisa Solheim Høstmark
June 2023

Norwegian University of Science and Technology
Faculty of Engineering
Department of Ocean Operations and Civil Engineering

NTNU
Norwegian University of
Science and Technology

Preface

After an engineering study program followed in the École Centrale de Nantes in France, this thesis concludes a one year Erasmus exchange done in the second year of the Naval Architecture Master of the Norwegian University of Science and Technology (NTNU) in Ålesund. It is a collaboration between the university and Vard Group.

The thesis focuses on bow design to limit the added resistance in waves. I have chosen this topic to gather my hydrodynamics, computational fluid dynamics (CFD) and naval architecture competences learnt during my years at École Centrale, during months of internship in naval study office and finally here in NTNU but also because it was a subject that interested me a lot.

Anyone involves in hydrodynamics, CFD, naval architecture or resistance optimization could find an interest of reading this thesis. The reader is expected to have basic knowledge in those topics even if some theoretical parts are included.

I would like to thank sincerely my supervisors, Karl Henning Halse at NTNU and Elisa Solheim Høstmark at Vard for their guidance, their advice and their availability throughout the semester.

Raphaël Kuntz
Ålesund, 8th of June 2023

Master Thesis 2023
-
Raphaël KUNTZ

Bow design for low added resistance in waves

Background

With the objective of improving the energy efficiency of ships and their sea-keeping performance, the bow design has an important role to play. Often designed for a reduced resistance in calm water and a specific speed, ship's bows are not always well adapted for the sea conditions encountered. Indeed, the study of the added resistance in waves requires important computational resources to obtain accurate results. Empirical formulas and linear potential methods do not provide good results for all the wave lenghts and their different headings. That is why using a time accurate fully non-linear boundary element method in Shipflow Motions to study the effect of bow designs characteristics on the added resistance in waves could be interesting.

Objectives of the research

The objective of this thesis is to better understand the ship's resistance in waves by highlighting the important parameters of bow design affecting the added resistance. Three or four ship's bows provided by VARD will be studied for this purpose. The calculations will be carried out thanks to CFD models in Shipflow Motions 7.0 provided by Flowtech (Gothenburg, Sweden) using a time accurate fully non-linear boundary element method. For each ship, the goal is to create a model and to investigate how to improve the bow shape in order to reduce their added resistance in waves.

This can lead to the following research questions :

- How will the ship motion affect the added resistance in waves ?
- What are the most important bow design parameters influencing the added resistance in waves ?
- How much can you improve the added resistance of a ship in waves by modifying the bow design ?

Scope of work

1 – Foundations of the thesis
The first step in this thesis is to conduct a literature review on the subject. It aims at highlighting different methods for studying the added resistance in waves, their pros and their cons. The theoretical approach and the empirical formulas will be discussed. This will also give an overview on the different hull parameters able to impact the added resistance.

2 – Modelisation
From ships provided by VARD, CFD models will be created in Shipflow Motions 7.0 and results will be compared to previous model tests in order to check the validity of the models.

3 – Analysis
The results obtained will permit to study different bow parameters impacting the added resistance in various sea states taking into consideration ship motions, time-averaged pressure distribution on the hulls, wave pattern...

4 – Bow improvement
Based on the parameters highlighted in the previous part, the bow design of the ships may be improved. The added resistance will then be recalculated and compared to original models.

The scope of work may prove to be larger than initially anticipated. Subject to approval from the advisor, topics from the list above may be deleted or reduced in extent.

The thesis should be written as a research report with summary, conclusion, literature references, table of contents, etc. During preparation of the text, the candidate should make efforts to create a well arranged and well written report. To ease the evaluation of the thesis, it is important to cross-reference text, tables and figures. For evaluation of the work a thorough discussion of results is needed. Discussion of research method, validation and generalization of results is also appreciated.

The thesis shall be submitted in electronic version according to standard procedures. Instructions are found on the NTNU website (Inspera) and on Blackboard. In addition, one paper copy of the full thesis together with an electronic device carrying all relevant documents and files shall be submitted to your supervisor.

Karl Henning Halse
Supervisor NTNU

Elisa Solheim Høstmark
Supervisor VARD Design AS

Delivery : June 2023

Signature candidate :

Abstract

With the aim of reducing the emissions of maritime traffic, the search for ship efficiency is crucial. In a seaway, waves are responsible for added resistance and increase a lot the power needed to move the ship forward. Added resistance is defined as the difference between the total resistance of a ship in a seaway and its resistance in calm water. The bows of the ships have a significant impact on the behaviour of the ship in waves on resistance but also on seakeeping performances. This Master thesis try to better understand the effects of the different bow design parameters and their impact on added resistance and motions.

Parameters such as the waterline entrance angle, the flare angle, the first shoulder shape and the underwater form of the bow have been studied. Regarding the large number of cases involved here, the tests have been carried out thanks to a Computational Fluid Dynamic (CFD) software, Shipflow Motions 7.0. The CFD models have been validated with towing tank results and a converence test.

What we can learn from these studies is that the motions and the resistance cannot be linked by some kind of rule, the parameters studied have varying degrees of impact on the added resistance and the motions but with a good combination we are able to reduce the total resistance in waves more than 9%.

By also considering the naval architecture constraints and the uses of the ship, the vessel could be able to reduce the power needed to sail. That means a reduction of emission and cost but also smaller engines required and maybe a better comfort onboard because of the reduction of motions.

List of Figures

2.1 Wavelength dependency of non-dimensional added resistance 5
2.2 R_W of KVLCC2 6
2.3 KVLCC2 R_W evaluation 7
2.4 KVLCC2 bow optimization 9

4.1 The ship studied 16
4.2 Mesh example 17
4.3 Evolution over time of the non-dimensioned resistance coefficient in calm water . 18
4.4 Evolution over time of standard deviation of the non-dimensioned standard deviation of the resistance in calm water 19
4.5 Evolution over time of non-dimensioned resistance coefficient in irregular waves . 19
4.6 Evolution over time of the non-dimensioned standard deviation of resistance in irregular waves 20
4.7 Relative errors on the different resistances for the three mesh densities 20
4.8 Total number of iteration for each mesh density 21
4.9 Comparison CFD calculations and tank tests 22
4.10 Waterline plane 23
4.11 3D view of the different waterline entrance angle studied 24
4.12 Flare profiles 25
4.13 3D views of the different flare studied 26
4.14 Waterline plane 27
4.15 3D view of the different first shoulder shape studied 27
4.16 U shape 28
4.17 V shape 29
4.18 Bulb shape 29

5.1 Resistance coefficients of the different waterline angles 30
5.2 Heave motions coefficient of the different waterline entrance angles 31
5.3 Standard deviation of heave motions coefficient for different waterline entrance angles 32
5.4 Pitch motions of the different waterline entrance angles 32
5.5 Standard deviation of pitch motions for different waterline entrance angles . . . 33
5.6 Global wave pattern of the different waterline entrance angles 34
5.7 Local wave pattern of the different waterline entrance angles 35
5.8 Pressure distribution on the different waterline entrance angles 36
5.9 Resistance coefficients of the different flare angles 37
5.10 Heave motions coefficient of the different flare angles 38
5.11 Zoom on heave motions coefficient of the different flare angles 38
5.12 Standard deviation of heave motions coefficient for different flare angles 39
5.13 Pitch motions of the different flare angles 39
5.14 Zoom on pitch motions of the different flare angles 40

5.15 Standard deviation of pitch motions for different flare angles 40
5.16 Global wave pattern of the initial hull and the case I 41
5.17 Local wave pattern of the initial hull and the case I 42
5.18 Pressure distribution on the initial design and the case I 42
5.19 Resistance coefficients of the different fisrt shoulder shapes 43
5.20 Heave motions coefficient of the different shoulder shapes 44
5.21 Standard deviation of heave motions coefficient for different shoulder shapes . . 44
5.22 Pitch motions of the different shoulder shapes 45
5.23 Standard deviation of pitch motions for different shoulder shapes 45
5.24 Global wave pattern of the different first shoulder shapes 47
5.25 Local wave pattern of the different first shoulder shapes 47
5.26 Pressure distribution on the different first shoulder shapes 48
5.27 Resistance coefficients of the different underwater forms 49
5.28 Heave motions coefficient of the different underwater bow forms 50
5.29 Standard deviation of heave motions coefficient for different underwater bow forms 50
5.30 Pitch motions of the different underwater bow forms 51
5.31 Standard deviation of pitch motions for different underwater bow forms 51
5.32 Global wave pattern of the different underwater bow forms 52
5.33 Local wave pattern of the different underwater bow forms 53
5.34 Pressure distribution on the different underwater bow forms 54
5.35 Waterline plane of the initial and final designs 56
5.36 Lines drawing of the final design versus the initial bow 56
5.37 3D view of the initial and final designs 57
5.38 Profiles of the initial and final designs 57
5.39 Resistance coefficients of the initial and final designs 58
5.40 Normalized resistance of the initial and final designs 58
5.41 Heave motions coefficient of the initial and final designs 59
5.42 Standard deviation of heave motions coefficient for the initial and final designs . 59
5.43 Pitch motions of the initial and final designs 60
5.44 Standard deviation of pitch motions for the initial and final designs 60
5.45 Global wave pattern of the initial hull and the final design 61
5.46 Pressure distribution on the initial and final designs 61

A.1 Global wave pattern of the different flare studied 64
A.2 Local wave pattern of the different flare studied 65
A.3 Dynamic pressure distribution of the different flare studied 66

List of Tables

4.1 Main particulars of the ship studied . . . 16
4.2 Sea water properties . . . 17
4.3 Convergence test case . . . 18
4.4 Calm water convergence test results . . . 18
4.5 Summary of the relative errors . . . 21
4.6 Sea states studied . . . 22
4.7 Waterline entrance angle . . . 24

5.1 Relative motion amplitude comparison for the different waterline entrance angles 33
5.2 Relative motion amplitude comparison for the different flare angles . . . 40
5.3 Relative motion amplitude comparison for the different shoulder shapes . . . 45
5.4 Relative motion amplitude comparison for the different underwater forms . . . 51
5.5 Relative motion amplitude comparison for the final design . . . 60

Nomenclature

The nomenclature defines important variables with explanation and unit.

$\dot{\xi}$	scalar amplitude of relative vertical velocity at any section between ship and wave surface	
γ	Spectrum form coefficient	
λ	Wavelength	m
ω	wave frequency	rad.s^{-1}
ρ	Density	kg.m^{-3}
ζ	Wave amplitude	m
a_{33}	Sectional heave virtual mass coefficient	
B	Shiph beam	m
b_{33}	Sectional heave virtual damping coefficient	
C_t	Resistance coefficient	
Fr	Froude number	
g	Potential acceleration	m.s^{-2}
H_s	Significant wave height	m
L	Ship length	m
L_{pp}	Length between perpendiculars	m
R_W	Added resistance	N
$S(\omega)$	Spectral energy density	
S_ζ	Wave spectrum	
S_b	Body surface	m^2
S_f	Free surface	m^2
T_p	Wave period	s
U_0	Ship speed	m.s^{-1}

Contents

Preface ii

Thesis agreement iii

Abstract iii

List of Figures v

List of Tables vi

Nomenclature vii

1 Introduction 1
- 1.1 Problem definition . . . 1
- 1.2 Motivation . . . 1
- 1.3 Scope . . . 1
- 1.4 Structure of the thesis . . . 2

2 State of the art 3
- 2.1 Irregular waves . . . 3
- 2.2 Added resistance in waves . . . 4
- 2.3 Study methods . . . 5
  - 2.3.1 Theoretical approach . . . 5
  - 2.3.2 Computational methods . . . 7
- 2.4 Hull optimization . . . 8
- 2.5 First finding . . . 9

3 Methodology 10
- 3.1 Overview of the method . . . 10
  - 3.1.1 Modelisation . . . 10
  - 3.1.2 Analysis . . . 10
  - 3.1.3 Improvement . . . 11
- 3.2 Assumptions and limitations . . . 11
  - 3.2.1 Shipflow Motions 7.0 assumptions . . . 11
  - 3.2.2 Limitiations of Shipflow Motions 7.0 . . . 14
  - 3.2.3 Resistance measurements . . . 14
  - 3.2.4 Assumptions about added resistance . . . 15

4 Case studies 16
- 4.1 The ship studied . . . 16
- 4.2 Model tests . . . 16
- 4.3 Shipflow model . . . 17

4.3.1 The model . . . 17
4.3.2 Convergence test . . . 17
4.3.3 Towing tank validation . . . 21
4.4 Bow parameters study . . . 22
4.4.1 Waterline entrance angle . . . 23
4.4.2 Flare angle . . . 24
4.4.3 First shoulder . . . 27
4.4.4 Bottom part . . . 28

5 Discussion of the results 30
5.1 Effect of the bow design parameters . . . 30
5.1.1 Waterline entrance angle . . . 30
5.1.2 Flare angle . . . 36
5.1.3 First shoulder . . . 43
5.1.4 Bottom part . . . 49
5.2 Summary . . . 54
5.3 Final bow design . . . 55
5.3.1 Geometry . . . 55
5.3.2 Results . . . 57

6 Conclusion 62
6.1 Concluding remarks . . . 62
6.2 Future work . . . 62

A 64

References 67

Chapter 1

Introduction

1.1 Problem definition

For many years ship hulls were optimized to limit the resistance in calm water. For this purpose most of the ships have been equipped with bulbous bows. However the encountered sea conditions are often quite different from calm water and bulbous bows are no longer perfectly suitable in this case and may involve increased resistance and poor sea-keeping performance.

The X-bow proposed by Ulstein, 2023 (Ulsteinvik, Norway) has shown that questioning classical design can be greatly beneficial to reduce the added resistance in waves and limit the motions of the ship at sea. The bow design of ships should now take into account the performance in waves in order to limit the added resistance and thus to get closer to the objective of better energy efficiency of ships. That is why VARD Group (Ålesund, Norway) wants to investigate the effect of waves on their bow designs to try to reduce the added resistance in waves.

The study of the added resistance in waves requires expensive model tests or important computational resources to obtain accurate results. Empirical formulas and linear potential methods do not provide good results for all the wave lengths and their different headings. Therefore it could be interesting to use a time accurate fully non-linear boundary element method in Shipflow Motions FLOWTECH, 2022 provided by Flowtech (Gothenburg, Sweden) to study the effect of bow designs characteristics on the added resistance in waves.

1.2 Motivation

The necessity of reducing the environmental impact of greenhouse gas emissions from global maritime traffic is now a major concern for ship owners and shipbuilders. One of the first elements to work on to reach this objective is the energy efficiency of the ships. The optimization of the performances of the ships in a seaway is one leverage to reduce the energy consumption of a ship. Moreover by limiting the power needed to move forward in waves, the shipowner will be able to make savings on energy consumption but also on the size of the ship's machinery.

1.3 Scope

The main objective of this Master thesis is to better understand the ship's resistance in waves by highlighting the important parameters of bow design affecting the addded resistance. A ship's bow provided by VARD will be studied for this purpose.

Based on 3D model provided by the company, the first objective is to determine accurately the added resistance of this ships. The calculations will be carried out thanks to Computational Fluid Dynamics (CFD) models in Shipflow Motions 7.0 FLOWTECH, 2022 using a time accurate fully non-linear boundary element method. The models will be validated thanks to previous towing tank tests conducted by the company.

The second objective consists in investigating the causes and the areas of the bow responsible for the added resistance in waves in order to then improve the bow shape.

Improving the bow design of those ships to reduce their added resistance in waves is the third objective. The effects of parameters as the waterline entrance angle, the flare angle or the bottom shape for example should be looked at.

From these objectives, three research questions can be highlighted:
RQ1: How will the ship motion affect the added resistance in waves?
RQ2: What are the most important bow design parameters influencing the added resistance in waves?
RQ3: How much can you improve the added resistance of a ship in waves by modifying the bow design?

1.4 Structure of the thesis

This Master Thesis will first present the state of the art on the added resistance in waves. From this background, the methodology, the assumptions and the limitations will be described. Then, different case studies of sea states, speeds and bow shape will be carried out. Following this, the results will be detailed and discussed. Finally, conclusions and recommendations will be covered.

Chapter 2

State of the art

2.1 Irregular waves

Ocean waves are a complex phenomena. Created by random winds, they can travel and propagate over large distances and long time. This leads to a free surface totally randomly structured. This section will not come back on regular waves theory but will focus on irregular sea states. It has been written with the help of Newman, 1977
Because of their randomness, irregular sea states have to be described with a probabilistic manner. It is explained that an irregular sea states can be modeled with a distribution of plane progressive waves coming from all the directions and with all the possible frequencies described by a complex amplitude $A(\omega, \theta)$. A Fourier method can be used to determine this amplitude function. In such a problem, we assume to describe the sea state on a finite free surface area and a finite amount of time.
The spectral density $S(\omega, \theta)$, which is a Fourier transform of the correlation function for the free surface elevation, corresponds to the spectral energy density and is commonly used. It is a directional energy spectrum that can be integrated over all the directions to obtain a frequency spectrum define by the following expression:

$$S(\omega) = \int_0^{2\pi} [S(\omega, \theta)] \, \mathrm{d}S \tag{2.1}$$

This expression can be sufficient to describe the wave environment if we consider that the sea state is unidirectional, or long crested.
With this assumption, and considering that the wave spectra have reached a steady state, $S(\omega)$ can be estimated by this semi-empirical expression:

$$S(\omega) = \frac{\alpha g^2}{\omega^5} \exp[-\beta (\frac{g}{U\omega})^4] \tag{2.2}$$

with α and β nondimensional parameters describing the spectrum, U the wind velocity at 19.5 meters above the free surface.
If $\alpha = 8.1 * 10^{-3}$ and $\beta = 0.74$ this spectrum is a Pierson-Moskovitz spectrum.

To give an idea of the waves amplitude, the significant wave higth H_s is used. It is the average of the highest one third of all the waves.

In this thesis we will use a Joint North Sea Wave Project (JONSWAP) spectrum expressed by Hasselmann, 1973. Its expression based on the Pierson-Moskovitz spectrum is the following:

$$S(\omega) = \frac{\alpha g^2}{\omega^5} \exp[-\frac{5\omega_p^4}{4\omega^4}] \gamma^{\exp[-\frac{(\omega - \omega_p)^2}{2\sigma^2 \omega_p^2}]} \tag{2.3}$$

with ω_p the peak pulsation, γ the form coefficient of the spectrum and σ the width of the spectrum.
It is common to describe a JONSWAP spectrum by its significant wave heigth H_s, the wave period T_p and the γ coefficient.

2.2 Added resistance in waves

The added resistance in waves for ships is not as well known as the resistance in calm water. However its study is necessary to predict accurately the ship performance in waves and its sea-keeping behaviour. Faltinsen, 2005 showed that a 198 m-long container vessel sailing on North Atlantic routes having a target speed of 22 knots recorded an average involuntary speed loss over a year of 1.7 knots westbound and 0.9 knots roundtrip voyage. This was mainly due to the added resistance in small sea states.

Faltinsen, 2005 defines the added resistance as a result of the interaction between incident waves and the ship. The added resistance in waves is linked to several factors. A summary of this is presented in Beck et al., 1989. The added resistance is made up of three components :
- The damping waves dissipating energy generated by the forced motions of the ship
- The phase shift between wave excitation and ship motions
- The reflection and refraction of the incoming waves on the hull.

However, the effects of the ship motions should be detailed a bit more. Pitching and heaving appear to have considerable impact on the added resistance. They create damping waves but they can also lead to other phenomena such as slamming or shipping water forward. As described in Beck et al., 1989, huge bow motion leads to its probable submergence and hence of shipping water on deck. The assessment of the effects of this water on deck can be done by computing the fraction of time that the foredeck is awash or that the deck edge is submerged at a specific longitudinal location.

Faltinsen, 2005 and Beck et al., 1989 agreed on the fact that the additional resistance is, as a first approximation, proportional to the square of the wave height. This come from the drift force induced by the waves. Figure 2.1 shows the dependency between the typical wavelength and the non-dimensional added resistance.

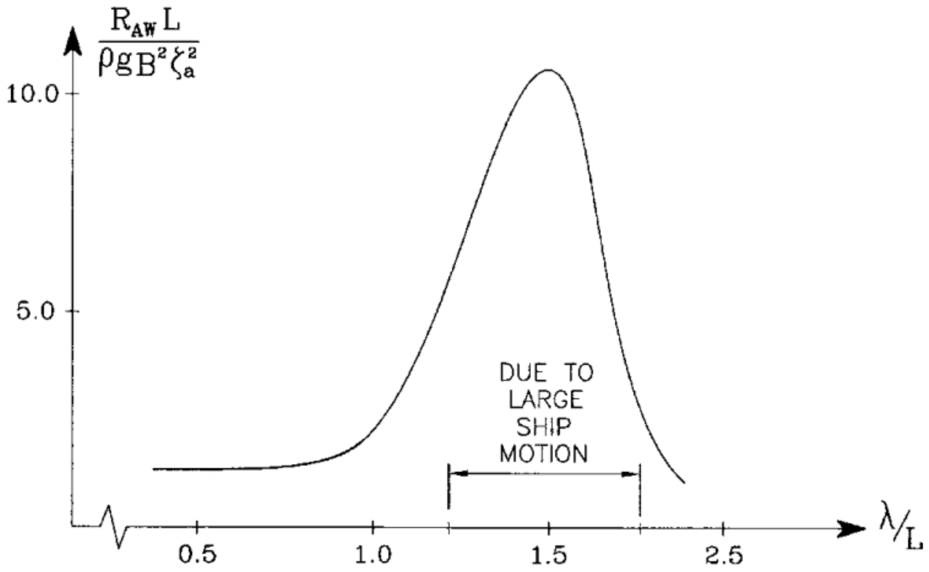

Figure 2.1: Typical wavelength dependency of non-dimensional added resistance a of a ship at forward speed in regular head sea waves. $R_{AW} = Added\ resistance$, $\zeta_a = amplitude\ of\ the\ incident\ waves$, $\lambda = wavelength$, $L = ship\ length$, $B = beam\ of\ the\ ship$, from Faltinsen, 2005

When the ratio λ/L is small the motions of the ship are not important. The finite added resistance in this case can be explained by the reflection of the waves on the hull.
The peak in the non-dimensional curve is due to large relative motions between the ship and the waves. It happens when the ship reaches resonant heave and pitch conditions.
If we consider now a large ratio λ/L, we can see the non-dimensional added resistance dropping to zero. In these conditions, the ship follows the free surface deformations and the relative motions between the ship and the waves decrease significantly.
Although the added resistance is really important around $\lambda/L = 1.5$, the finite added resistance for short waves matters because it represents most of the conditions encountered by the ship.

2.3 Study methods

2.3.1 Theoretical approach

The added resistance in waves is a complex physical phenomena. The different theoretical approaches need to make some assumptions to express it with equations.
Firstly, one can assume that the added resistance results of the damping waves radiated from the oscillating ship's hull. In Beck et al., 1989, a theoretical approach made is in accordance with this assumption. They arrived at a relation for a ship in regular head seas :

$$< \delta R >= (\pi/\lambda\omega_e) \int b(x)|\dot{\xi}|^2(x)dx \tag{2.4}$$

where $< \delta R >= added\ resistance\ in\ regular\ head\ sea$, $\lambda = wavelength$, $\omega_e = frequency\ of\ encounter$,
$b(x) = b_{33}(x) - U_0\frac{da_{33}(x)}{dx}$,
$\dot{\xi} = scalar\ amplitude\ of\ relative\ vertical\ velocity\ at\ any\ section\ between\ ship\ and\ wave\ surface$,
$b_{33}(x) = sectional\ heave\ virtual\ damping\ coefficient$,
$a_{33}(x) = sectional\ heave\ virtual\ mass\ coefficient$

However this relation cannot be used for irregular seas or for oblique waves. Moreover, because its focus on the ship motions, it is not applicable for short waves mostly creating reflection. That is why another relation is usually used according to Beck et al., 1989. It is based on the theory of quadratic, non-linear systems and allows to calculate the added resistance in irregular waves. The usual estimator for its mean value is :

$$< \delta R_W >= 2 \int [\delta R(\omega_e)/\bar{\zeta}^2] S_\zeta(\omega_e) d\omega_e \tag{2.5}$$

where $[\delta R(\omega_e)/\bar{\zeta}^2] = normalized\, mean\, value\, of\, added\, resistance\, in\, regular\, waves\, of\, amplitude\, \bar{\zeta}$, $S_\zeta(\omega_e) = encountered\ variance\ spectrum\ of\ wave\ elevation$

Bolbot and Papanikolaou, 2016 mentioned that another approach can be made. The added resistance R_W may be decomposed into two components : R_{AWM} due to ship motions and R_{AWR} due to wave reflection. Figure 2.2 shows the distribution of these parameters for different wavelength for a large ship such as the standard ITTC KVLCC2 tanker.

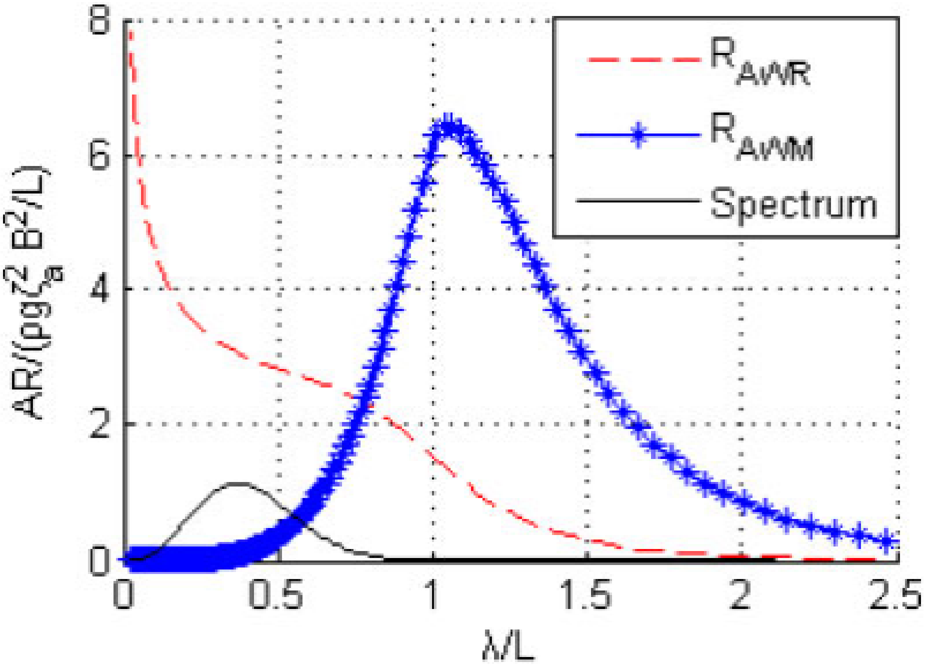

Figure 2.2: The non-dimensional R_W of KVLCC2 ship for different wavelengths, from V. Bolbot and A. Papanikolaou Bolbot and Papanikolaou, 2016.

One can notice that this distribution agrees with the previous dependency between added resistance and wavelength seen in Figure 2.1. The effect of short-crested waves cannot be neglected even if the shop motions are responsible for a peak in the added resistance. With this reasoning, the added resistance may be written :

$$R_W = \int_0^\infty [R_{AWR}(\omega) + R_{AWM}(\omega)] \frac{S(\omega)}{\zeta^2} d\omega \tag{2.6}$$

With $\omega = wave\ frequency$ and $S(\omega) = sea\ spectrum$

In this approach, R_{AWR} is estimated thanks to semi-empirical methods based on the pressure integration over the waterline. R_{AWM} is also calculated thanks to another semi-empirical

formula based on basic ship's parameters.
For the KVLCC2, the Mean Absolute Percentage Error (MAPE) of this method is close to 25%. The results for this ship are compared with model tests in Figure 2.3.

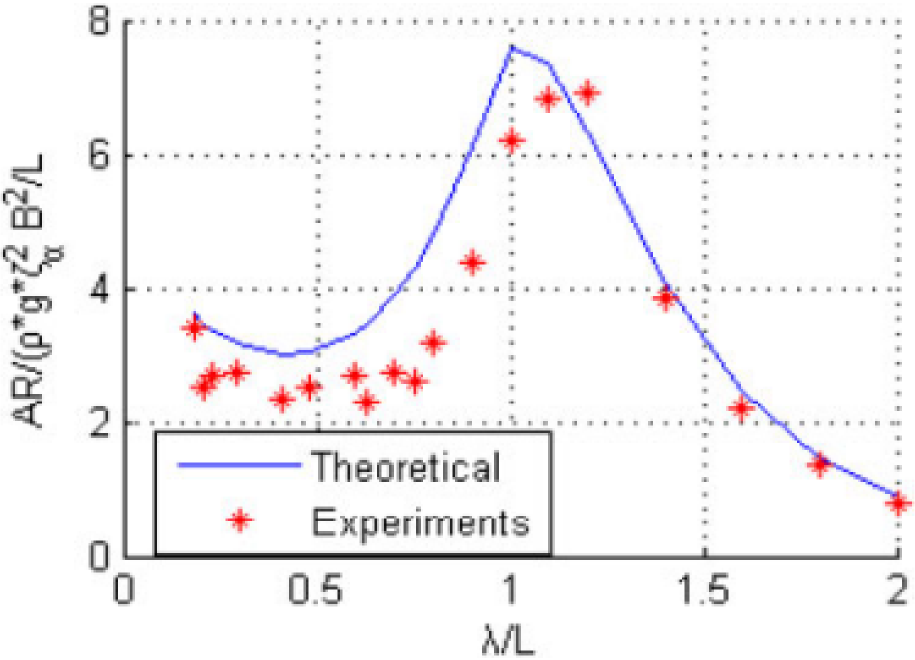

Figure 2.3: The non-dimensional R_W of KVLCC2 at $Fr = 0.142$ for different wavelengths, from V. Bolbot and A. Papanikolaou Bolbot and Papanikolaou, 2016.

Faltinsen, 2005 described another first approximation method based on the pressure distribution over the time-dependent wetted area. However this approach took into account only one of several contributions to the added resistance.

2.3.2 Computational methods

As seen in the previous section, expressing the added resistance is not easy, requires several assumptions and provides results with not negligible errors. Numerical methods may help to obtain more accurate results. Several methods exist. Söding and Shigunov, 2015 have compared some of them.

Firstly they discussed about the **Rankine source method** which is based on the linearisation of the flow and ship motions due to incoming waves. This method takes into account interactions between the steady non-linear flow and the ship in calm water. It was previously well described by Söding, Graefe, et al., 2012. Here the fluid is assumed inviscid, incompressible and irrotational. Söding and Shigunov, 2015 have obtained suitable results to predict an estimation of the added resistance with this method even in short waves.

The **Strip method** (PDSTRIP), detailed by Newman, 1977 is another potential method. It consists in dividing the submerged part of a slender ship into a finite number of strips. The fluid motions are formulated as a 2D problem. 2D hydrodynamic coefficients can be computed for each strip and summed over the length of the hull. For Söding and Shigunov, 2015, the strip method gave inaccurate results for wavelength exceeding $0.8L_{pp}$ and unacceptable results for shorter wavelengths. In their numerical studies in oblique sea conditions, Park et al., 2019 obtained an accurate tendency of their Strip method results compared to the experimental tests even though the added resistance was overestimated.

The **Lee method** is applicable to short head waves in which periodic ship motions are small. The dependence of the flow potential on the vertical coordinate z is approximated by the function $\exp -kz$ with k the wave number as mentionned by Söding and Shigunov, 2015. The results obtained are quite similar to those coming from the Rankine source method.

Reynolds-averaged Navier-Stokes (RANSE) equations are time-averaged equations of the motion of a fluid flow. By taking in account turbulent flows and viscous effects, they are known to provide accurate results in the estimation of seakeeping performances in comparison to model tests. However, solving these equations requires a too huge computational time when several loading conditions, speeds, wave period or headings need to be assessed.

A **fully non-linear unsteady potential flow boundary element code** can also be used. This code will be used in this thesis thanks to FLOWTECH, 2022 software, Shipflow Motions. It is based on a Mixed Eulerian-Lagrangian approach and includes a non-linear decomposition of the velocity potential and the wave field. It will be more detailled in the next chapter. Coslovich et al., 2021 used this method to estimate the added resistance and the heave and pitch motions of the KVLCC2. The results in heave and pitch showed a great accuracy compared to the experimental test carried out at SSPA Sweden AB. The added resistance was compared to several others results obtained with different methods such as a linear potential flow, a partially non-linear potential flow, an Euler method, a Unsteady Reynolds-Averaged Navier-Stokes method and the experimental results. In general, there was a good agreement with the other methods and the model test results.

2.4 Hull optimization

Once the added resistance and the ship motions can be estimated accurately, the next step is to optimize the design to improve these performances. Beck et al., 1989 highlight the fact that the sea-keeping aspects should appear earlier during the design phase of a boat than the resistance in calm water. Indeed, calm-sea resistance characteristics of a hull design are more sensitive than sea-keeping characteristics to local hull geometry changes. As seen in the previous sections, ship motions are determining in the added resistance in waves. Beck et al., 1989 mention several design aspects able to impact the heave and pitch motions. The size of the ship and its speed are two main parameters but fixed most of the time. The deck wetness and slamming impacts may cause huge speed loss. A large flare limits deck wetness but increases slamming impacts. The slamming impacts can be reduced by a more important V-form in the forebody. Design choices are a matter of compromise.

In term of optimization, Larsson and Raven, 2010 described a method aiming at reducing the wave making of a hull moving forward in calm water. The first step consists in studying the visualization of the wave pattern and determining what components are prevalent. Then, the created waves have to be linked to hull form features. For this step, L.Larsson and H.C.Raven stated that the relations between the hull form and the hydrodynamic pressure distribution have to be first considered. The pressure distribution is later related to wave making. The final step is to carry out the new wave pattern obtained after the hull form optimization. A similar approach could be interesting to implement considering incoming waves to reduce the added resistance in waves.

Some studies focused on hull optimization. Here we will focus on bow design optimization. Yang and Kim, 2017 compared three bows for the KVLCC2 ship using a Cartesian-grid method: the original one, a Ax-bow type and a Leadge-bow type. These bows are represented in Figure 2.4a. As shown in Figure 2.4b, the Ax-bow leads to smaller added resistance than the original one but the Leadge-bow is even better. This one provides approximately 30% reduction of added resistance.

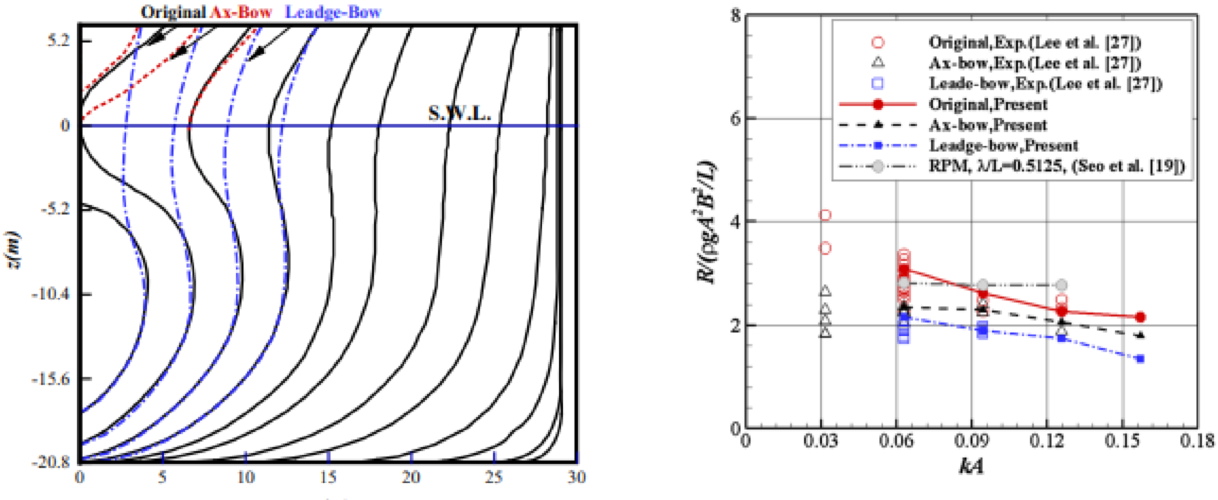

(a) Body plans for KVLCC2 with different bow shape, from Yang and Kim, 2017.

(b) Comparison of added resistance in short waves for different bow shapes and different waves amplitude, from Yang and Kim, 2017.

Figure 2.4: KVLCC2 bow optimization

The Leadge bow concept had also good results in Bolbot and Papanikolaou, 2016 study. They obtained a bow shape close to the Leadge bow during their optimization work of the KVLCC2 tanker in terms of added resistance and calm water resistance.

The X-bow from Ulstein company and a wave-piercing monohull have been compared by Chen et al., 2022 thanks to an incompressible two-phase unsteady Reynolds Averaged Navier–Stokes equations solver using the finite volume method. Here the results were not so clear-cut. For small wave heights the X-bow appeared to have a smaller added resistance. However, for larger wave heights, the results showed the opposite. A similar comparison could be made regarding the ship speed. For low Froude number, the ship motions were more significant for the wave-piercing monohull but when the speed increased, the X-bow had a larger motion response.

2.5 First finding

It can then be interesting to compare different bow shape of a ship as Yang and Kim, 2017 did with the KVLCC2 but this time by taking into account more specific parameters such as the ones mentioned in Beck et al., 1989. By varying the flare angle, the waterline angle, the shape of the first shoulder or the form of the bulb one by one, we might be able to highlight their respective impacts on the added resistance in waves. Linking the pressure distribution and the wave pattern to the geometry as presented by Larsson and Raven, 2010 could also allow to better understand the effects of those bow parameters.

Doing those different tests can be very costly especially if model tests have to be conducted. That is why using an accurate but not too costly method such as a fully non-linear unsteady potential flow boundary element code could be a great compromise.

Chapter 3

Methodology

3.1 Overview of the method

In order to reach the objectives fixed, the thesis will be divided in three work-packages.

3.1.1 Modelisation

Shipflow models The first step will consist in creating accurate CFD models in Shipflow Motions 7.0. This software use a time accurate fully non-linear boundary element method to calculate the added resitance in waves. The models will be created from existing ship models built by VARD.

Validation of the CFD models For the ships mentioned, VARD has at its disposal several seakeeping tests. The goal will be to reproduce the sea conditions used during those model tests in the Shipflow models. A comparison of the results will allow to validate them.

3.1.2 Analysis

Ship motions If the CFD models provide satisfying results in Shipflow, the study of the added resistance and the behaviour of ships in waves will be dug a little further. One important parameter to assess is the ship motion. As seen in the literature review, ship motions seem to have a significant impact on the added resistance. Moreover, this element is a determining factor in the use of the vessel.

Pressure distribution Assessing the time-average pressure distribution on the hull and especially on the bow might be a way to highlight the areas of the bow affecting the added resistance in waves. A similar method was described in the literature review for the resistance in calm water.

Wave pattern The wave resistance in calm water can be a major part of the total resistance. The study of the wave pattern often permits to detect some design effect on this wave resistance. In waves it could also be interesting to look at it to see how the waves can be deflected. It is also important to ensure that this wave pattern will not be overly degraded by an optimization that would reduce the added resistance.

3.1.3 Improvement

Bow design improvement Depending on the results obtained in the previous work batches, some bow design parameters may be modified on the ship studied. These modifications will aim at improving the behaviour in waves and at reducing the added resistance without degrading the performances in calm water or impacting the use of the vessel.

New performances Once a new design is proposed, its performances have to be assessed and compared to the initial ones. The added resistance and the resistance in calm water will be calculated to evaluate the new design. A particular attention will also be paid to possible side effects that the optimization could have created.

3.2 Assumptions and limitations

3.2.1 Shipflow Motions 7.0 assumptions

Some assumptions are made in Shipflow Motions 7.0 to solve the hydrodynamic equations in a reasonable amount of time. Shipflow Motions 7.0 is based on a fully nonlinear unsteady potential flow solver for free surface flows. It can include single or multiple bodies with six degrees of freedom. This section is based on Shipflow Motions 7.0 Users manual FLOWTECH, 2022 and Coslovich et al., 2021 paper.

Coordinate systems

In Shipflow Motions 7.0, six different coordinate systems are used.

The first one is an earth-fixed Cartesian right handed coordinate system in wich the origin is set at an arbitrary position on the calm free surface. It is used for the incoming waves, the free surface evolution and for the equations governing the fluid flow.

The second coordinate system is a body-fixed one where the origin is at the center of gravity of the body.

The offset coordinate system is the third one. The offset file or the imported mesh are described thanks to it. It's origin is at the baseline, aft perpendicular.

The fourth coordinate system is a computational one which is a horizontally aligned body-fixed coordinate system with the origin on the horizontal plane and vertically below the center of gravity of the body.

An initial coordinate system using the same orientation as the offset coordinate system. The origin is place at the water plane in the middle between the aft and the fore perpendiculars.

The last one is a body-fixed sub-body coordinate system with the origin and the orientation defined by the user.

Potential flow

The assumption of an inviscid, incompressible and irrotational flow is made to solve the Navier-Stokes equations governing the fluid. They reduce the expenses in terms of computational power. One can define a scalar quantity ϕ describing the motions of the fluid with

$$\nabla\phi = (\frac{\partial\phi}{\partial x}, \frac{\partial\phi}{\partial y}, \frac{\partial\phi}{\partial z}) = (u, v, w) = \vec{u} \tag{3.1}$$

where u, v, w, are the fluid velocity in the x, y and z direction in the earth-fixed Cartesian right-handed coordinate system.

The incompressible assumption implies : $\vec{\nabla}.\vec{u} = 0$
So it leads to the Laplace equation : $\Delta\phi = 0$

Boundary conditions

In order to solve the different partial differential equations governing the problem, boundary conditions have to be described.

The kinematic free surface boundary condition A fluid particle on the free surface will always belong to the free surface. It means that there is no material flow through the surface. This kinematic boundary condition can be expressed as :

$$\frac{D\vec{x}}{Dt} = (\frac{dx}{dt}, \frac{dy}{dt}, \frac{dz}{dt}) = (u, v, w) = \nabla\phi \tag{3.2}$$

where $\vec{x} = (x, y, z)$ is the position of a fluid particle on the free surface, ϕ is defined as $\nabla\phi = (u, v, w)$ and the material derivative is defined as $\frac{D}{Dt} = \frac{\partial}{\partial t} + \nabla\phi * \nabla$.

The dynamic free surface boundary condition The equilibrium between the hydrodynamic and hydrostatic pressure and the absence of jumps in pressure across the free surface are required. The pressure at the surface is then equal to the atmospheric pressure. This condition can be expressed as :

$$\frac{D\phi}{Dt} = -gz + \frac{1}{2}\nabla\phi.\nabla\phi - \frac{p_a}{\rho} \tag{3.3}$$

where g is the gravitational acceleration, ρ is the fluid density and p_a is the atmospheric pressure.

The body surface boundary condition There is no fluid flow through the body surface. The fluid velocity in the normal direction of the body surface is equal to zero. This condition implies :

$$\nabla\phi.\vec{n} = \frac{\partial\phi}{\partial n} = \vec{n}.(\vec{v} + \vec{\omega} * \vec{r}) \tag{3.4}$$

where $\vec{n}$ is the unit normal vector pointing into the fluid domain, $\vec{r}$ is the radius vector from the body center of rotation, $\vec{v}$ and $\vec{\omega}$ are the translatory and angular velocities of the body.

Unsteady pressure and forces

The pressure on the hull is calculated thanks to the Bernoulli's equation:

$$p = -\rho * (\frac{\partial\phi}{\partial t} + \frac{|\nabla\phi|^2}{2} + g * z) \tag{3.5}$$

The hydrodynamic forces acting on the body can be assessed by integrating the pressure on the wetted body surface S_b:

$$(F_1, F_2, F_3) = -\iint_{S_b} p * \vec{n}\,\mathrm{d}S \tag{3.6}$$

$$(F_4, F_5, F_6) = -\iint_{S_b} p * (\vec{r}.\vec{n})\,\mathrm{d}S \tag{3.7}$$

Nonlinear decomposition

In order to decrease the time of computations, a nonlinear decomposition of the solution has been used. The velocity potential ϕ and the free surface elevation ζ have been decomposed into an incident term describing the undisturbed incident wave field and a scattered term describing the disturbances of the incident wave field.

$$\zeta = \zeta^I + \zeta^S \ and \ \phi = \phi^I + \phi^S \tag{3.8}$$

This leads to a new formulation of the free surface boundary conditions:

$$\frac{D\vec{x}}{Dt} = \nabla(\phi^I + \phi^S) \tag{3.9}$$

$$\frac{D\phi}{Dt} = -gz + \frac{1}{2}\nabla(\phi^I + \phi^S).\nabla(\phi^I + \phi^S) - \frac{p_a}{\rho} \tag{3.10}$$

The incident wave field is a solution of the Laplace equation so we obtained for the scattered solution:

$$\nabla^2\phi^S = 0, \ x \ \in \ D \tag{3.11}$$

$$\phi^S = \phi - \phi^I, \ x \ \in \ S_f \tag{3.12}$$

$$\nabla\phi^S.\vec{n} = (\vec{v} + \vec{\omega}.\vec{r}).\vec{n} - \nabla\phi^I.\vec{n}, \ x \ \in \ S_b \tag{3.13}$$

with D the fluid domain, S_f the free surface ans S_b the body surface.

Then the pressure can be evaluated estimating the scattered part by means of backward-differences or using the acceleration potential.

Numerical method

The boundary value problem is solved thanks to a Boundary Element Method (BEM). The ship surface and the free surface are discretized with means of quadrilateral panels with an unknown constant strength source distribution. The Green's function allows to obtain the source strength σ. For two points P and Q in the domain the Green's function can be written:

$$G = \frac{1}{4\pi r(P,Q)} \tag{3.14}$$

with

$$r(P,Q) = \sqrt{(x_P - x_Q)^2 + (y_P - y_Q)^2 + (z_P - z_Q)^2} \tag{3.15}$$

The velocity potential at a point P if the sources are located on the boundary S of the domain becomes thanks to the Green's theorem:

$$\phi(P) = -\frac{1}{\alpha}\iint_S [G\frac{\partial\phi(Q)}{\partial n}] \, \mathrm{d}S \tag{3.16}$$

with G the Green's function, n the normal direction of the panel and α the solid angle.

A Mixed Eulerian-Lagrangian (MEL) method is used for the evolution in time of the free surface. Some markers trace the free surfqce and its velocity potential. Each iteration is then divided into two steps. The first one is the Eulerian step in which the boundary value problem is solved with the BEM. The velocity potential and velocity are then known at the marker.

The second step consists in integrating in time the free surface boundary conditions and update the position of the markers. Once those steps are done, the surface elevation is interpolated to create a new free surface mesh. The boundary conditions for the future Eulerian step are calculated thanks to the interpolation of the velocity potential of the markers.
The mesh is more described in the convergence test section.

Friction model

The friction part of the resistance is computed thanks to the ITTC'57 friction line. It can be based on the instantaneous wetted surface area and the horizontal speed of the body or based on the tangential friction forces on each individual panel using the local flow velocity.

3.2.2 Limitiations of Shipflow Motions 7.0

Some applications might not be supported or treated accurately by the software because of the assumption of non-lifting potential flow and the numerical model for evolving the free surface in time.
These applications include :
- Severe wave breaking
- Potential flow lifting surfaces
- Planing hulls
- Viscous effects, even if they can be modelled by additional motion damping terms.

3.2.3 Resistance measurements

Because we are focusing on irregular waves, the resistance cannot be estimated as the integral body force in the x-direction only.
The resistance is estimated by Shipflow Motions thanks to the time series data. According to the User's Manual FLOWTECH, 2022, the resistance is calculated with this scheme : the Integral body force in the x-direction named FBD1 using a backward-difference scheme. Then FBD1mean is calculated, it is an exponentially smoothed value of the time series tail (90% tail for irregular waves) of FBD1. Finally, FBD1mean-mean is used as the resistance value. It is estimated as the mean value of FBD1mean over the last 50% of the time series.
When the simulation has converged, FBD1mean-mean gives the estimation of the resistance in irregular waves.

To present the resistance results, we will use non-dimensioned values. Here the total resistance coefficient described by the International Towing Tank Conference "ITTC - Recommended Procedures and Guidelines" 2011 by the equation 3.17 will serve us for calm water resistance, added resistance in waves and the total resistance.

$$C_t = \frac{R}{0.5 * S * \rho * V_{ship}^2} \tag{3.17}$$

R is the resistance we want to study, ρ is the volume weight of the water, S is the wetted surface and V is the speed of the ship.

In order to reach convergence the simulations will last enough time to allow the ship to encounter at least 100 waves. We will see in the convergence test in the next section that the convergence is reached for 100 waves.

3.2.4 Assumptions about added resistance

The literature review has shown that the added resistance in waves can be defined as a sum of different and complex phenomena as ship motions, reflection and refraction of waves, slamming or shipping water forward. Regarding the objectives and the limits imposed by the CFD software some phenomena may be neglected in this study. This list highlights the phenomena not taken into account in this thesis :

- Slamming loads
- shipping water forward on deck

Chapter 4

Case studies

4.1 The ship studied

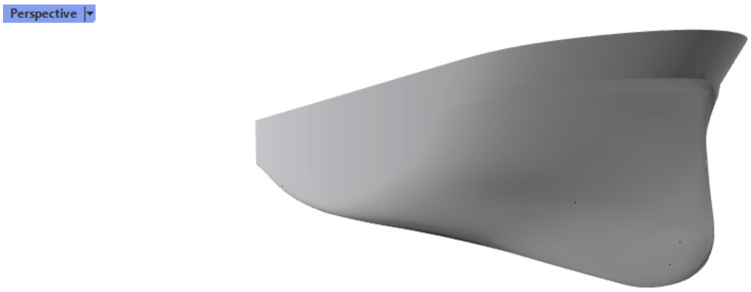

Figure 4.1: The ship studied

The ship studied in this thesis is an expedition vessel. Its main characteristics are described in the table 4.1. For industrial secrecy reasons, the ship will not be named, the parameters and the results will be non-dimensional.

L_{pp}/B	8.31
Design Froude number	0.19

Table 4.1: Main particulars of the ship studied

4.2 Model tests

Some model tests were performed by The Hamburg Ship Model Basin (HSVA). The results concerning the added resistance in waves will be used to check the validity of the CFD models. The model scale from those tests was 1:18.953. According to the HSVA report, the model is equipped with a pair of retractable fin stabilizers, two pairs of bilge keels and three bow thruster tunnels as shown in figure **??**. For the added resistance tests, the azimuth thruster units were not installed on the model. The tests were performed at a 6.0 m draught.

The heave, roll, and pitch motions were completely free but the surge, sway, and yaw motions were restrained with soft springs allowing the cyclic motions of the model in seaway, but keeping it softly on its course and position.

4.3 Shipflow model

4.3.1 The model

The CFD model is based on the geometry of the hull provided by Vard. This geometry does not take in account the bilge keels, the retractable stabilizers, the three bow tunnels nor the azimuth thrusters.
Shipflow Motions 7.0 is set up to be as close as possible to the model tests conditions.

The sea water properties assumed here are the following:

	Sea water	
Temperature	15	°C
Density	1026.02	kg/m^3
Viscosity	$1.1892.10^{-6}$	$m^2.s^{-1}$

Table 4.2: Sea water properties

4.3.2 Convergence test

Shipflow Motions 7 integrates an automatic mesher for the CFD calculations. It meshes the body and the free surface according to the density set. The hull panelization and the free surface mesh are automatically refined in the important or critical areas such as the water line, the bow or the stern for the body and around the hull for the free surface as illustrated by the figure 4.2. However, the hull mesh is kept constant while the free surface mesh evolves over time.

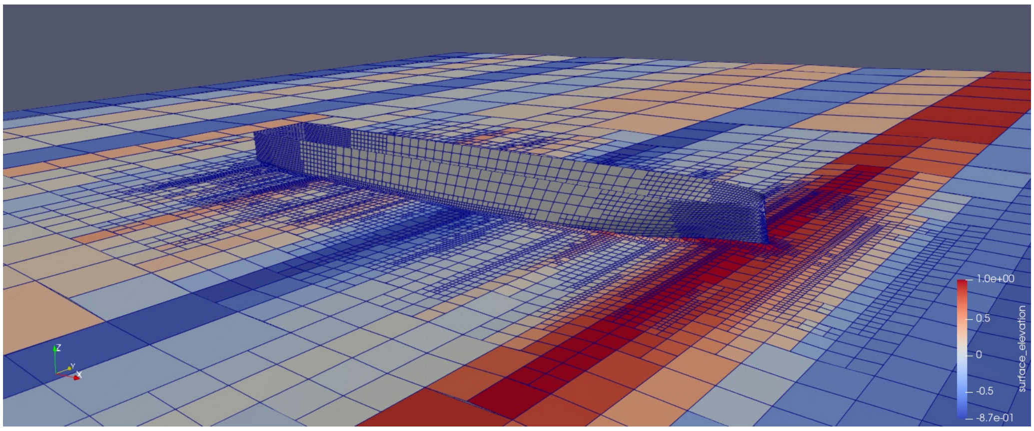

Figure 4.2: Mesh example

In order to check the convergence of the calculations, a convergence test will be carry out. Different densities of mesh will be set and the convergence of the results will be compared. Shipflow Motions propose three degrees of mesh density : Coarse, Medium and Fine. Those three levels will be studied initially.
For this convergence test, the cases chosen is composed of medium irregular waves and calm water at a medium speed.

Spectrum	JONSWAP	
Hs	3	m
Tp	11	s
γ	3.3	
Froude number	0.15	

Table 4.3: Convergence test case

Convergence in calm water

The first step consists in comparing the results obtained for the three mesh density in calm water. The table 4.4 summarizes the resistance coefficient calculated thanks to equation 3.17.

Case	Calm water C_t	Error (%)
Model test	0.00197	
Coarse	0.00209	6.10
Medium	0.00204	3.55
Fine	0.00204	3.55

Table 4.4: Calm water convergence test results

The evolution over time of the mean of the mean of the integral body force in the x-direction (FBD1mean_mean), corresponding to the total resistance, has been used to plot the resistance coefficient in figure 4.3 for the different cases (see section 2 for more explanation). The values are negatives because the force is applied in the opposite direction of the x-direction. The evolutions over time of the standard deviations of those values are shown in figure 4.4.

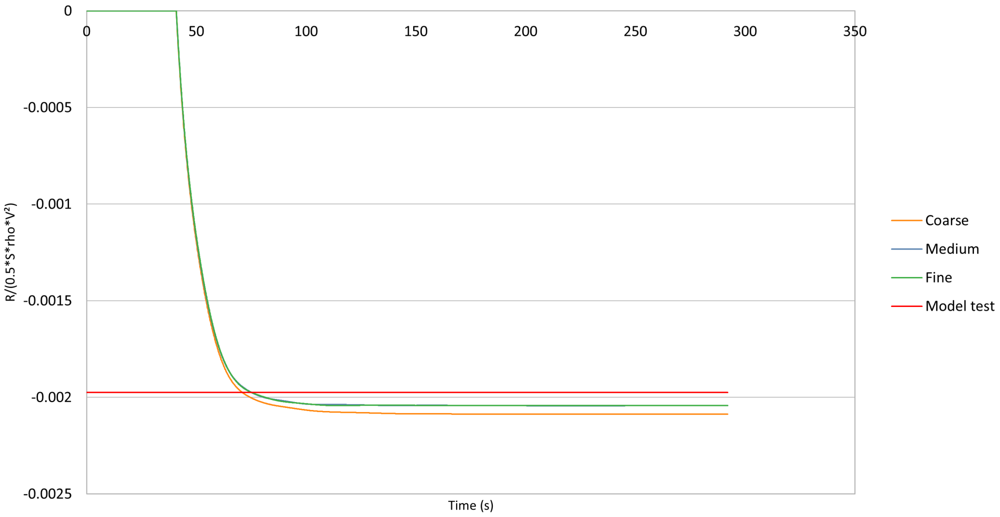

Figure 4.3: Evolution over time of the non-dimensioned resistance coefficient in calm water

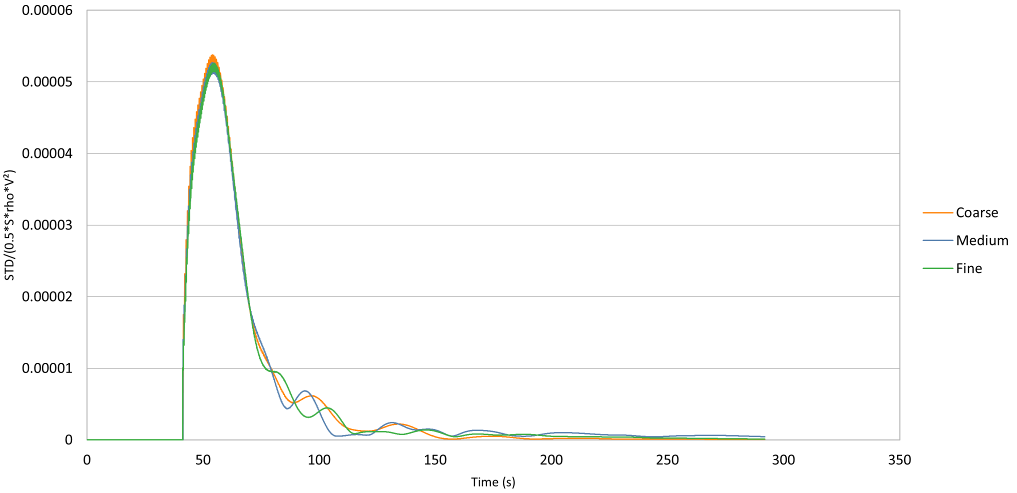

Figure 4.4: Evolution over time of the non-dimensioned standard deviation of the resistance in calm water

The three cases converge quite similarly. One can notice that the final error on the resistance coefficient is a bit higher with the coarse mesh but identical with the medium and the fine mesh. The peak at the begining of the simulation corresponds to the transient state.

Convergence in irregular waves

In wave condition described in the table 4.3 and as for the calm water test, the evolution over time for the mean of the mean of the integral body force in the x-direction has been used to plot the resistance coefficient in figure 4.5: The evolutions over time of the non-dimensioned standard deviations are shown in figure 4.6. The simulations have been set up so that at least a hundred waves encounter the ship and to reach a convergence point.

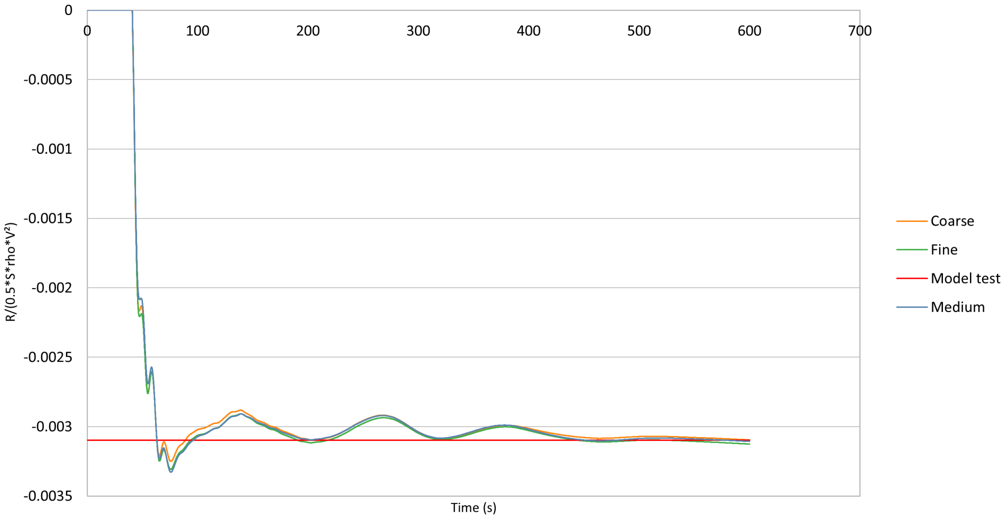

Figure 4.5: Evolution over time of the mean of the non-dimensioned resistance coefficient in irregular waves

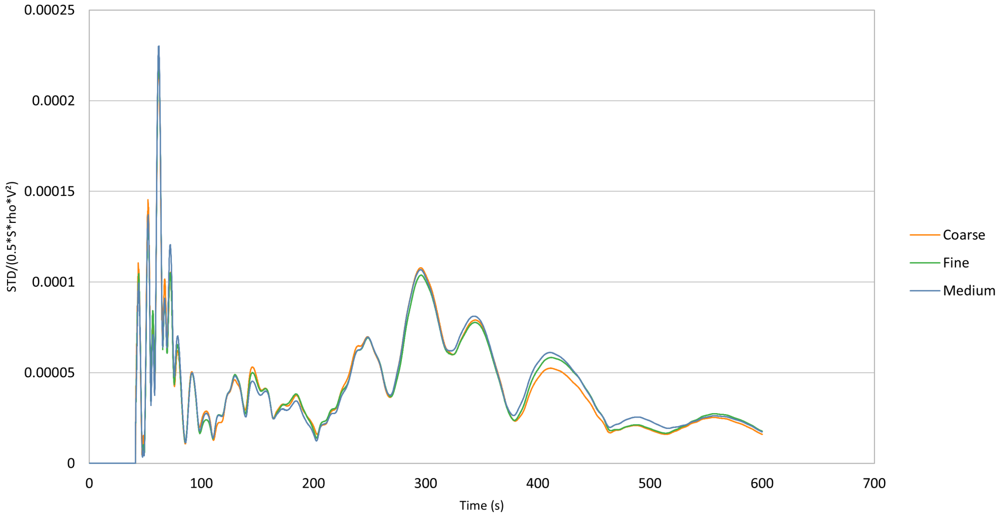

Figure 4.6: Evolution over time of the non-dimensioned standard deviation of resistance in irregular waves

Analysis

First of all, by simulating at least 100 waves, the convergence is reached as we can see on figure 4.5.
The behaviour of the three mesh densities is hardly distinguishable. Therefore we can look at the relative errors (4.1) on the results. The added resistance in waves is determined by subtracting the resistance in calm water from the total resistance, also calculated with the corresponding mesh density. Figure 4.7 shows the relative errors obtained with the different mesh densities in comparison with the model test results.

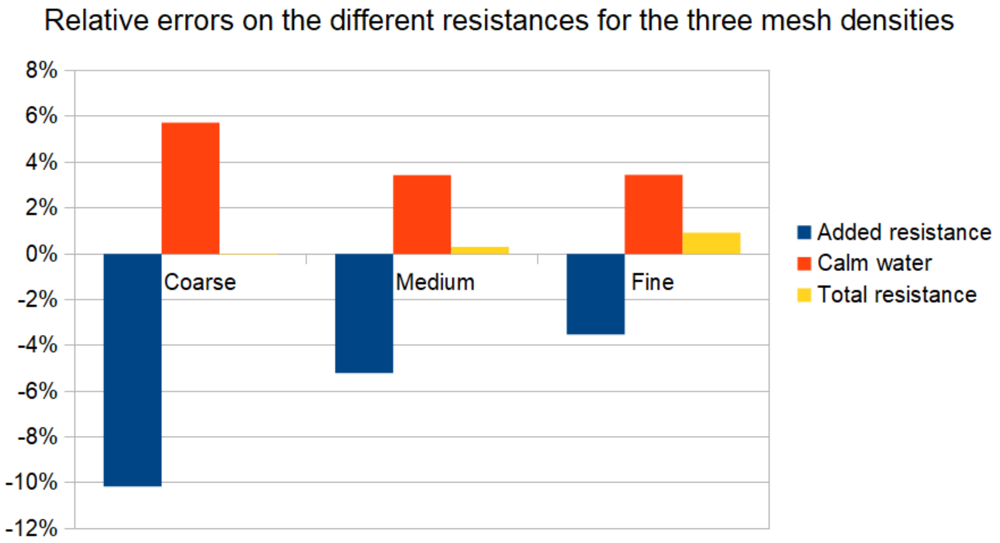

Figure 4.7: Relative errors on the different resistances for the three mesh densities

The relative errors are obtained using the following formula :

$$relative\ error = \frac{CFD\ results - model\ test\ results}{|model\ test\ results|} \tag{4.1}$$

The three mesh densities do not require the same amount of computational resources and therefore the same time of calculation. The figure 4.8 highlights the total number of iterations needed to determine the added resistance in waves for each mesh level.

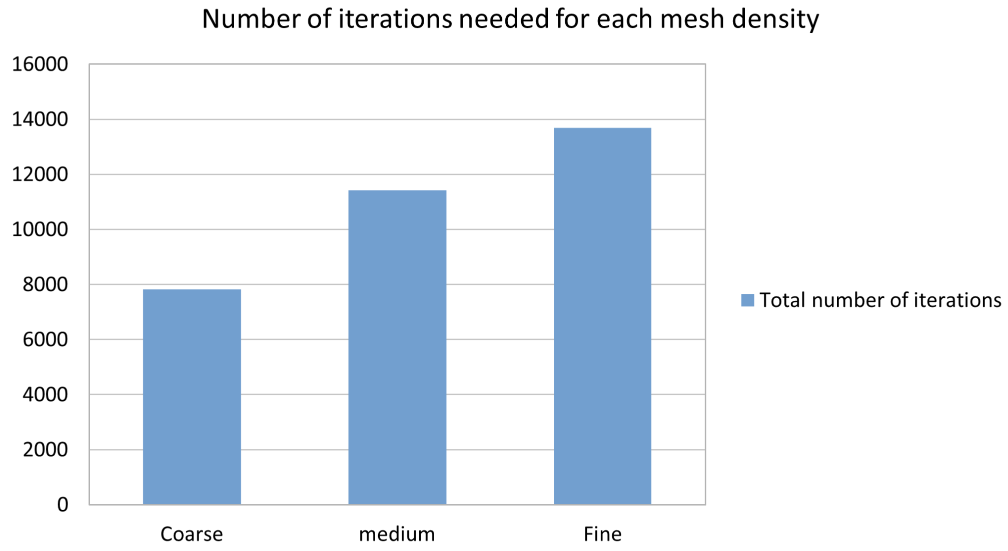

Figure 4.8: Total number of iteration for each mesh density

To give an order of idea of the simulation time, for a medium mesh for approximately a hundred irregular waves using a computer node with the following specifications: 28-core 2,4GHz, 256 GB RAM, the calculation time was around ten hours.

Conclusion

The errors obtained from the resistance results obtained for this convergence test are summarized in the table 4.5.

Case	Total resistance (%)	Calm water resistance (%)	Added resistance (%)
Coarse	-0.03	5.73	-10.16
Medium	0.31	3.45	-5.21
Fine	0.93	3.46	-3.53

Table 4.5: Summary of the relative errors

4.3.3 Towing tank validation

The convergence test has shown that the medium mesh refinement was a good compromise between time of calculation and accuracy. Before studying the effect of the bow parameters on the added resistance we will check the accuracy of the CFD model in different sea states with the medium mesh refinement. The results will be compared to model test data. The table 4.6 describe the sea states used for this study.
The figure 4.9 present the results obtained.

Sea states	1	2	3	
Spectrum	JONSWAP			
Hs	1.5	3	5	m
Tp	9	11	13	s
γ	3.3			

Table 4.6: Sea states studied

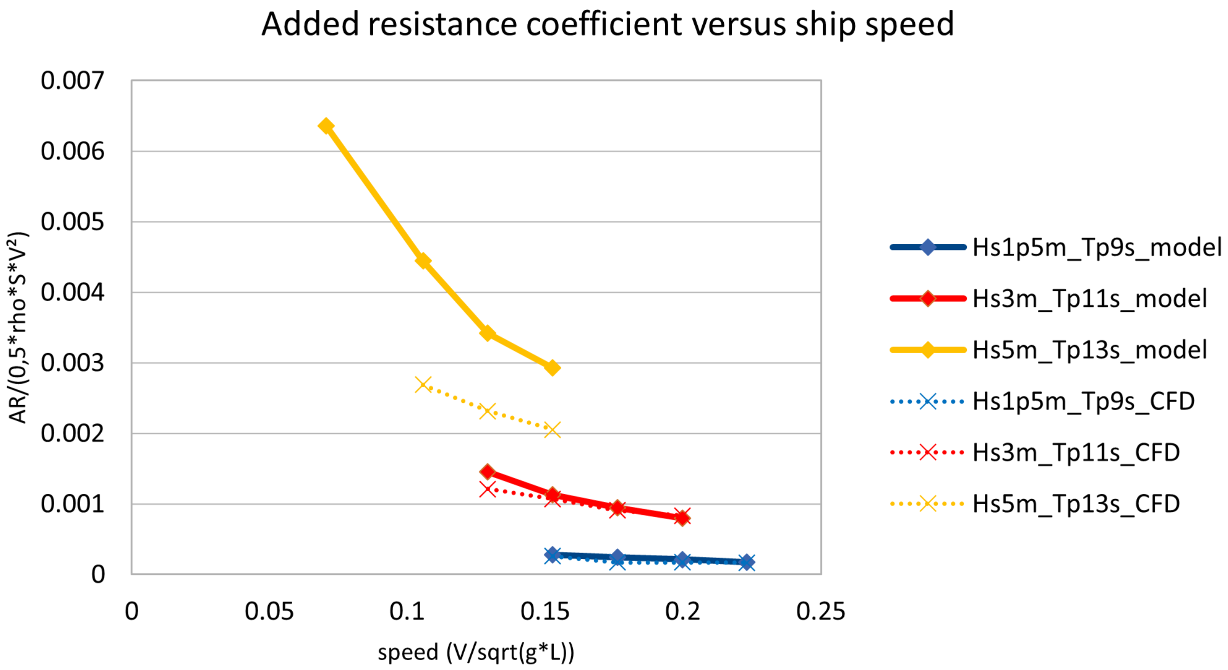

Figure 4.9: Comparison CFD calculations and tank tests

The CFD model is really reliable for the two lowest sea states (1 and 2) and especially when the speed is high. When the speed is really low, some differencies appear for the sea state 2. However, when the size of the waves increase (sea state 3) the errors become significant and the CFD model loses its reliability. This is one of the limitations of Shipflow. It cannot deal well with severe wave breaking. In this case the resistance is underestimated compare to the model tests.
For the following studies, we will focus on the sea state 2 with a target speed high enough. This permits to have significant waves and ship motions but also a good accuracy.

4.4 Bow parameters study

The bow shape might influence significantly the behaviour of the ship in waves. The motions of the ship, the added resistance in waves or the comfort can be improved or degraded by modifying it.
In this Master thesis we will not use optimization process. The goal is to highlight and understand the effects of the different design parameters of a bow in a seaway.
The ship studied is already well optimized that is why this thesis does not necessarily claim to improve this design but rather to give hints on effective design in waves.
In this part, several parameters such as the waterline entrance angle, the flare angle, the shape

of the first shoulder or the shape of the bottom part of the bow will be investigated. As it is hard to change one parameter without modifying another, some constraints over those modifications will be announced for each case. The waterline length of the ship, the draft and the entire rear and middle section will not be modified.
For this study, the ship will be placed in irreular waves defined by a JONSWAP spectrum with $Hs = 3m$, $Tp = 11s$ and $\gamma = 3.3$. The target non-dimensional speed of $Fr = 0,1940$ defined by the equation 4.2 will be used.

$$Fr = \frac{V}{\sqrt{g * L_{pp}}} \tag{4.2}$$

4.4.1 Waterline entrance angle

In this part, we focus on the waterline area. Several entrance angle have been chosen to study this parameter. The figure 4.10 shows those different shape from above. They are captioned from A to D. A is always the initial design. Each entrance angle is referenced in the table 4.7
For this bow design modification, the position of the first shoulder is fixed, the shape of the bottom part is unchanged and the modified area tries to connect naturally to the original shape. The figure 4.11 illustrate the different shape studied here.

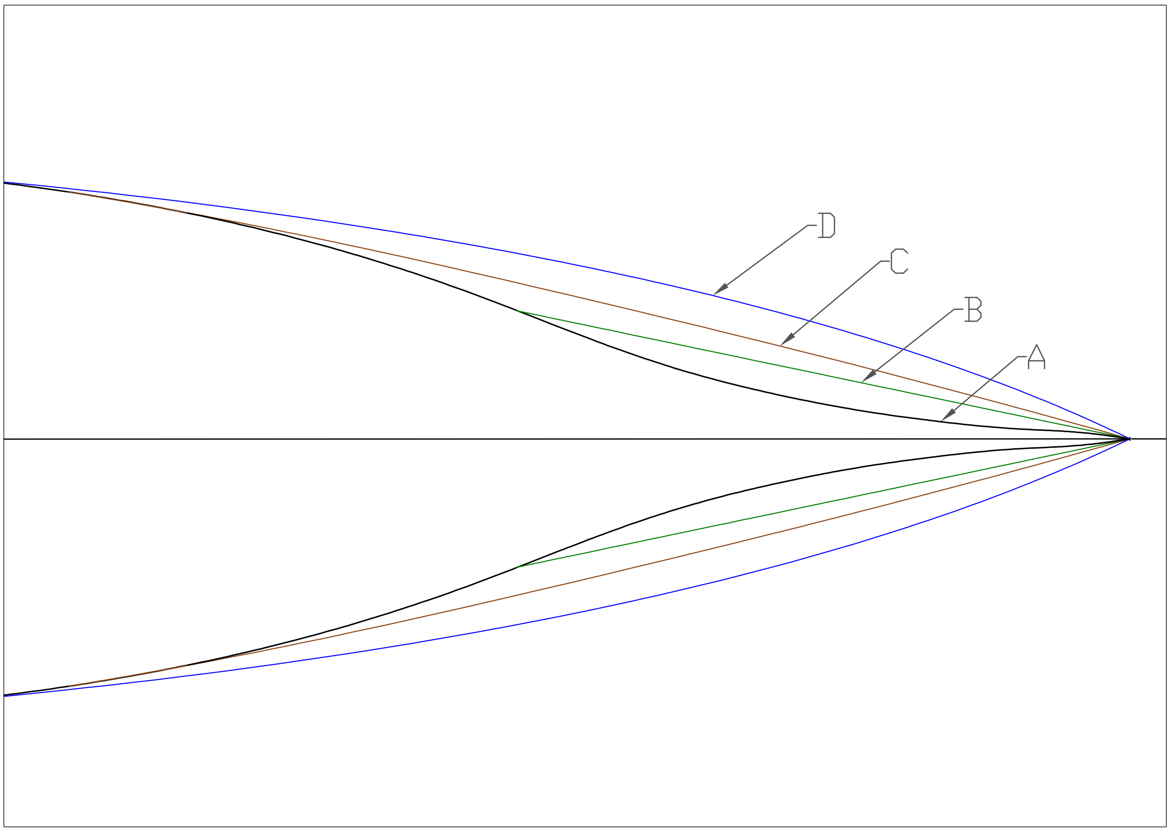

Figure 4.10: Waterline plane

Case	Angle (°)
A (initial)	8
B	12
C	16
D	26

Table 4.7: Waterline entrance angle

(a) Case A (initial)

(b) Case B

(c) Case C

(d) Case D

Figure 4.11: 3D view of the different waterline entrance angle studied

4.4.2 Flare angle

The flare angle of the bow is susceptible to have a significant effect on the behaviour of the ship in waves especially regarding the induced motions. Indeed the shape of the flare changes the pitching righting torque by modifying the volume distribution over the free surface.
In this section the bottom part, under the waterline will stay unchanged. The top part will be modified until the first shoulder of the ship. The figure 4.13 shows the different shapes studied and the figure 4.12 highlights the different profiles of those flare angles, captioned from E to H with A the initial hull.
In this section, very different geometries have been chosen for this study in order to have significant differences in the behaviours and not to optimize precisely the flare angle. Shapes such as inversed bow, straight flare, convex or concave flare will be used.

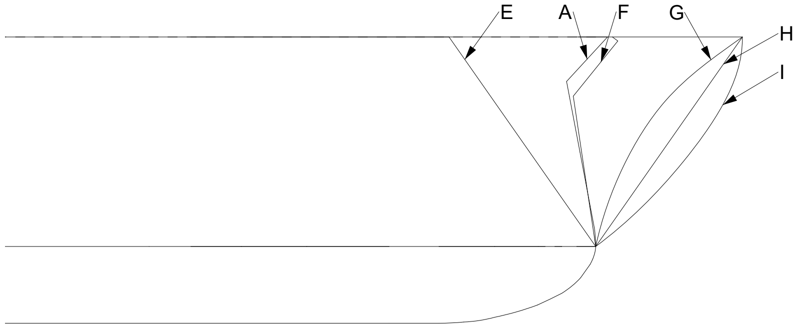

Figure 4.12: Flare profiles

(a) Case A 3D view (initial)

(b) Case A profile (initial)

(c) Case E 3D view

(d) Case E profile

(e) Case F 3D view

(f) Case F profile

(g) Case G 3D view

(h) Case G profile

(i) Case H 3D view

(j) Case H profile

(k) Case I 3D view

(l) Case I profile

Figure 4.13: 3D views of the different flare studied

4.4.3 First shoulder

Previously, several waterline entrance angles had been presented. The first shoulder was there fixed and common for all the geometries. In this part, the waterline entrance angle of the very fore part of the bow will be based on the initial bow geometry but the shape of the first shoulder will be modified. The figure 4.14 highlights those different first shoulder geometry on the waterline plane.

The bottom part is similar for the three new geometries but does not include the thin bulbous shape of the initial hull. However the top part of the freeboard is the same for all of them. The figure 4.15 shows the 3D view of these new designs. They are captioned from J to L with A the initial hull.

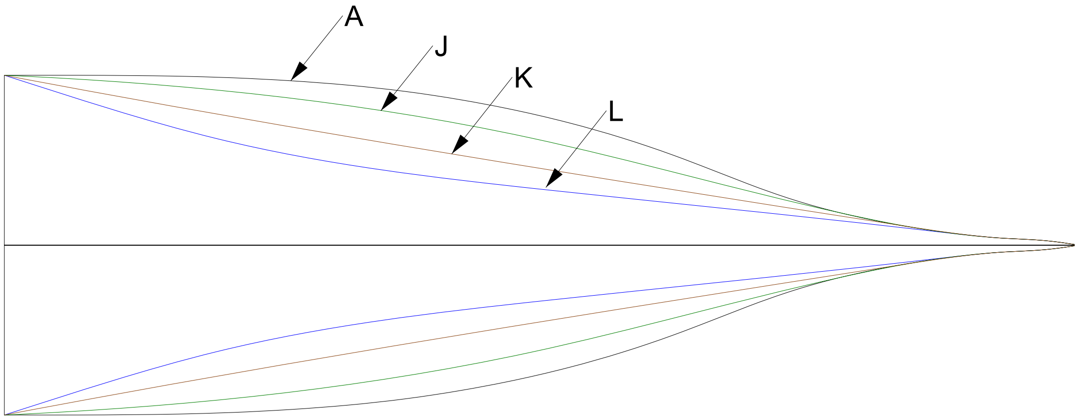

Figure 4.14: Waterline plane

(a) Case A (initial)

(b) Case J

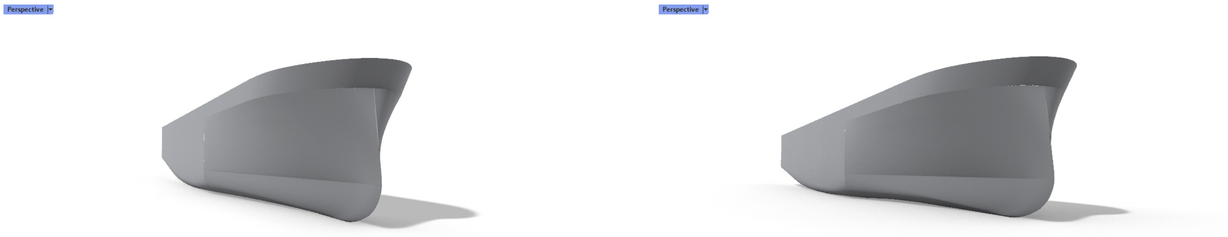

(c) Case K

(d) Case L

Figure 4.15: 3D view of the different first shoulder shape studied

4.4.4 Bottom part

The last part of the bow which has not been modified yet is the bottom part, the underwater geometry. In this section, the figures 4.16, 4.17 and 4.18 show the different geometries studied here. The left side of the lines drawing is the initial hull and the right side, the modified one. The keel line and the waterline are fixed and the same for the different shapes and will be used as limitations in order to compare a similar boat. A U-shape, close to the initial design but without any kind of bulb, a V-shape sharper than the initial design and a more voluminous bulbous shape are presented here. As for the rest of this thesis, the shapes are not optimized.

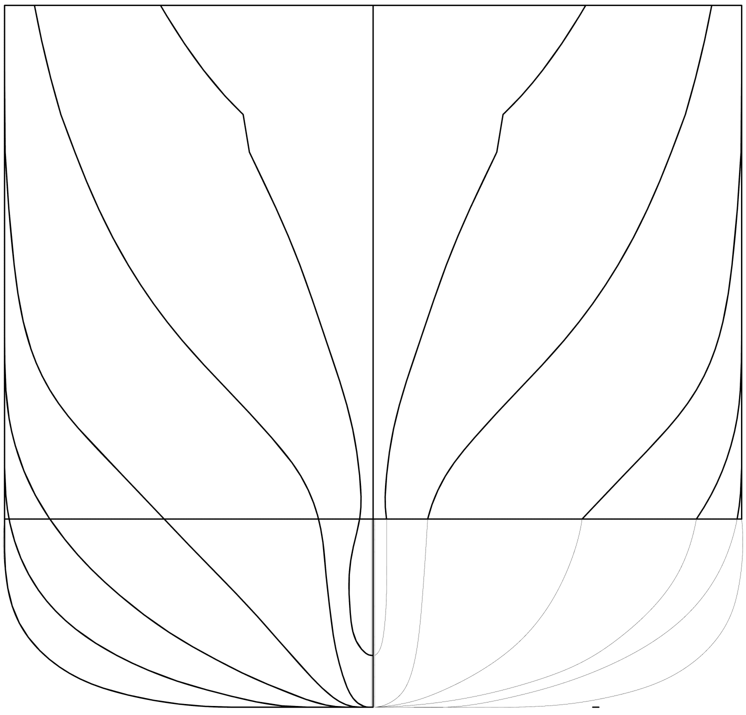

Figure 4.16: Lines drawing of the bottom U-shape versus the initial bow

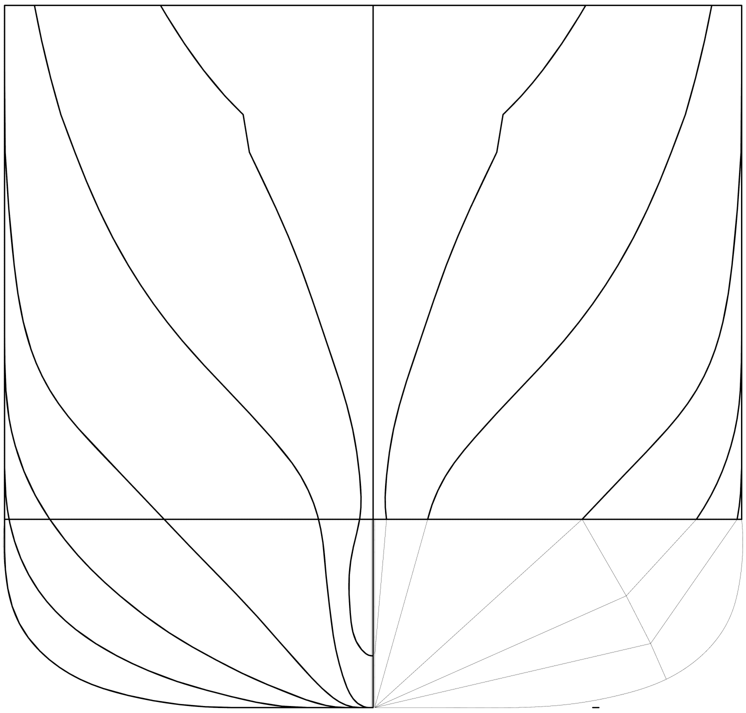

Figure 4.17: Lines drawing of the bottom V-shape versus the initial bow

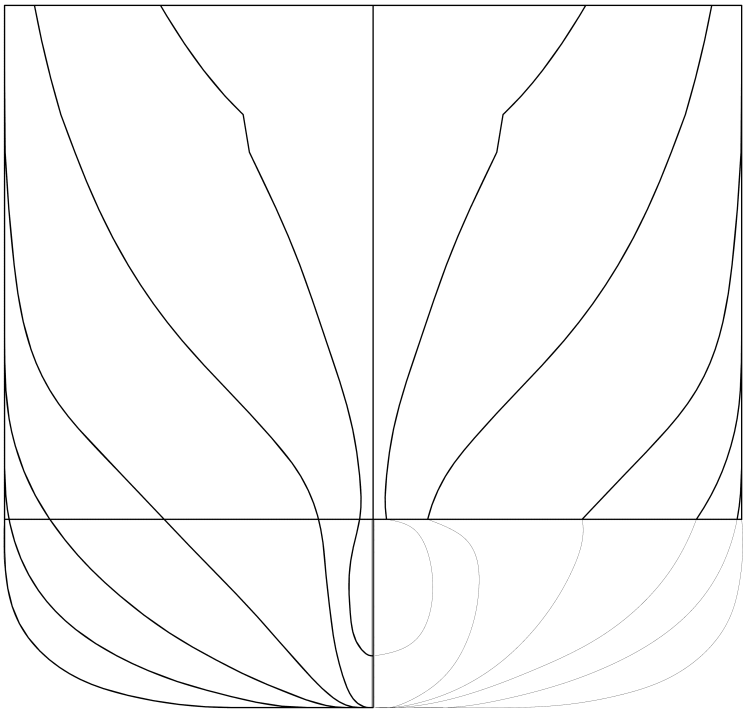

Figure 4.18: Lines drawing of the bottom bulb-shape versus the initial bow

Chapter 5

Discussion of the results

5.1 Effect of the bow design parameters

The results obtained for the different geometries studied will be highlighted in this part. The focus will be on the resistances, the movements of the ship but also on the wave pattern and the pressure distribution.

5.1.1 Waterline entrance angle

Resistance performances

For the bow shapes described in figures 4.10 and 4.11 differences in the performances appear. The figure 5.1 summarizes the different resistance coefficients obtained. The main gaps can be found on the calm water resistance. The smaller the entrance angle is, the more efficient is the hull. Here, the friction component stay approximately the same. The main differences in calm water come from the wave resistance component. However those gaps stay globally the same in waves as one can notice that the added resistance in waves is quite constant from one geometry to another. Reminder : the incidence A corresponds to the initial geometry.

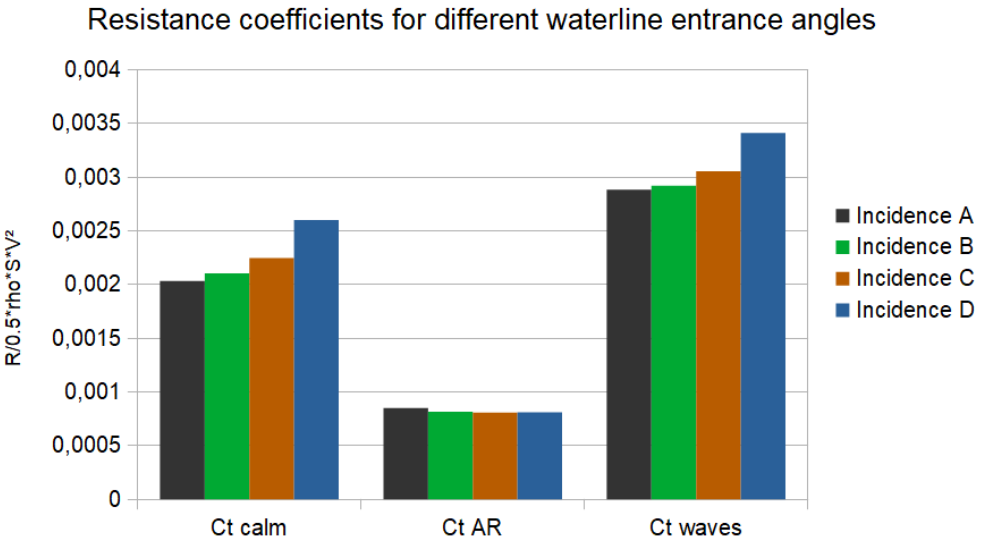

Figure 5.1: Resistance coefficients of the different waterline angles

The small differences of the wetted surface area have been taken in account in the calculation of the coefficients.

We have to keep in mind the fact that the initial hull shape has been better optimized than the new waterline entrance angles for which the rest of the bow shape has not been modified and might not fit perfectly.

Motions of the ship

Waves arriving from the front of the ship are mainly responsible for pitch and heave movements. Surge, sway, roll and yaw stay approximately constant or null in this case.
Heave and pitch motions are plotted in the figures 5.2 and 5.4 respectively for 100 seconds extracted of the simulations.
The standard deviations of heave and pitch motions of the whole simulation are shown in figure 5.3 and 5.5 respectively.

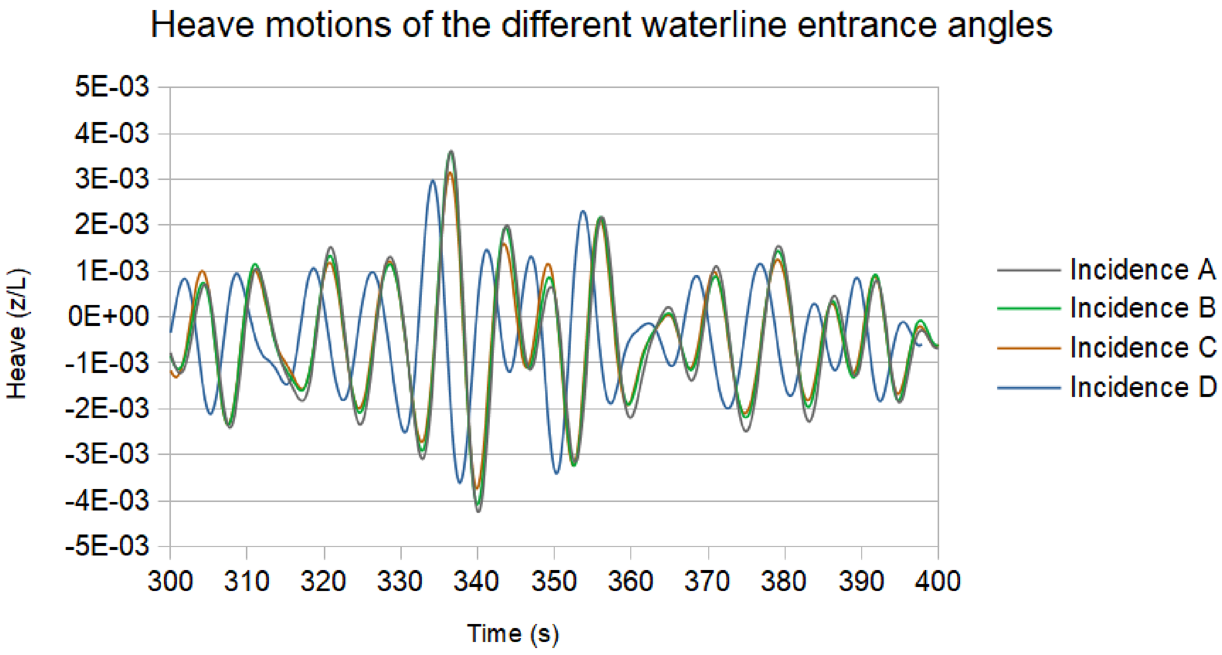

Figure 5.2: Heave motions coefficient of the different waterline entrance angles

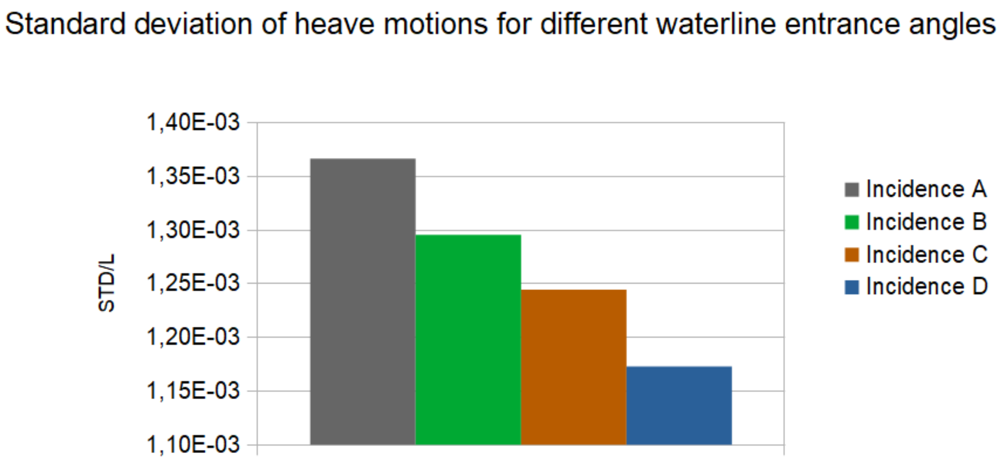

Figure 5.3: Standard deviation of heave motions coefficient for different waterline entrance angles

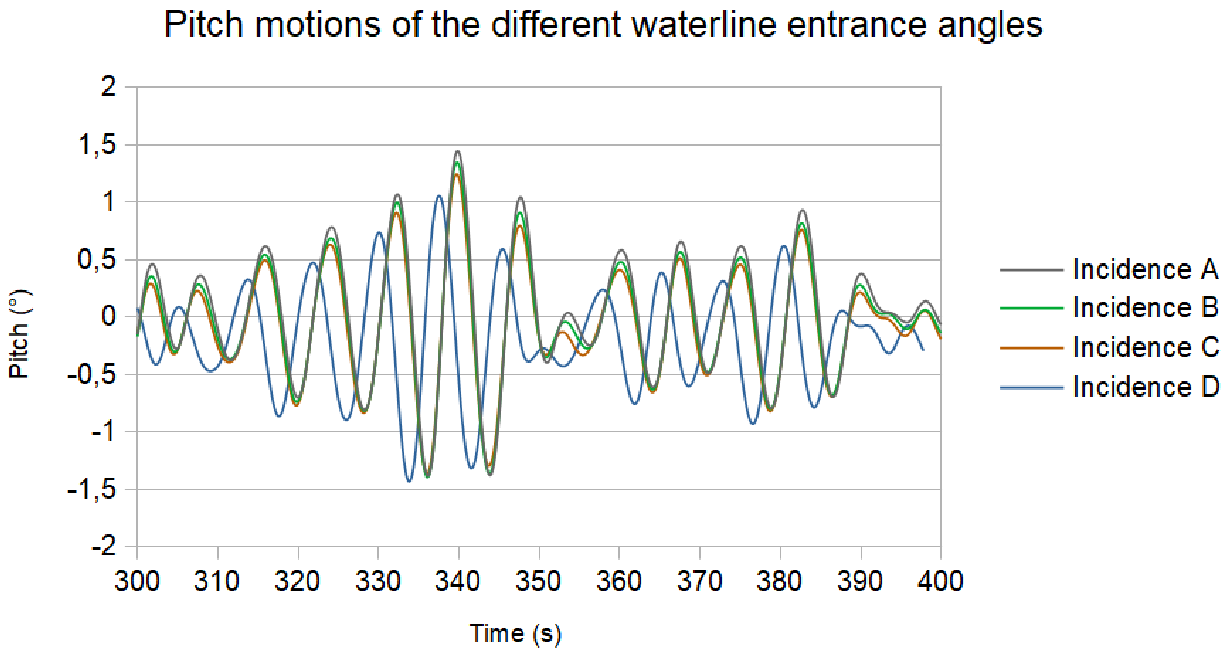

Figure 5.4: Pitch motions of the different waterline entrance angles

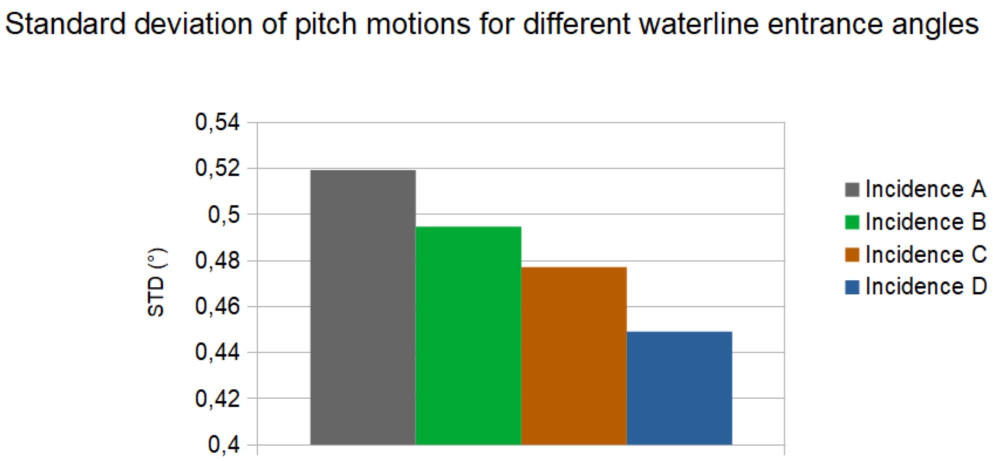

Figure 5.5: Standard deviation of pitch motions for different waterline entrance angles

The motions induced by the different waterline entrance angles have the same behaviour but not exactly the same amplitudes. In pitch or in heave, one can notice that the greater the entrance angle is the smaller are the motions amplitudes. This is confirmed by the standard deviations levels of the different incidence angles in heave and in pitch. The table 5.1 summarizes the differences with the initial hull in the maximum amplitude obtained during the simulations unsing the formula 5.1.

$$relative\ amplitude = \frac{Max\ amplitude\ X - Max\ amplitude\ A}{|Max\ amplitude\ A|} \tag{5.1}$$

Case	Heave relative amplitude (%)	Pitch relative amplitude (%)
A (initial)	0	0
B	-2.96	-3.04
C	-5.19	-7.45
D	-10.23	-11.99

Table 5.1: Relative motion amplitude comparison for the different waterline entrance angles

This highlights the fact that a greater entrance angle inducing a more voluminous bow allows to reduce the motion amplitudes.

Wave pattern

Changing the geometry of the bow has an impact on the resistance and the motions of the ship. Differences in resistance and motions can be related to the wave pattern. The figure 5.6 and the figure 5.7 show respectively the global and a more localized view of the wave pattern of the different waterline entrance angles.
The irregular waves of the sea state are here clearly visible. The time step chosen corresponds to the instant when a significant wave is hitting the bow of the ship.
Firstly, we can mention that the wave created by the bow when the ship is moving forward is more significant when the waterline entrance angle is increasing. This explains the differences in resistance obtained in calm water. As the frictional parameter of the resistance stays quite constant because the wetted surface area does not change much, the gaps are caused by the

waves created by the ship in calm water. So bigger waterline entrance angle leads to larger bow wave and then greater resistance.

Secondly, the wave created by the ship in irregular waves are a sum of the waves created by the ship moving forward, the reflected incoming waves on the hull and the damping waves created by the motions of the ship. By modifying the waterline entrance angle, we saw that the wave component in calm water and the motions are not the same anymore. As a result one can notice that the wave pattern is affected by those changes. The different arrows on the figures 5.6 d and 5.7 d highlight some discontinuities in the divergent waves. The angle of these divergent waves is also increasing when the waterline entrance angle is getting bigger.

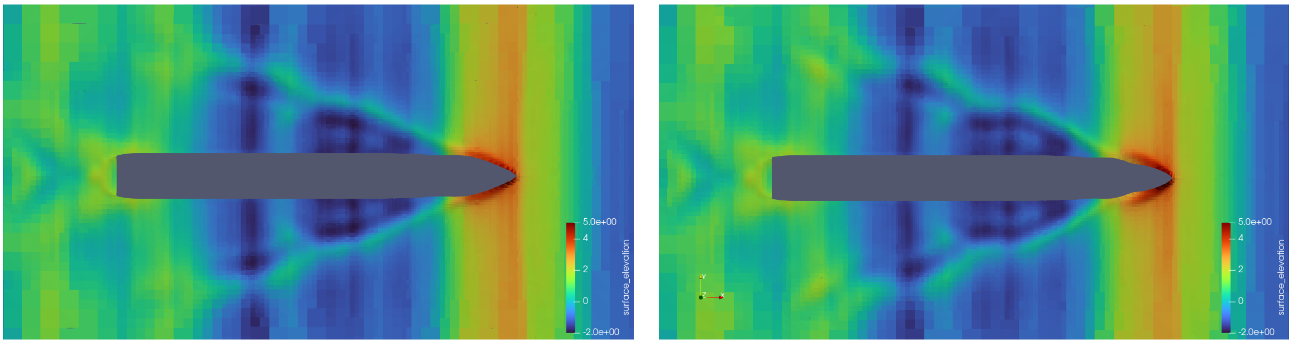

(a) Case A (initial)

(b) Case B

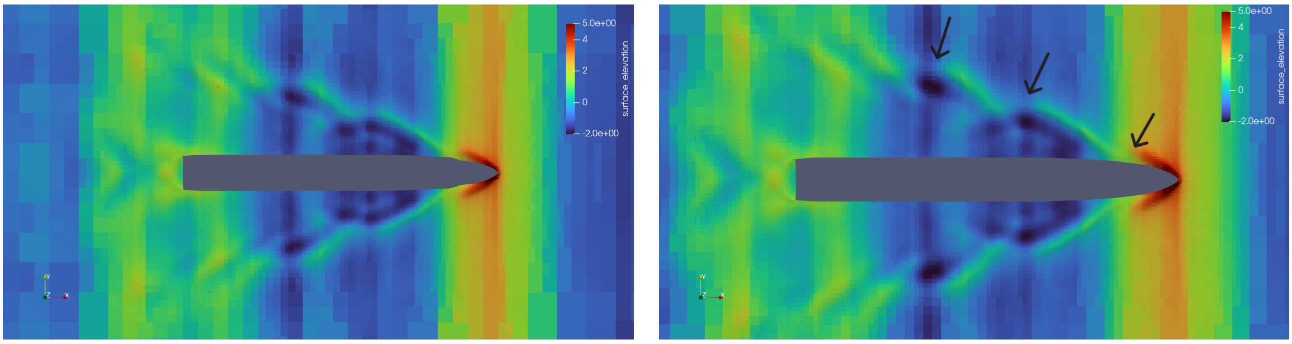

(c) Case C

(d) Case D

Figure 5.6: Global wave pattern of the different waterline entrance angles

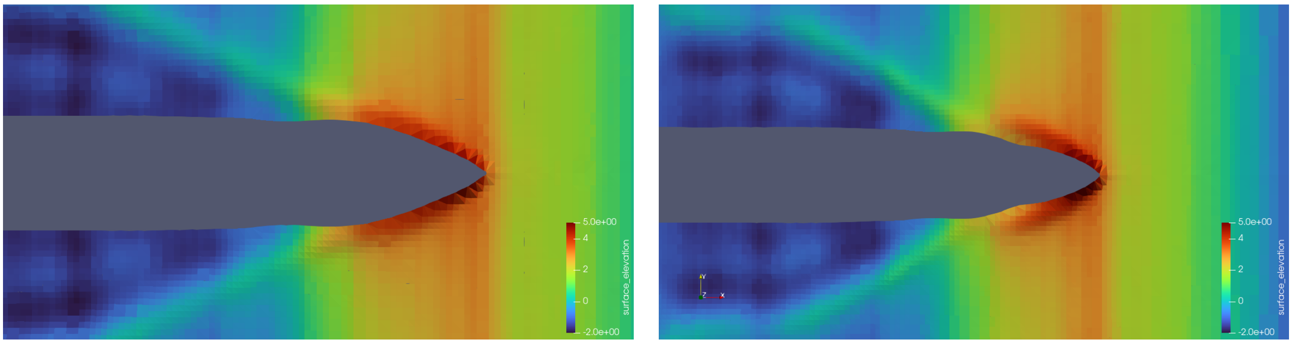

(a) Case A (initial) (b) Case B

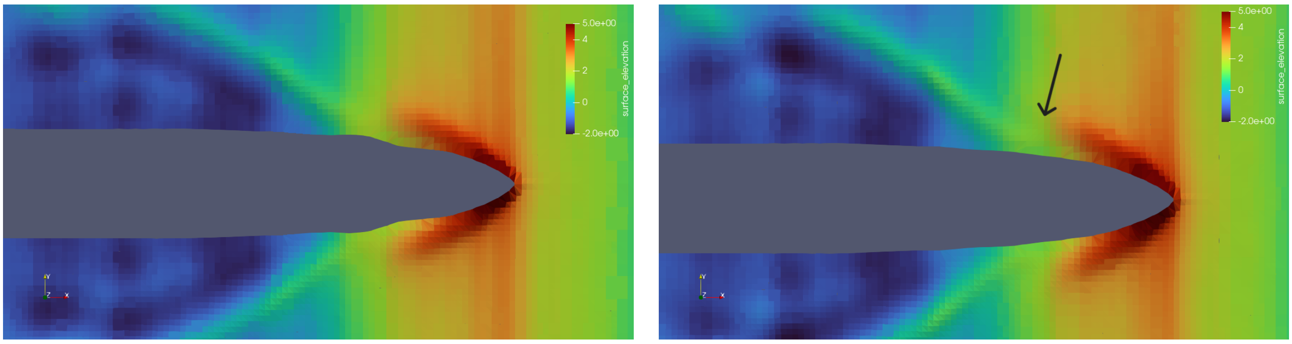

(c) Case C (d) Case D

Figure 5.7: Local wave pattern of the different waterline entrance angles

Dynamic pressure distribution

The increase in resistance by changing the waterline entrance angle can also be explained by looking at the dynamic pressure distribution on the bow. Figures 5.8 shows the pressure distribution of each case in face and in profile. One can clearly notice that the pressure level is raising when the entrance angle is increasing. This can be linked to the previous section : the pressure level is a direct consequence of the amount of water pushed forward by the ship. And, as we saw, the wave at the bow becomes bigger when the waterline entrance angle is increasing. When increasing the waterline entrance angle, the main differences on the dynamic pressure distribution appear on the very fore part of the bow. Along the waterline there is no major changes.

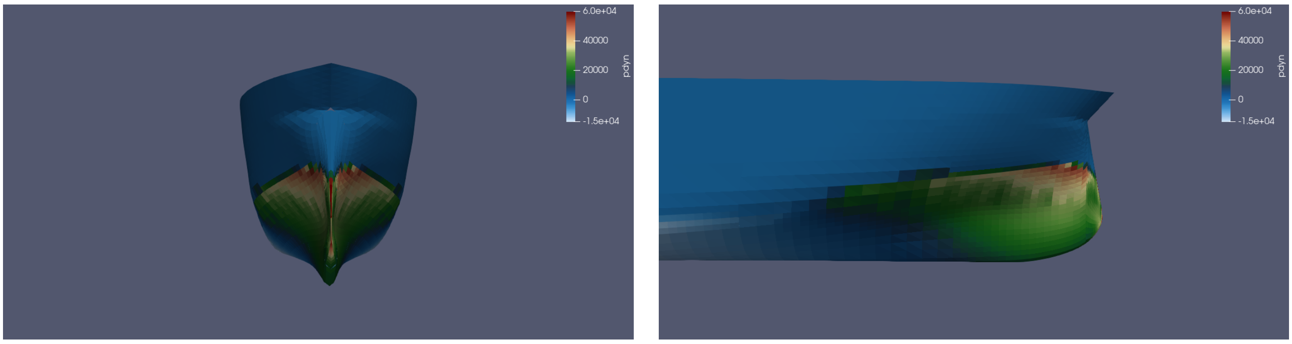

(a) Case A face (initial) (b) Case A profile (initial)

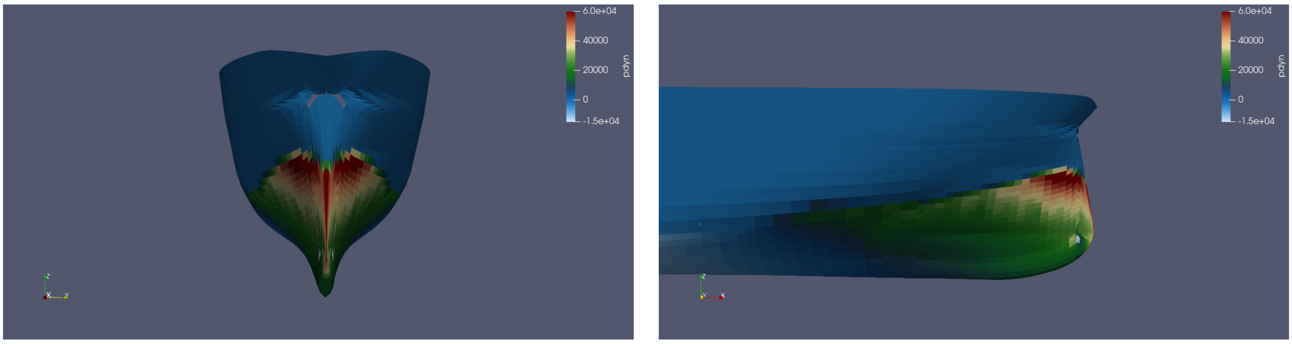

(c) Case B face (d) Case B profile

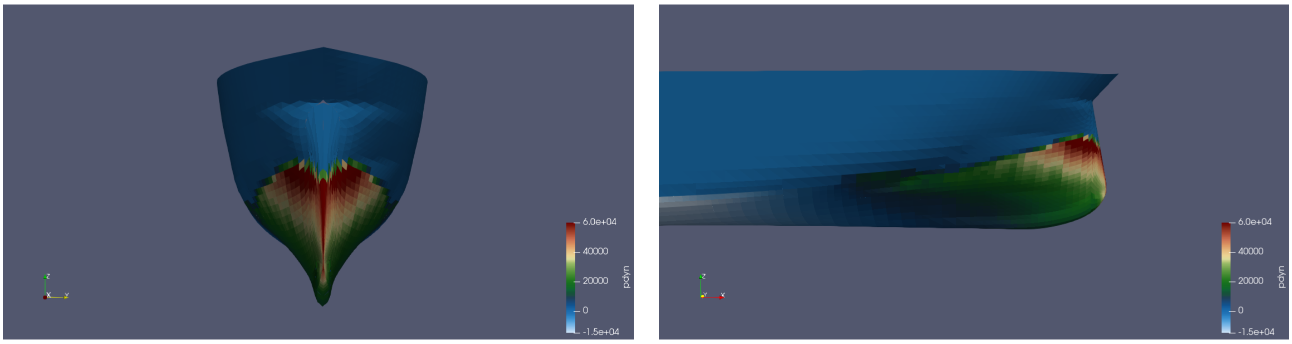

(e) Case C face (f) Case C profile

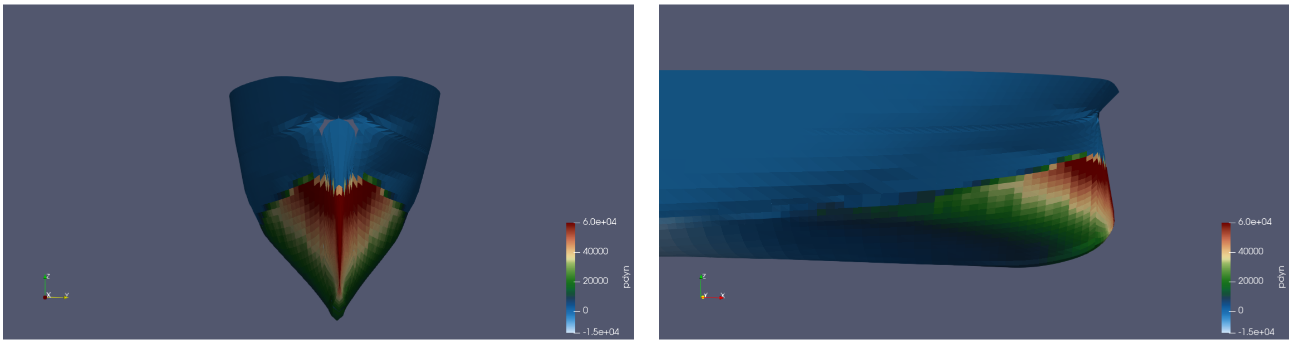

(g) Case D face (h) Case D profile

Figure 5.8: Pressure distribution on the different waterline entrance angles

5.1.2 Flare angle

Resistance performances

For the different flare angle studied, the figure 5.9 shows the resistance coefficients obtained in calm water, for the added resistance and in waves. The tendency is not as clear as the one we could highlight for the waterline entrance angle. Indeed, quite different shape have been modelled here. One can notice that the case E and F corresponding respectively to an inversed bow and a straight bow close to the initial one do not improve much the performances in waves regarding the added resistance coefficient. The small reduction on the total resistance come mainly from a reduced resistance in calm water. However, when the volume increased above the free surface and when it is pushed a bit forward, some significant reduction appear. Both in calm water and in a seaway. The reduction in total resistance of the case I is 10,3% of the initial resistance.

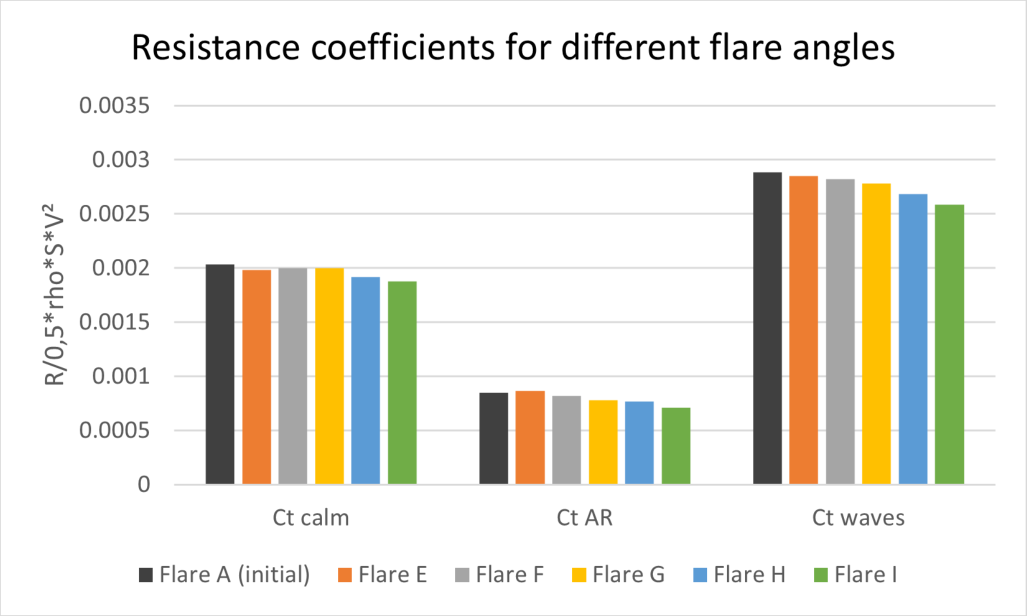

Figure 5.9: Resistance coefficients of the different flare angles

Motions of the ship

As we did for the waterline entrance angle, we can take a look at the pitch and the heave motions of the different flare shapes studied here. The figures 5.10 and 5.13 show respectively the heave and pitch motions of 100 seconds of simulation. Figures 5.11 and 5.14 are a zoom of the two previous figures to discuss more easily of the behaviour of the different cases. Finally, the figures 5.12 and 5.15 describe the standard deviation of the heave and pitch motions of the simulations and the table 5.2 summarizes the differences with the initial hull in the maximum amplitude obtained during the simulations using the formula 5.1.

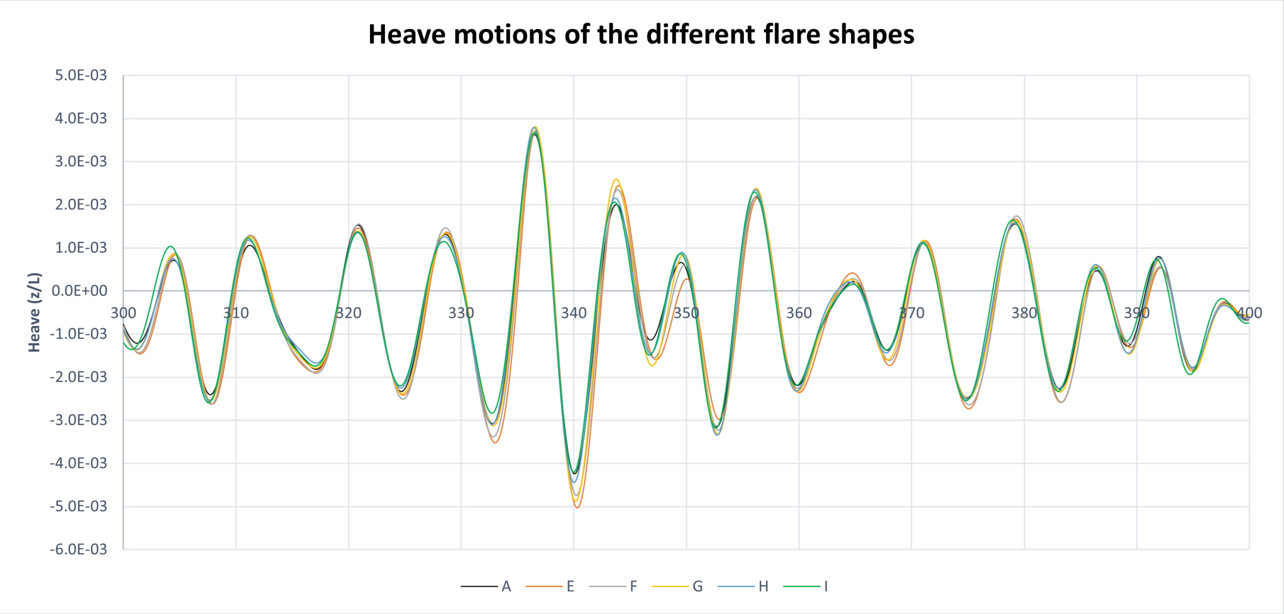

Figure 5.10: Heave motions coefficient of the different flare angles

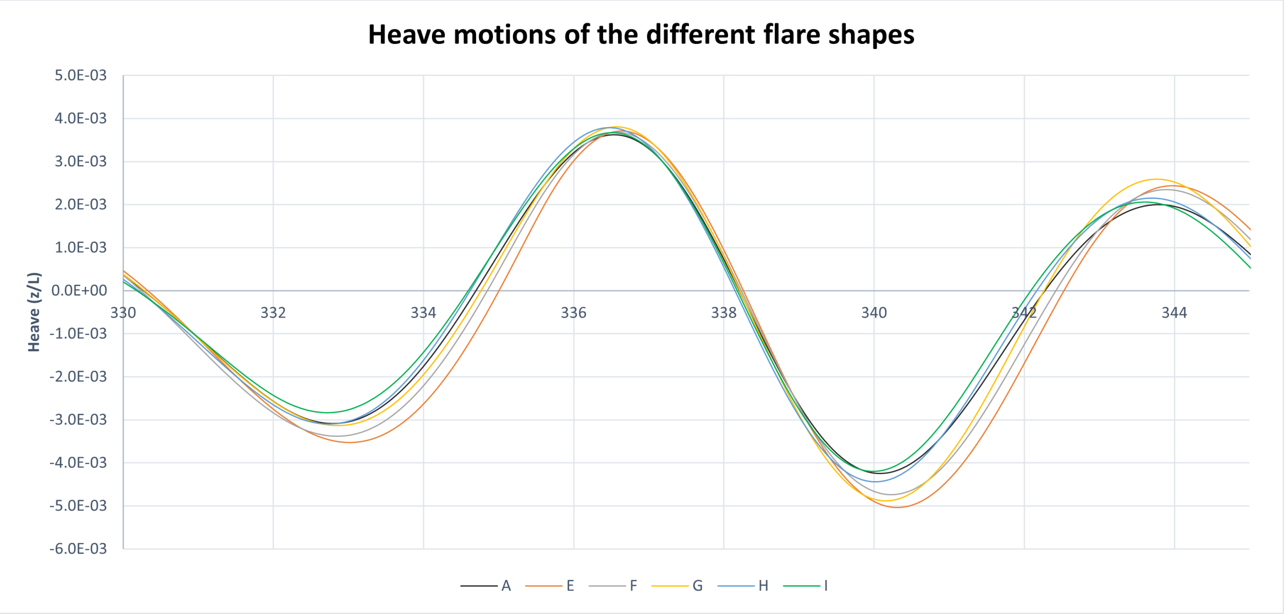

Figure 5.11: Zoom on heave motions coefficient of the different flare angles

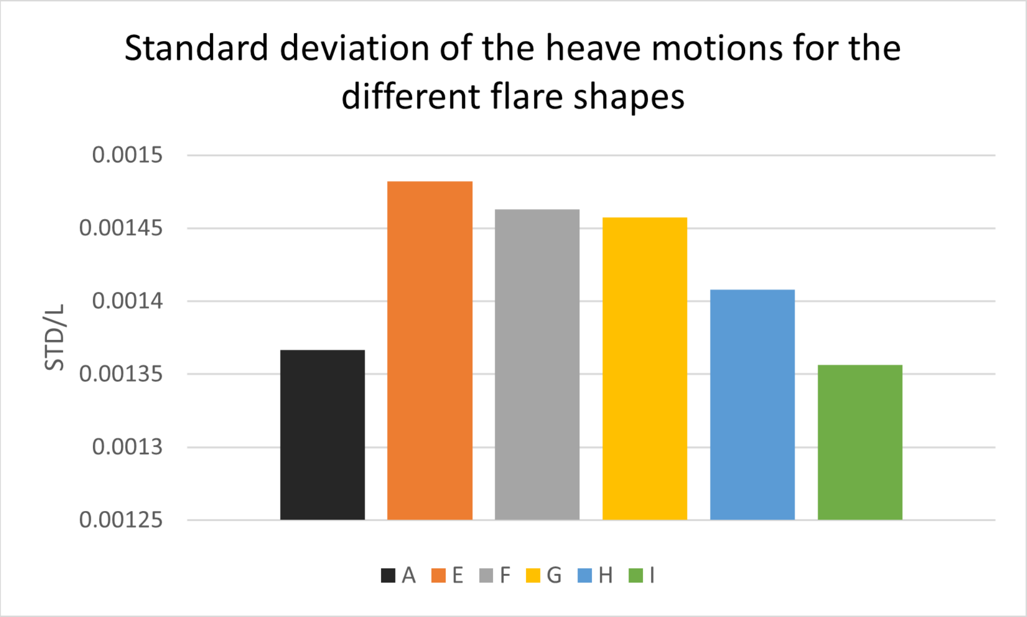

Figure 5.12: Standard deviation of heave motions coefficient for different flare angles

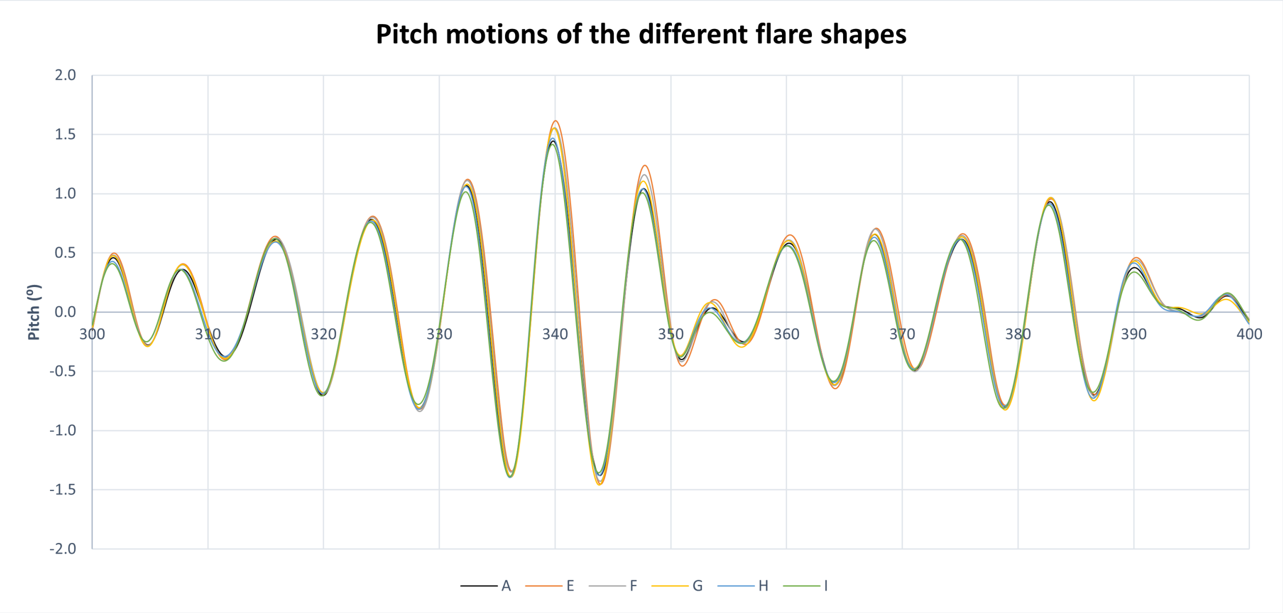

Figure 5.13: Pitch motions of the different flare angles

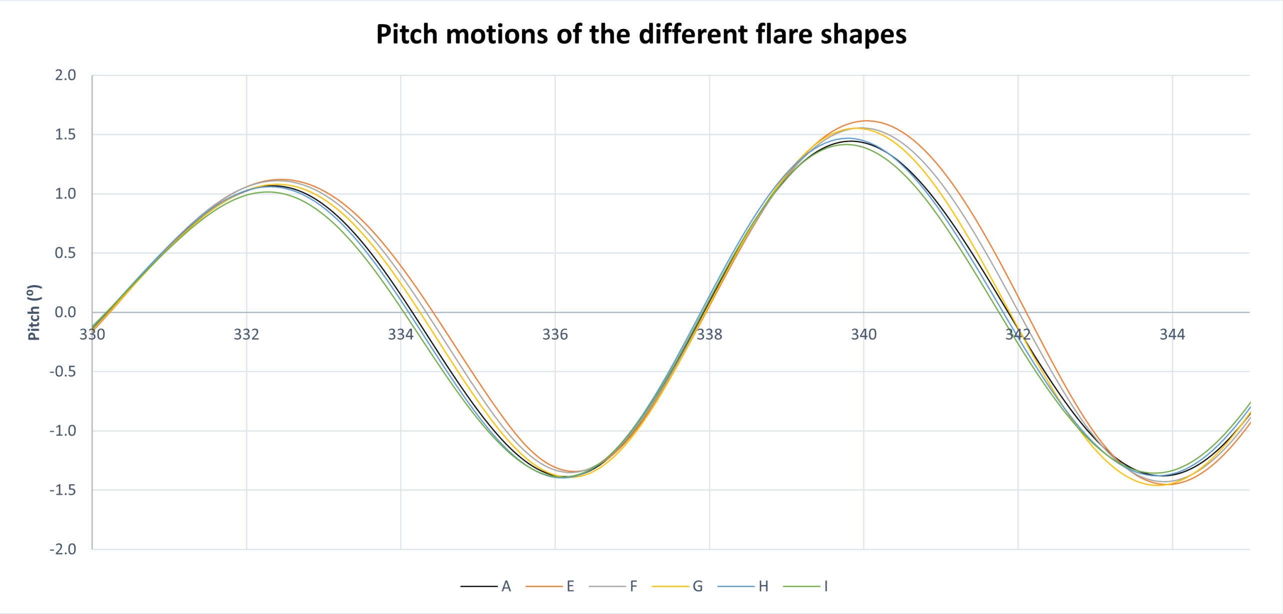

Figure 5.14: Zoom on pitch motions of the different flare angles

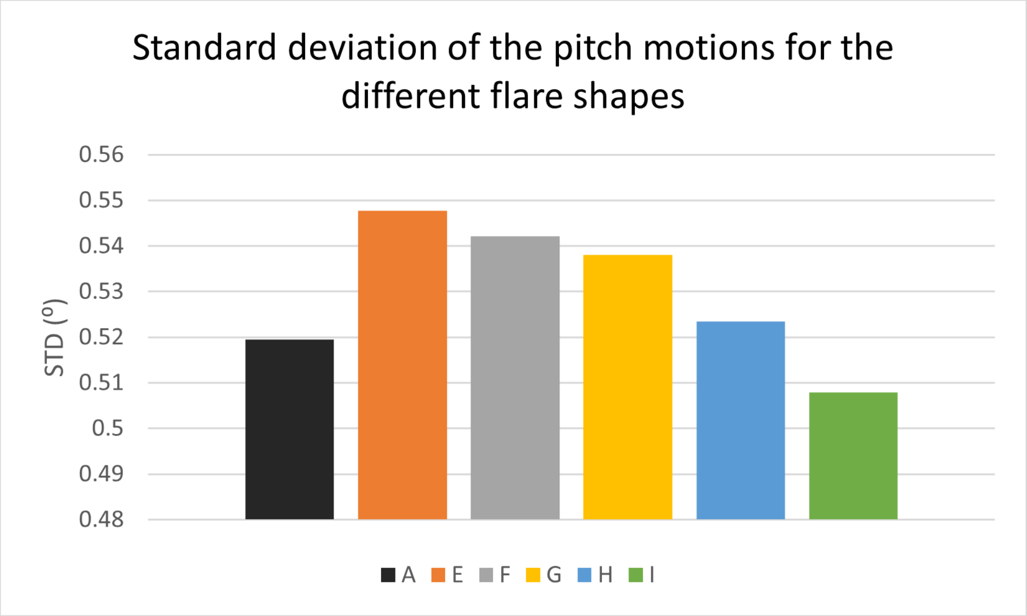

Figure 5.15: Standard deviation of pitch motions for different flare angles

Case	Heave relative amplitude (%)	Pitch relative amplitude (%)
A (initial)	0	0
E	7.48	8.53
F	4.58	5.73
G	7.73	6.52
H	5.07	1.27
I	-1.42	-0.84

Table 5.2: Relative motion amplitude comparison for the different flare angles

Even if the different geometries are slightly different, the behaviour in waves does not change much. However, we can point two major tendencies :

1) From the geometry E to the I, the amplitudes in pitch and heave motions are decreasing progressively. The temporal data are not that easy to compare but the study of the standard deviation and the relative motion amplitude comparison allow to show this decrease clearly. The pitch data in the table 5.2 are especially highlighting the main differences.
2) Again, from geometry E to I, the "peaks" in the time series happen earlier and earlier. It is particularly visible on the zoomed figures 5.11 and 5.14.

Those differences might be explained by the changes in the volumetric distribution of the bow above the free surface. The more voluminous is the upper part of the bow, the more reduced are the motions and the earlier the response reach its maximum. But case A behave a bit different. Contrary to the new flare design tested here which have the volume increasing smoothly from the very fore part to the first shoulder, the initial case has a fairly pronounced and sudden increase in volume just before the first shoulder. This can explain the differences in motions in particular with the case F: similar resistance but lower motions for the initial hull. Indeed, these two designs are quite similar on the fore part but different arriving to the first shoulder. The next section on the first shoulder shape might enlighten us about it.

It is interesting to notice that the motions are more important for most of the cases but with a smaller resistance in waves. We will come back to it.

Wave pattern

The wave pattern of all the different cases are shown in Appendix. The different wave pattern are very close from one another. So we will focus and compare only the initial hull and the most efficient case, the case I in figures A.1 and A.2.
Even if the wave pattern is approximately the same, we can mention the fact that the height of the bow wave is a bit lower in case I and especially when moving back along the ship. This can be explained by the smaller motions of this case.
The divergent wave seems to be also a little smaller in case I. It can explain the differences in resistance in calm water particularly.

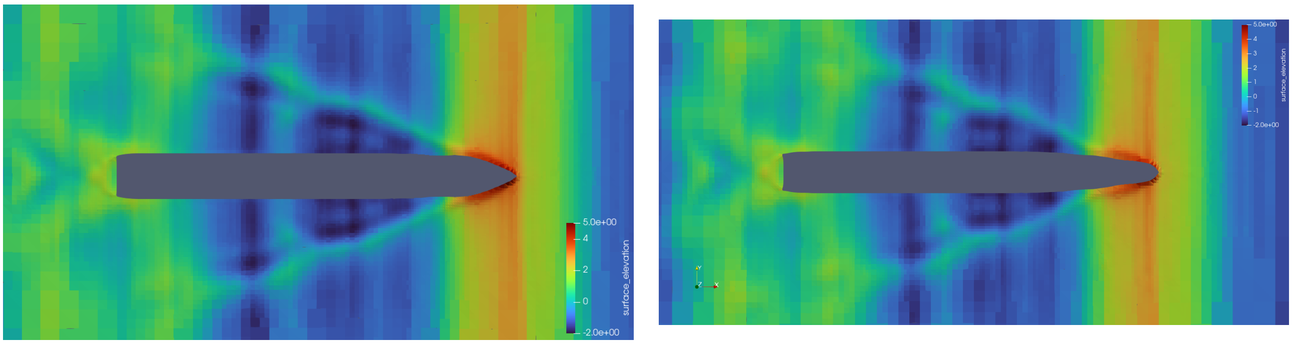

(a) Case A (initial)

(b) Case I

Figure 5.16: Global wave pattern of the initial hull and the case I

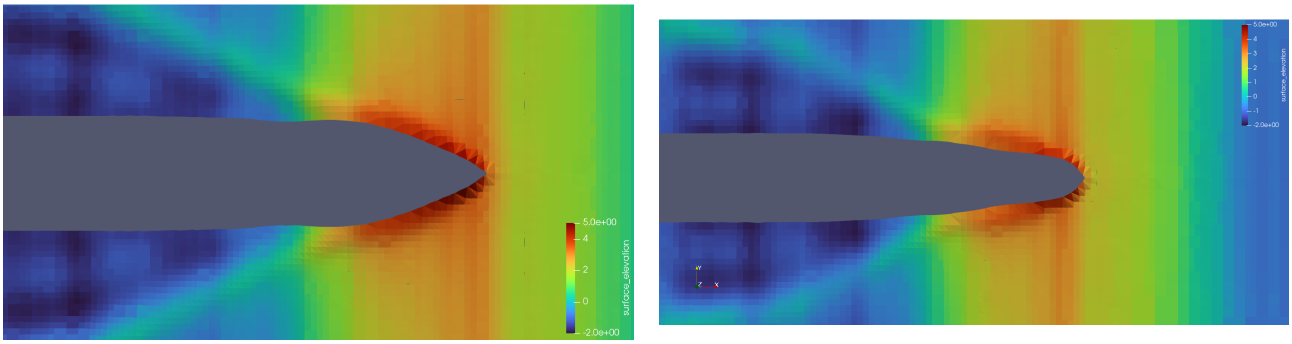

(a) Case A (initial)

(b) Case I

Figure 5.17: Local wave pattern of the initial hull and the case I

Dynamic pressure distribution

As for the wave pattern, the pressure distribution on all the cases is presented in Appendix. We will focus on the cases A and I in this section. Figure 5.18 show the pressure distribution on these two geometries.

In the first shoulder part, the two design experienced the same level of dynamic pressure. It is also quite similar for the bottom part.

The differences appear at the very fore part of the bow. The dynamic pressure on initial hull is more concentrated and in a higher level. On the case I, this pressure is more evenly distributed. The fact that the above waterline part of the case I is longer and then more voluminous helps in this manner. When hitting the incoming wave, the design in case I breaks the wave smoothly and redirects it to the sides while the initial hull penetrates into the wave without breaking it firstly. But then the wave meets a wider part of the bow and crashes more violently on it creating higher levels of dynamic pressure. This might also explain why the case I has lower motions in waves.

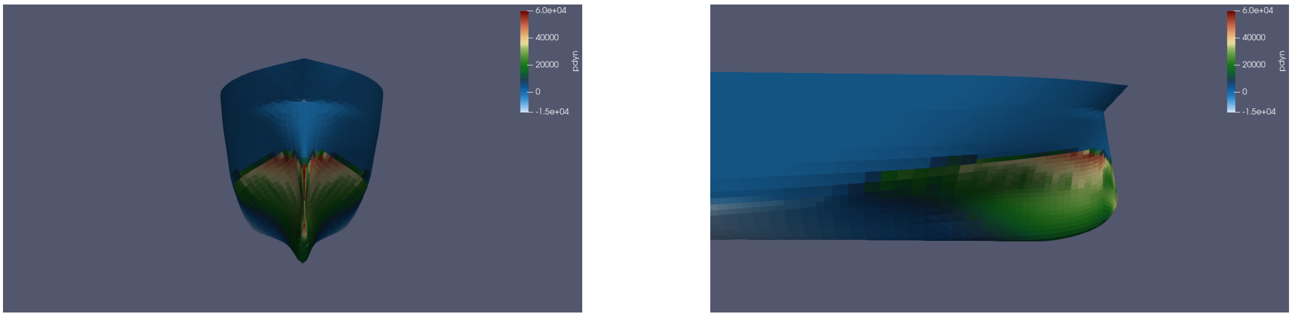

(a) Case A face (initial)

(b) Case A profile (initial)

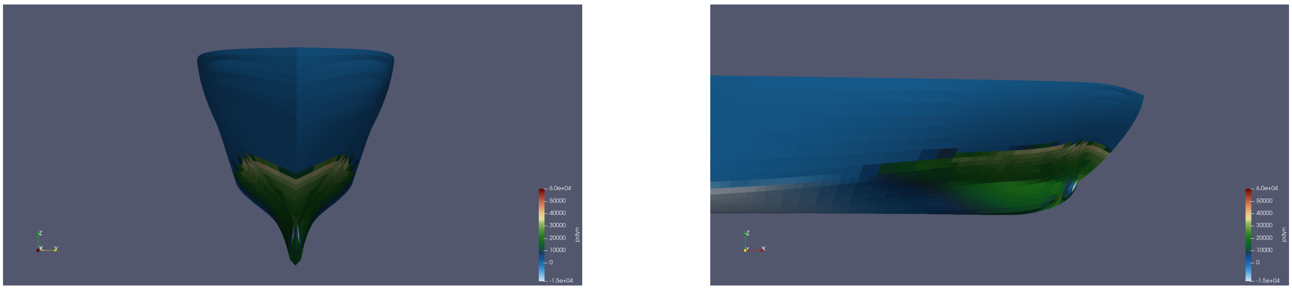

(c) Case I face

(d) Case I profile

Figure 5.18: Pressure distribution on the initial design and the case I

5.1.3 First shoulder

Resistance performances

The performances of the different first shoulder design are summarized in the figure 5.19. In calm water, the cases J and K are as efficient as the initial case but the case L is completely inefficient. In waves, smoothing the first shoulder permits to reduce the resistance up to 8,1% for the case K. However, reversing the curvature (case L) does not help.

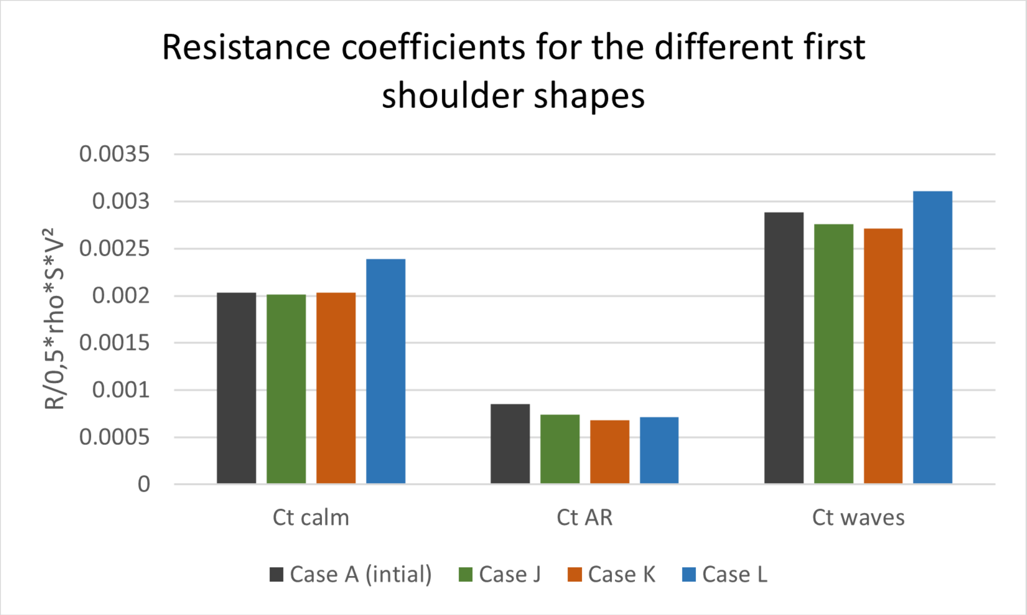

Figure 5.19: Resistance coefficients of the different first shoulder shapes

Motions of the ship

Once again, the pitch and the heave motions of the different first shoulder design are going to be studied here. The figures 5.20 and 5.22 show respectively the heave and pitch motions of 100 seconds of simulation and the figures 5.21 and 5.23 expose the standard deviation of the heave and pitch motions of the simulations. The table 5.3 allow to compare the maximum amplitudes with the initial hull using the formula 5.1.

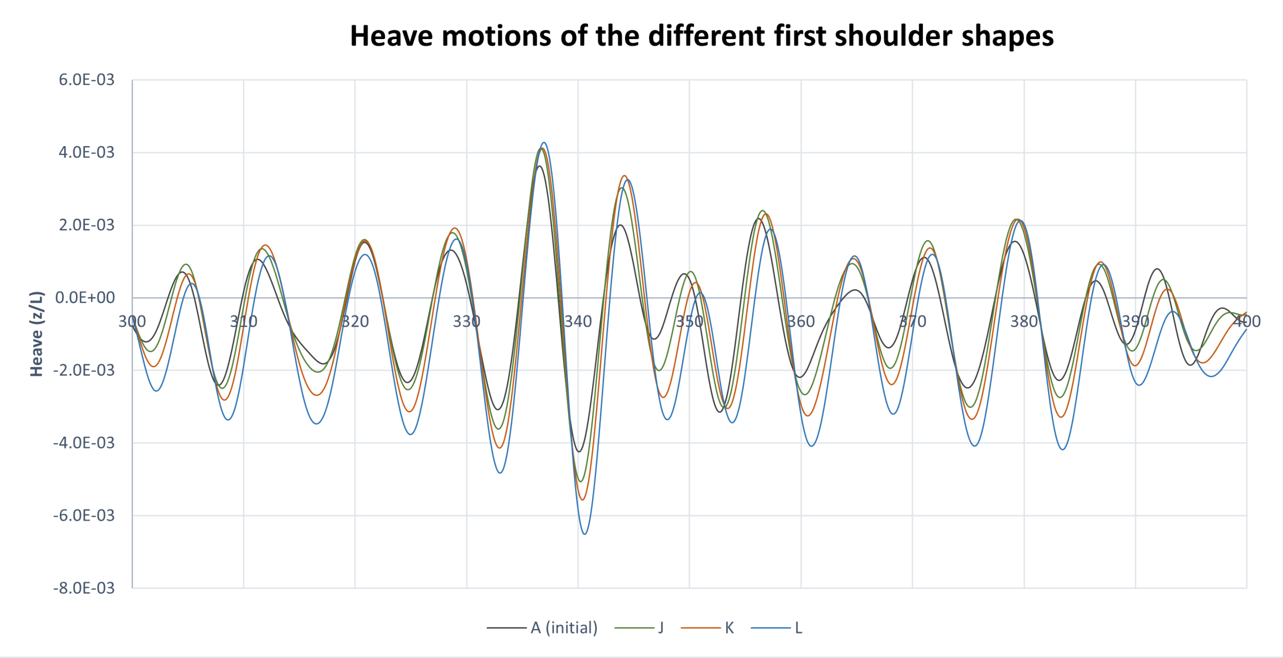

Figure 5.20: Heave motions coefficient of the different shoulder shapes

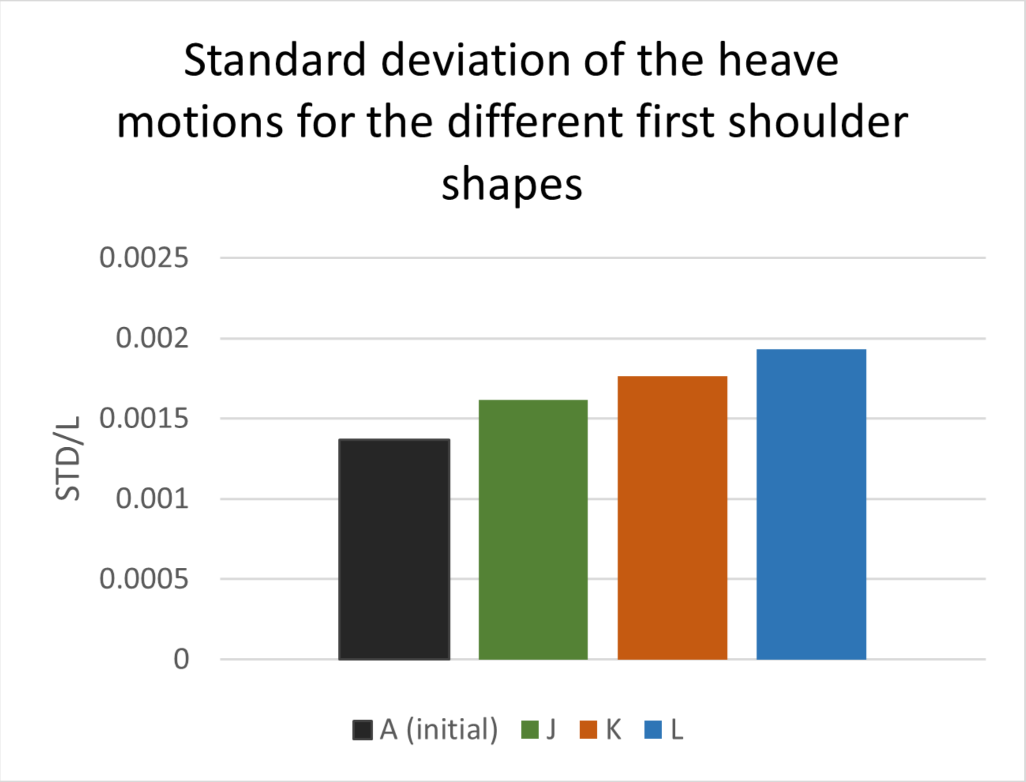

Figure 5.21: Standard deviation of heave motions coefficient for different shoulder shapes

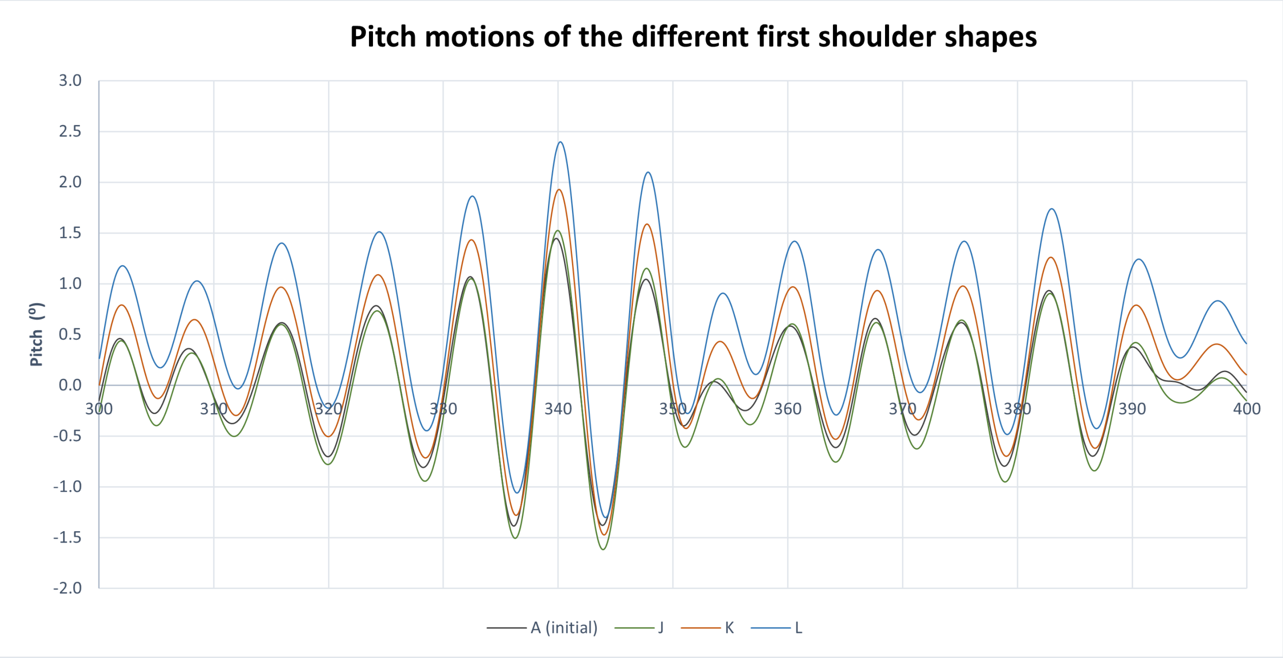

Figure 5.22: Pitch motions of the different shoulder shapes

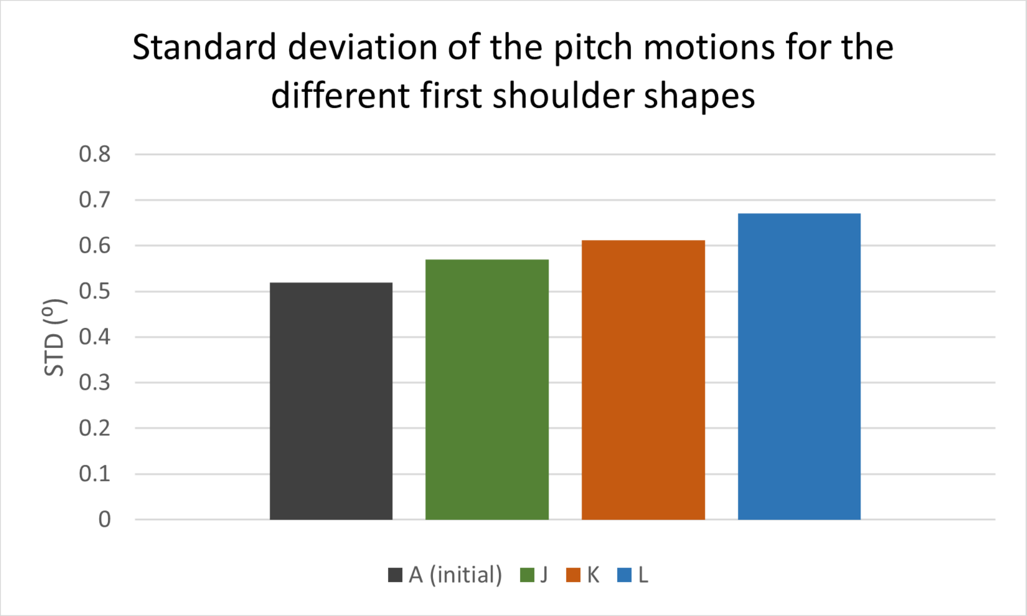

Figure 5.23: Standard deviation of pitch motions for different shoulder shapes

Case	Heave relative amplitude (%)	Pitch relative amplitude (%)
A (initial)	0	0
J	15.15	11.02
K	23.32	20.19
L	32.17	31.26

Table 5.3: Relative motion amplitude comparison for the different shoulder shapes

The analysis is quite easy for this case. All the different figures above show and agree on the fact that the narrower is the part leading to the first shoulder (ie the less voluminous is

the bow) the higher is the motion response in waves. The table **??** present very high variation compare to the initial hull. This means that the shape of the first shoulder has definitely a huge impact on the behaviour of the ship in a seaway.
However, one can notice an interesting point: in one hand the motions are largely increased in case J and K, the resistance in waves is, in the other hand, highly smaller compare to the initial hull (see previous section). This echoes what we question in the flare angle section.
As a last comment, the figure 5.22 showing the pitch motions highlights also that the cases J, K and L have a steady state trim angle if we take the mean value of the different cases. It can be explain by the reduction of volume on the fore part of the ship. As the center of gravity is still at the same position for all the cases, a reduction of volume in this parts leads to a slight sinking of the bow at the equilibrium.

Wave pattern

The figure 5.24 and the figure 5.25 show respectively the global and a local view of the wave pattern for the different first shoulder shapes.
The instant chosen corresponds to the same moment used in the previous wave patterns studies (ie when significant wave is hitting the bow of the ship).
The different wave patterns shows several phenomena:
1) When inversing the curvature linking the fore part of the bow and the first shoulder, then creating a sharper angle (see figure 4.14), the effect of this first shoulder seems to be more visible. For the cases K and L one can notice that a second divergent waves is created just after the first one.
2) While a second divergent wave is created after the first shoulder, we can also mention the fact that the initial divergent wave starts a bit further back when changing the shape from case J to L.
3) Finally, a wave trough appear right after the shoulder on cases K and L.
4) The angles of the different divergent waves seems to be similar.

The facts 1 and 3 should lead to an increase of the resistance because the free surface is more deformed and then dissipates more energy. For the case L it is obvious that the second divergent wave is responsible for the increase in resistance in calm water as seen in the figure 5.19. For the case K it is harder to conclude. Indeed the resistance is lower than the initial hull but a second divergent wave is also visible on its wave pattern. What can explain this is the fact that the divergent waves generated in the case K are a bit smaller than the one generated by the initial hull. So two small divergent waves leads to a lower resistance than one bigger divergent wave.

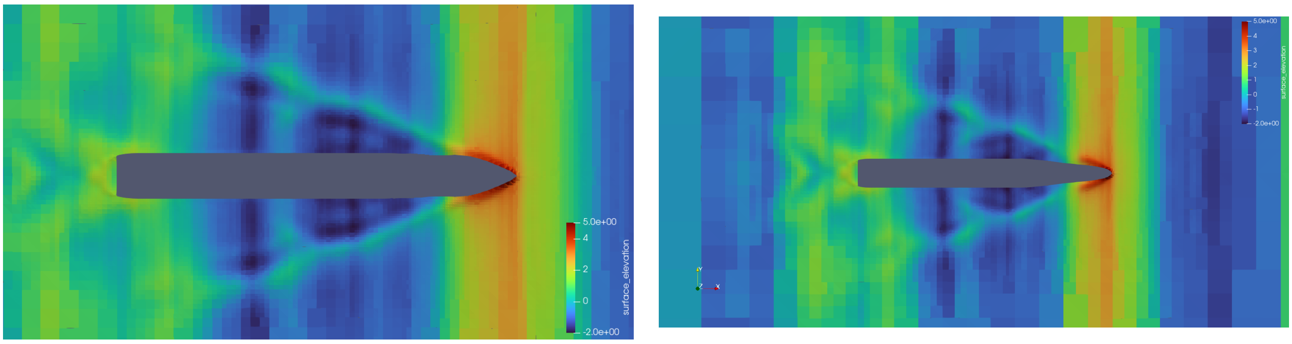

(a) Case A (initial)

(b) Case J

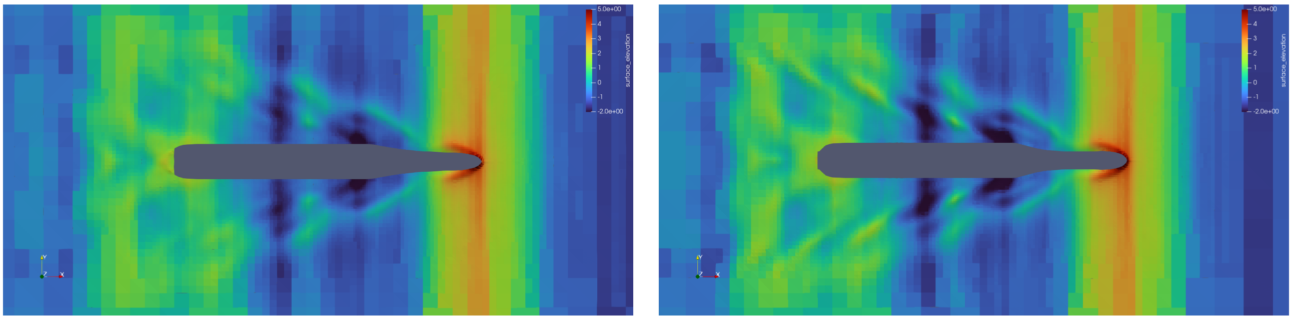

(c) Case K

(d) Case L

Figure 5.24: Global wave pattern of the different first shoulder shapes

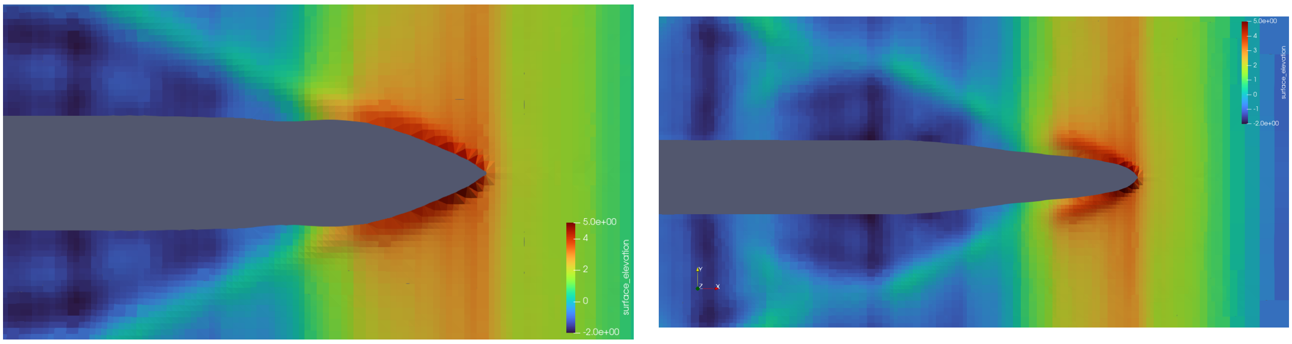

(a) Case A (initial)

(b) Case J

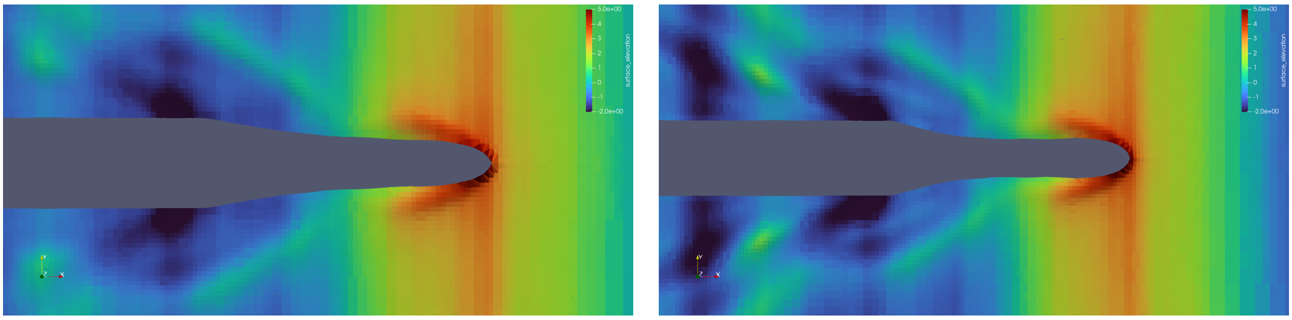

(c) Case K

(d) Case L

Figure 5.25: Local wave pattern of the different first shoulder shapes

Dynamic pressure distribution

The dynamic pressure distribution on the three different first shoulder shapes is presented in the figure 5.26.
The first obvious thing to notice is the increase in trim angle as mention in the study of the

pitch motions. Indeed, the less voluminous is the fore part of the ship, the higher is the pressure boundary created by the bow wave.

Secondly, the level of pressure increase from case A to L. As the very fore part of the boat is identical on the different cases, this pressure increase is not due to a reflected wave or the wave resistance but it is rather linked to the increase in motion amplitude.

There is no major differences in pressure distribution near the first shoulder area.

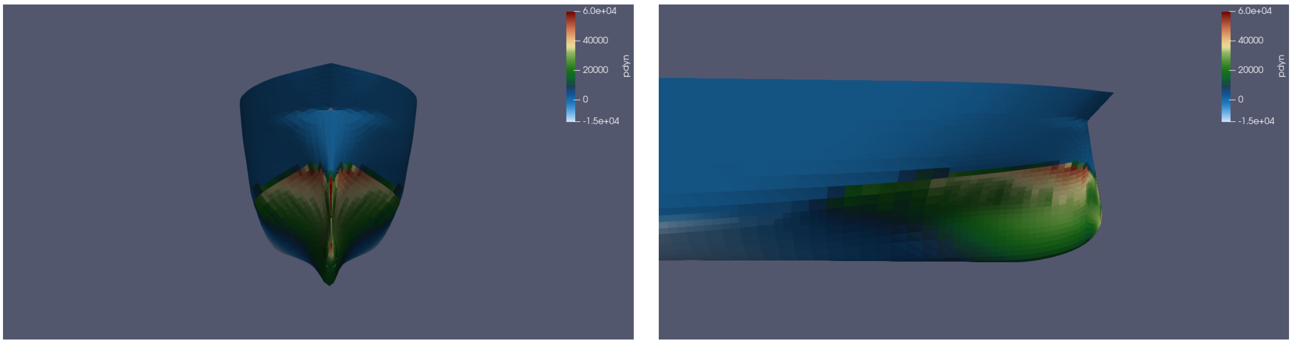

(a) Case A face (initial) (b) Case A profile (initial)

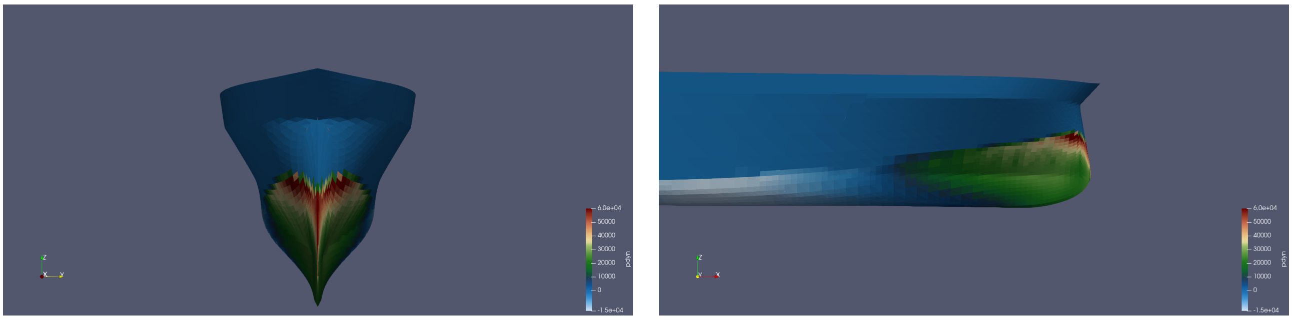

(c) Case J face (d) Case J profile

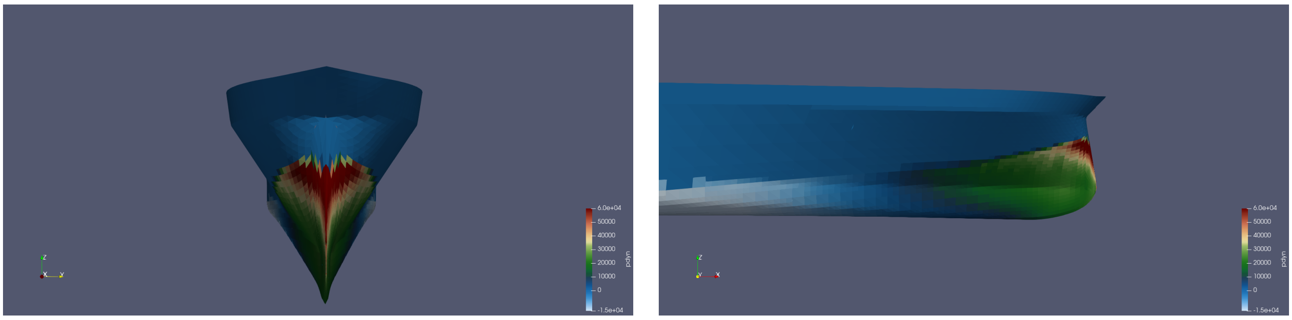

(e) Case K face (f) Case K profile

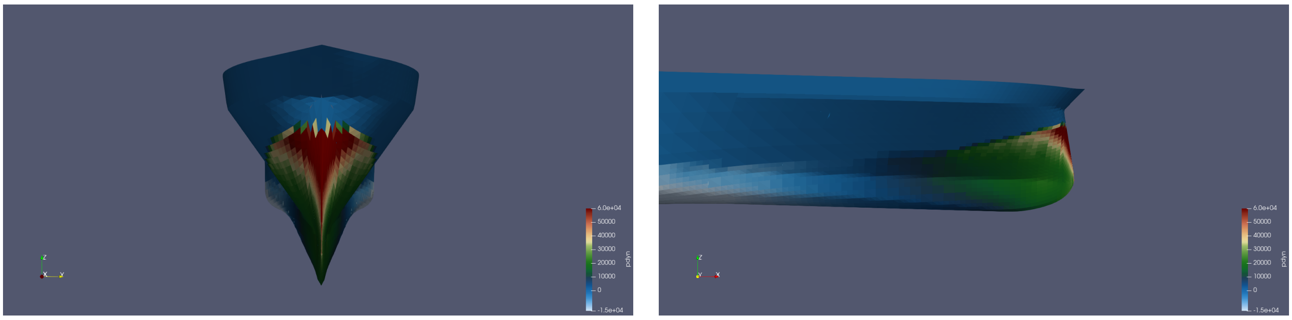

(g) Case L face (h) Case L profile

Figure 5.26: Pressure distribution on the different first shoulder shapes

5.1.4 Bottom part

Resistance performances

The performances obtained with different underwater bow form are described by their resistance coefficients in the figure 5.27.
The initial hull is already well optimized for calm water resistance. However, the V-shape induce a bit lower resistance both in calm water and in waves. As we can see, the bulb-shape is not well optimized at all. It ends with the lowest added resistance coefficient but this is due to the very high calm water resistance. The U-shape is quite similar to the initial hull but has poorer performances as well.

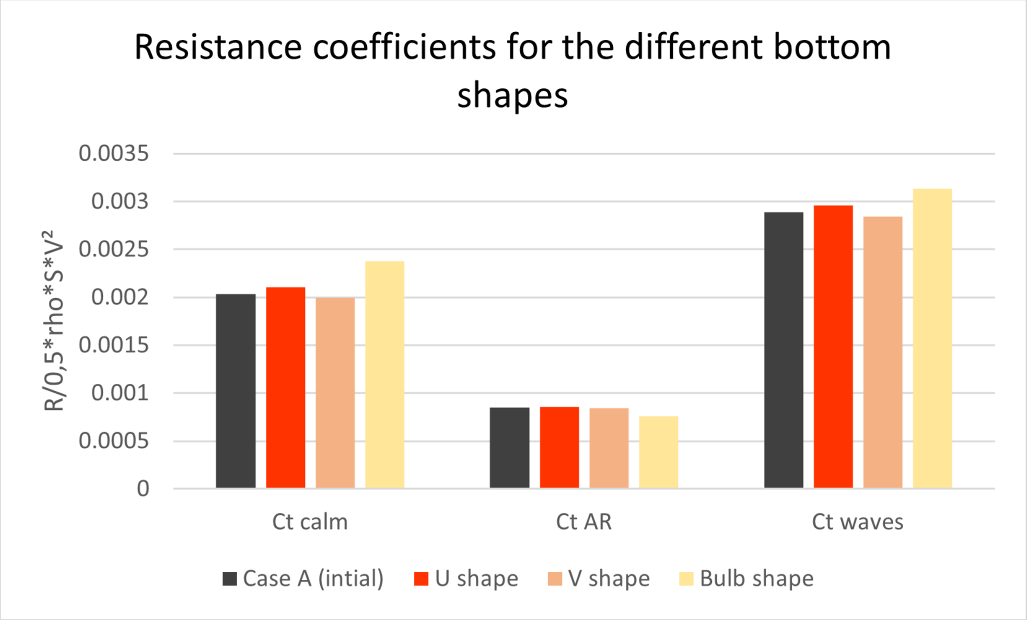

Figure 5.27: Resistance coefficients of the different underwater forms

Motions of the ship

The figures 5.28 and 5.30 show respectively the heave and pitch motions of 100 seconds of simulation and the figures 5.21 and 5.23 describe the standard deviation of the heave and pitch motions of the simulations. The table 5.4 compares the maximum amplitudes with the initial hull using the formula 5.1.

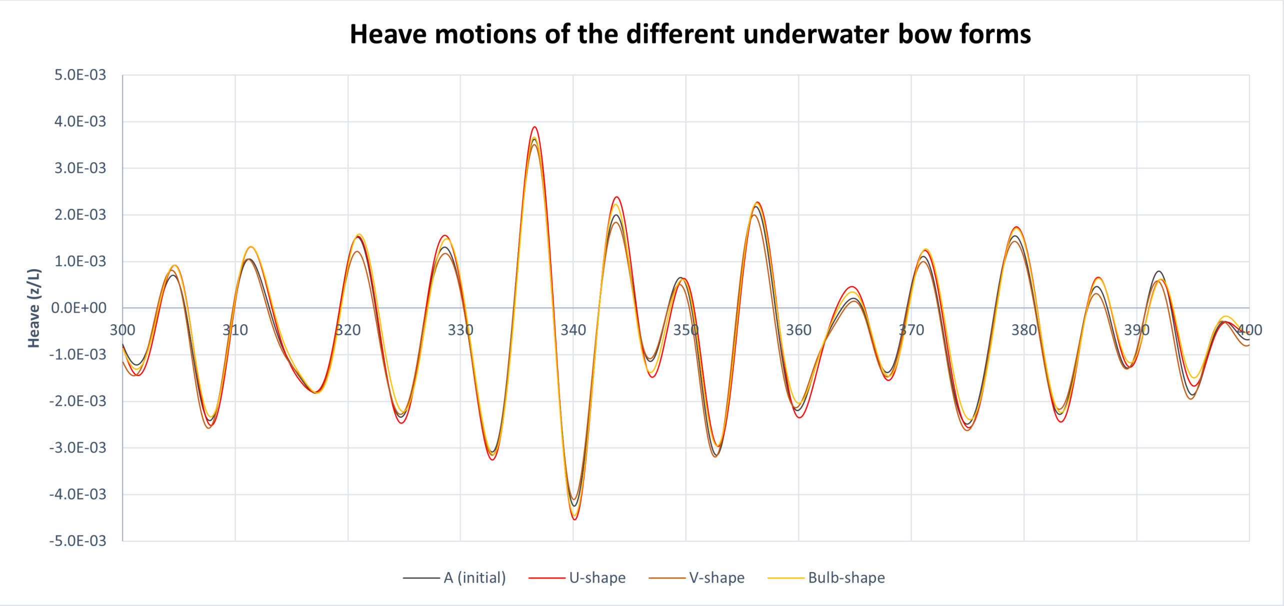

Figure 5.28: Heave motions coefficient of the different underwater bow forms

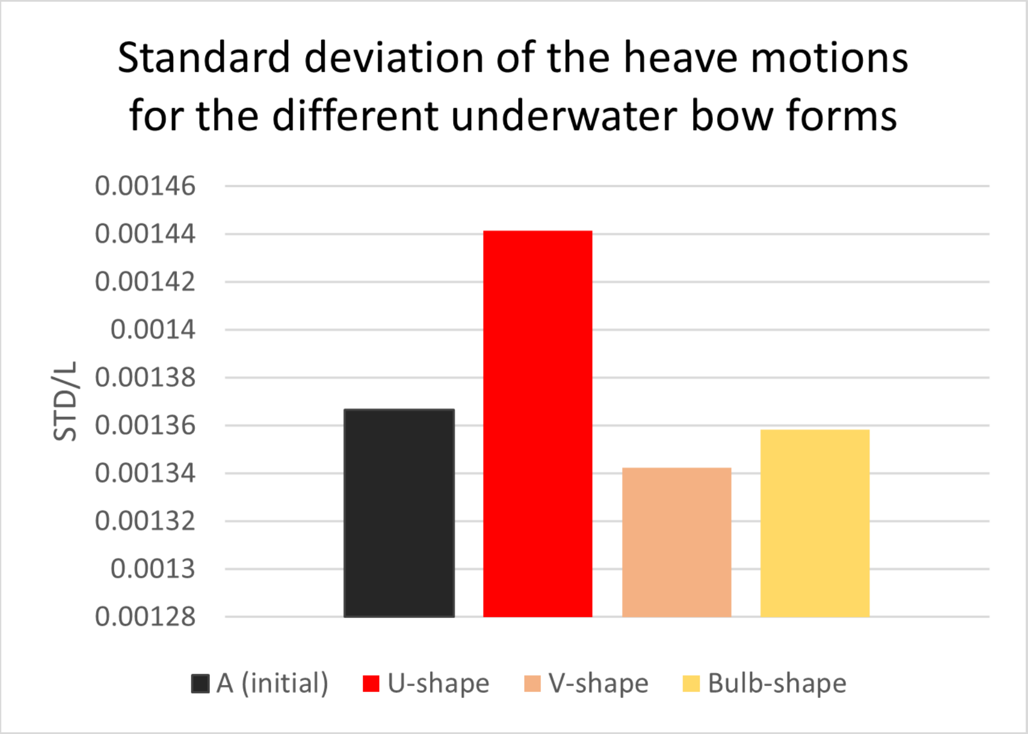

Figure 5.29: Standard deviation of heave motions coefficient for different underwater bow forms

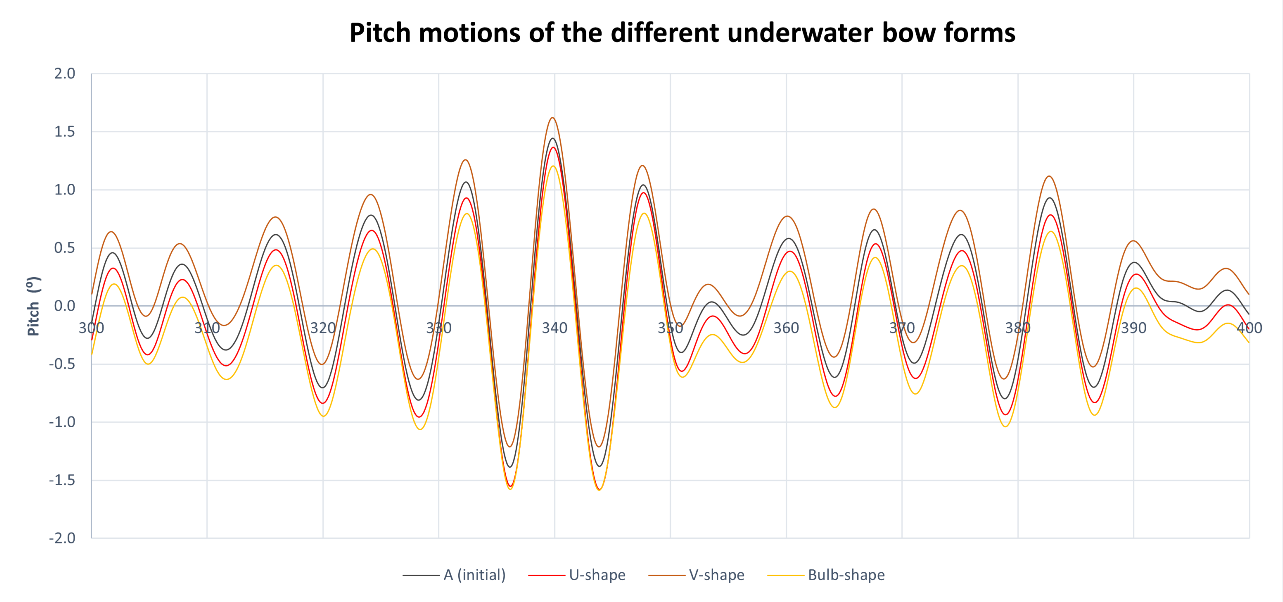

Figure 5.30: Pitch motions of the different underwater bow forms

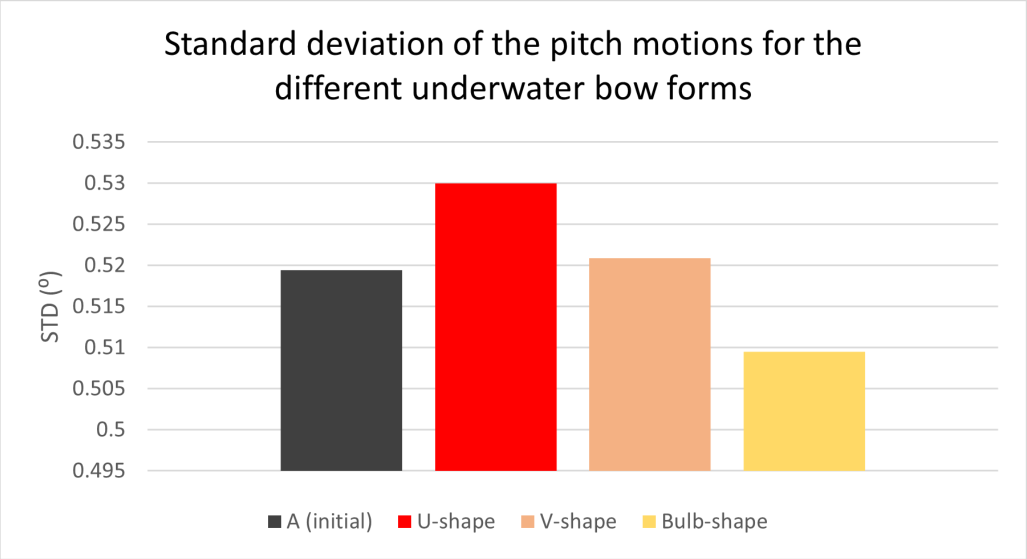

Figure 5.31: Standard deviation of pitch motions for different underwater bow forms

Case	Heave relative amplitude (%)	Pitch relative amplitude (%)
A (initial)	0	0
U-shape	6.77	4.08
V-shape	-1.84	0.16
Bulb-shape	-1.23	-1.33

Table 5.4: Relative motion amplitude comparison for the different underwater forms

The differences in motions are not really significant for this case. We can however see that the U-shape induce greater motions than the other designs and that the V-shape appear to be a good compromise between heave and pitch motions. The bulb-shape implies smaller motions but its resistance coefficients prevent us to consider it as a competitive solution. Finally, as for the shoulder shape, we can notice that changing the bottom part of the bow may induce differences in the volume distribution along the hull. This leads to several trim angle highlighted by the mean values of the pitch motion data. The V-shape is less voluminous than the initial hull but the U-shape and the bulb-shape are more voluminous.

Wave pattern

As we can see on the figure 5.32, the wave pattern is not really impacted by the changes of geometry in the underwater part of the bow. For the U-shape, the V-shape, the bulb-shape or the initial hull, the wave pattern resulting is the same.

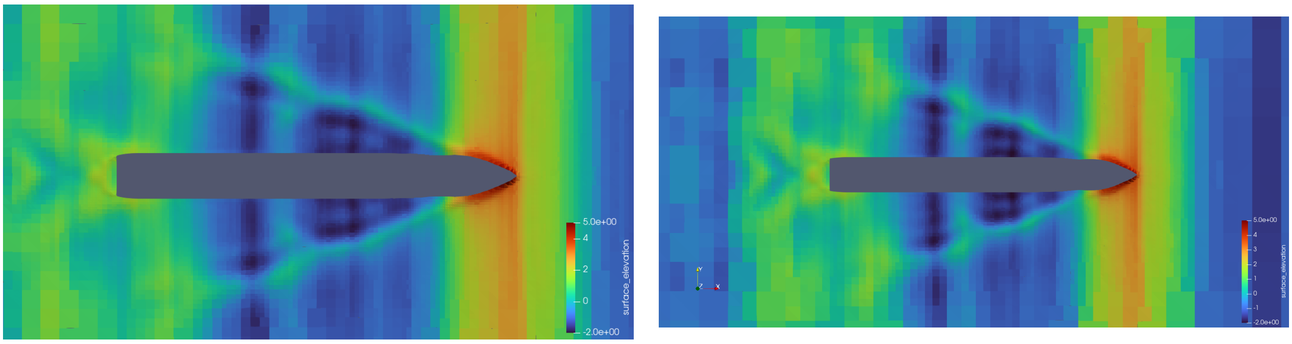

(a) Case A (initial)

(b) U-shape

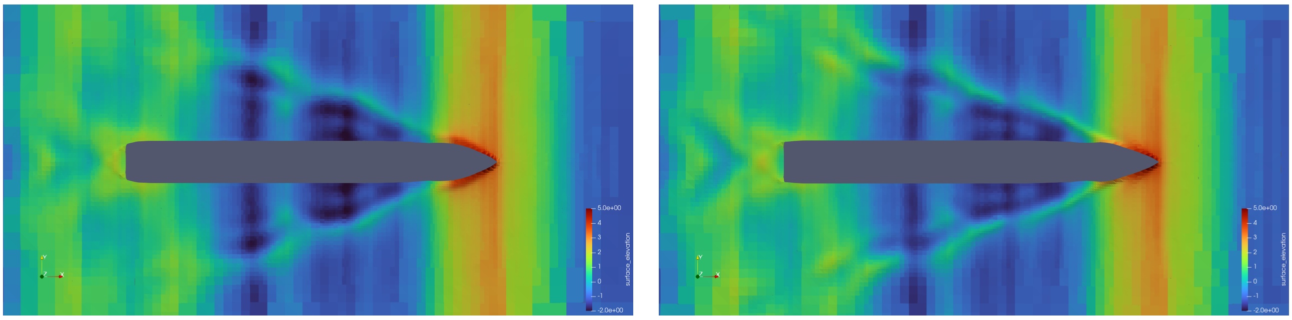

(c) V-shape

(d) Bulb-shape

Figure 5.32: Global wave pattern of the different underwater bow forms

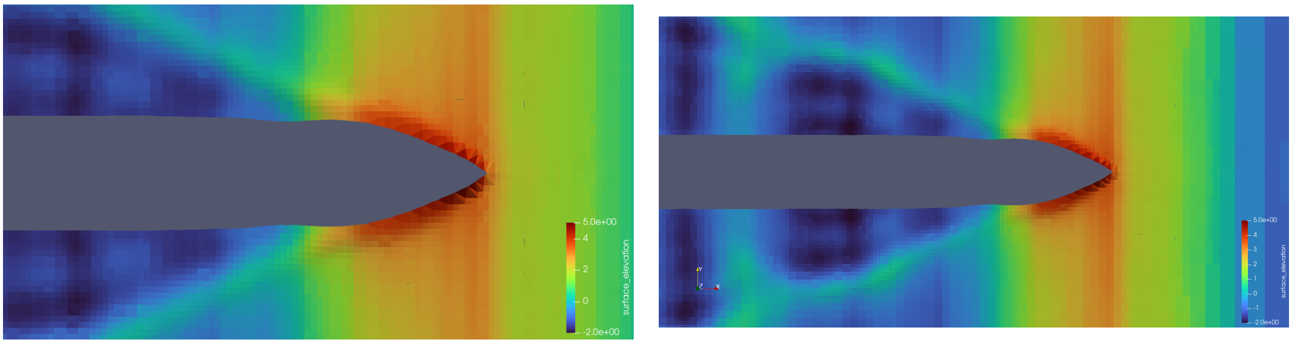

(a) Case A (initial)

(b) U-shape

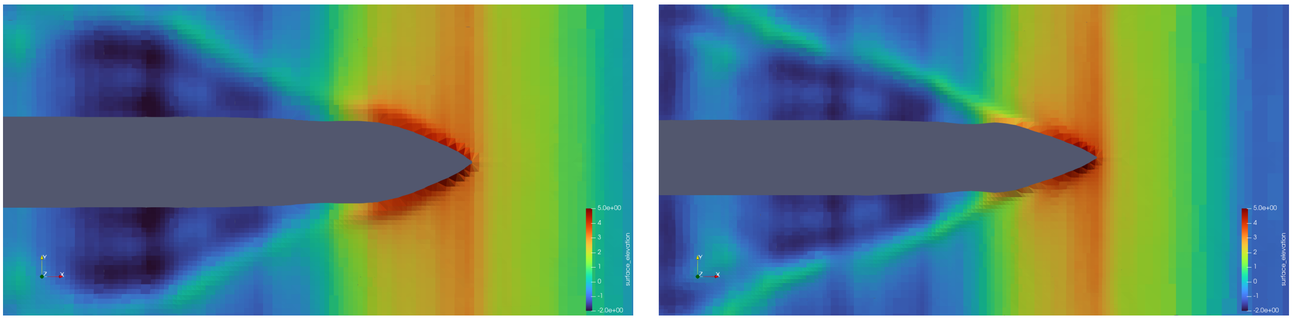

(c) V-shape

(d) Bulb-shape

Figure 5.33: Local wave pattern of the different underwater bow forms

Dynamic pressure distribution

As we saw for the wave pattern, the dynamic pressure distribution on the hull described by the figure 5.34 is not really affected by the changes on the underwater part of the bow. The areas concerned by high pressure levels are the same and the levels of pressure themselves are comparable.

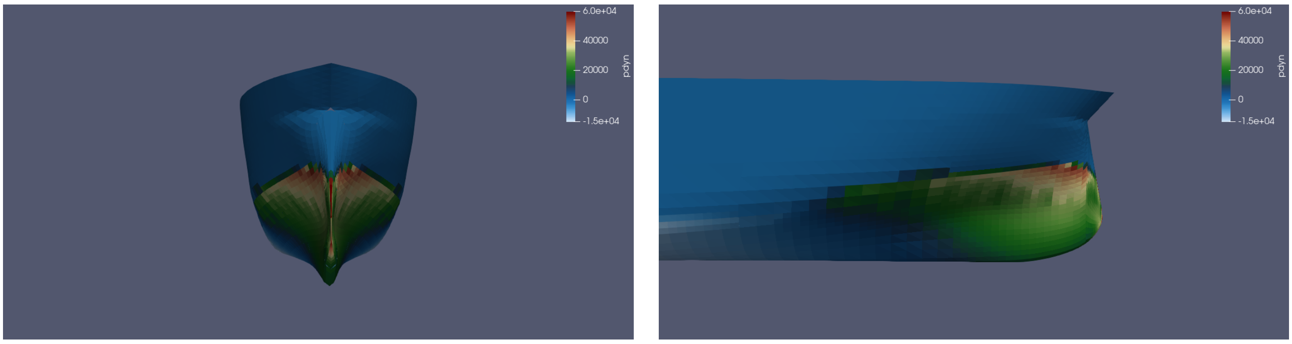

(a) Case A face (initial) (b) Case A profile (initial)

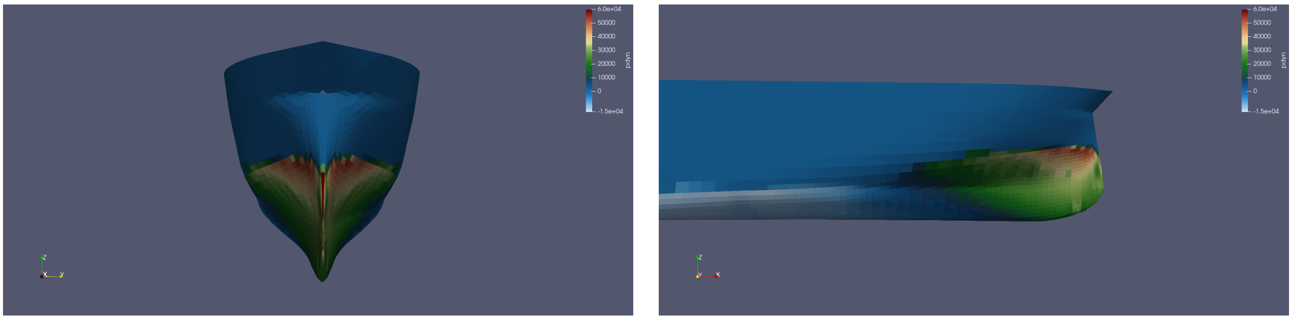

(c) U-shape face (d) U-shape profile

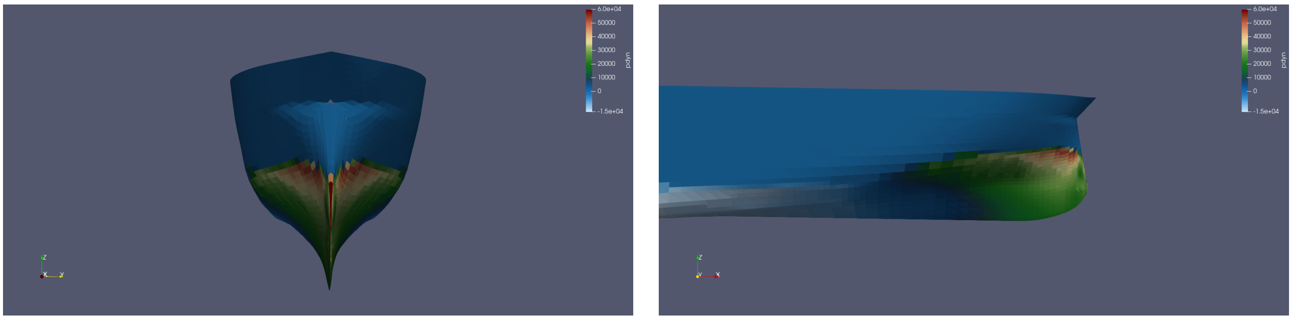

(e) V-shape face (f) V-shape profile

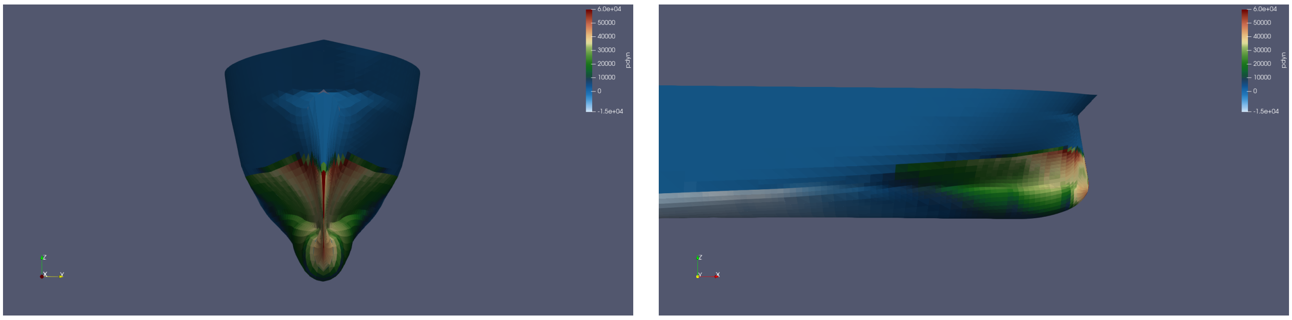

(g) Bulb-shape face (h) Bulb-shape profile

Figure 5.34: Pressure distribution on the different underwater bow forms

5.2 Summary

All the cases studied allow us to draw a summary of the effects of the bow design parameters on the added resistance in waves and the motions of the ship.

- **We cannot establish an universal rule linking the resistance in waves and the motions of the ship.** Indeed, for some design, the resistance was lower but with higher motion amplitudes and the opposite was also true.

- **The different parameters have various effects on the resistance.** Some bow design parameters affect more the resistance in calm water than in waves. It is the case for the waterline entrance angle. The changes of the flare angle and the first shoulder shape have a great importance on the resistance values especially in waves. The modification of the bottom part does not have a great impact on the resistance except if a bulbous form is introduced.

- In general terms, **a more voluminous bow leads to less motions but can also affected negatively the resistance** if the increase in volume is located under or on the waterline. So a narrow bow at the waterline permits to reduce the resistance but increase the motions as well.

- A good compromise might be to have a narrow but not too narrow bow near the waterline with a larger volume just above it to limit motions in waves.

Such a design, trying to gather the benefits of each bow design parameter, will be studied in the following section.

5.3 Final bow design

5.3.1 Geometry

This final design has been modelled regarding the results obtained for the different cases studied discussed in Chapter 4. It gathers the best compromise of each bow design parameter.
So it is a narrow but not too narrow bow near the waterline with a larger volume above it and with a V-shape in the underwater part.
The figure 5.35 shows the waterline plane of the initial design (in black) and of the final design (in green). The lines drawing of the initial hull are drawn on the left side of the figure 5.36 while the right side corresponds to the final design. Figures 5.37 and 5.38 are respectively the 3D view and the profiles of those two designs.

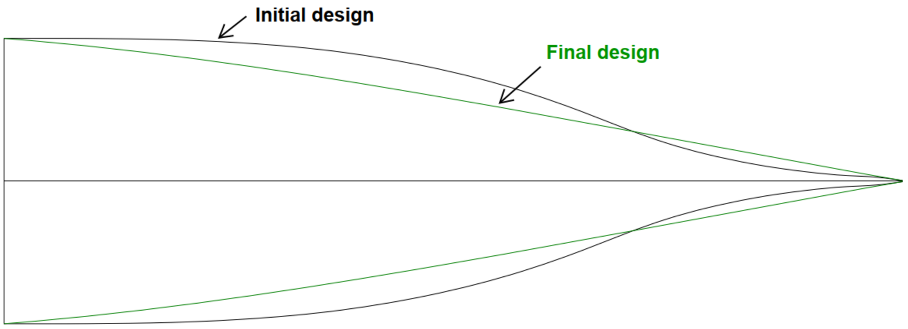

Figure 5.35: Waterline plane of the initial and final designs

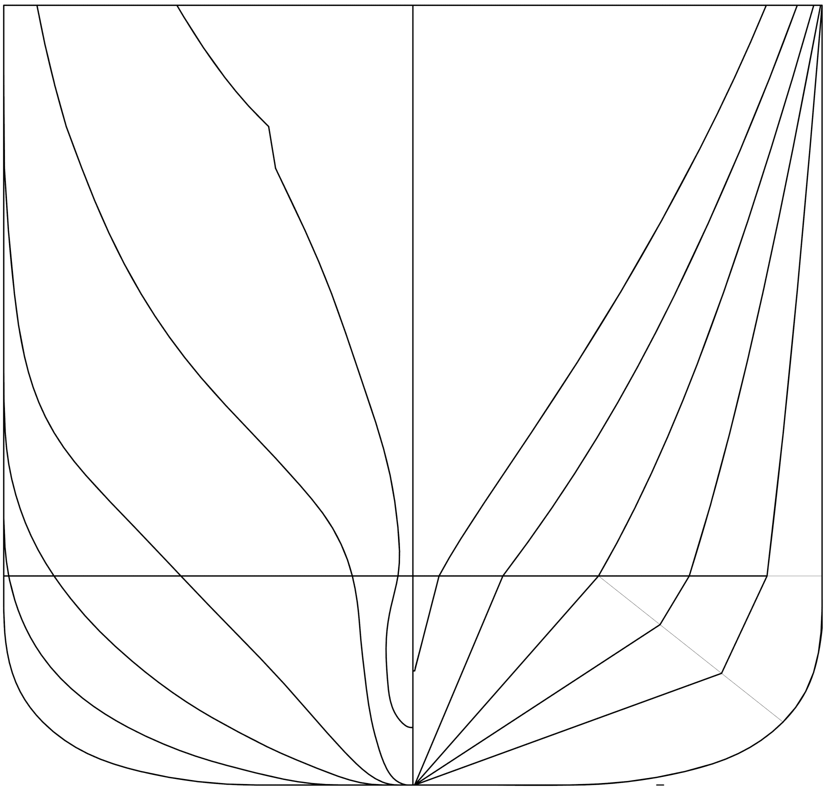

Figure 5.36: Lines drawing of the final design versus the initial bow

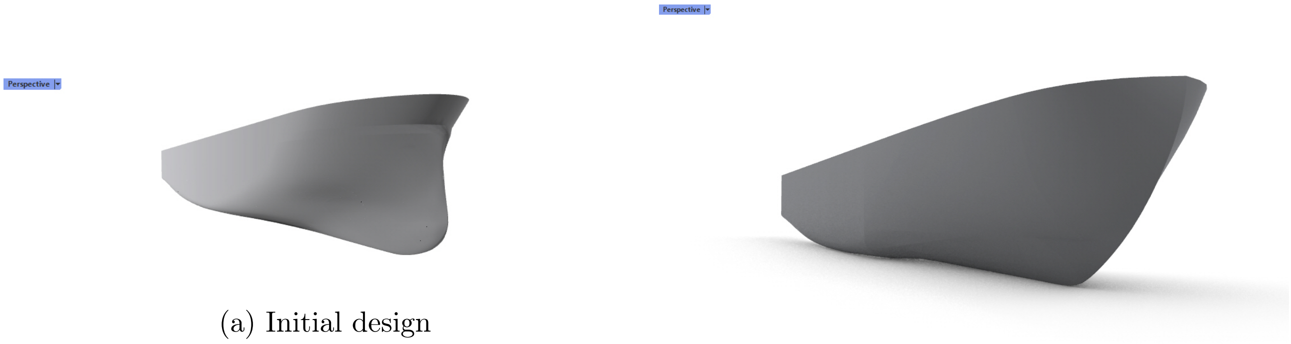

(a) Initial design

(b) Final design

Figure 5.37: 3D view of the initial and final designs

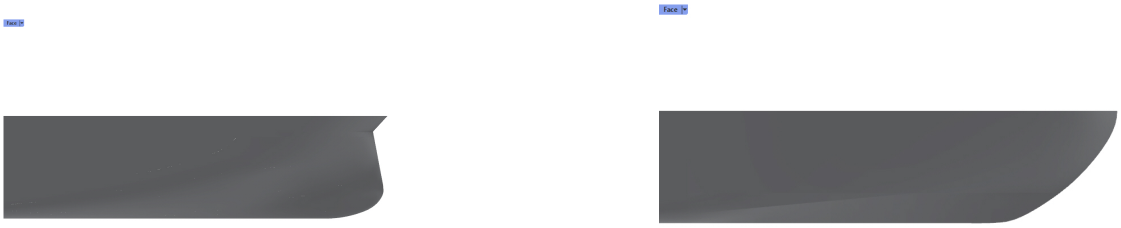

(a) Initial design

(b) Final design

Figure 5.38: Profiles of the initial and final designs

5.3.2 Results

In this part, we will discuss about the results obtained for this final design.

Resistance performances

The figure 5.39 highlights the different resistance coefficients of the initial and the final bows while the figure 5.40 presents the total resistance as a sum of the added resistance and the calm water resistance normalized on the initial total resistance.

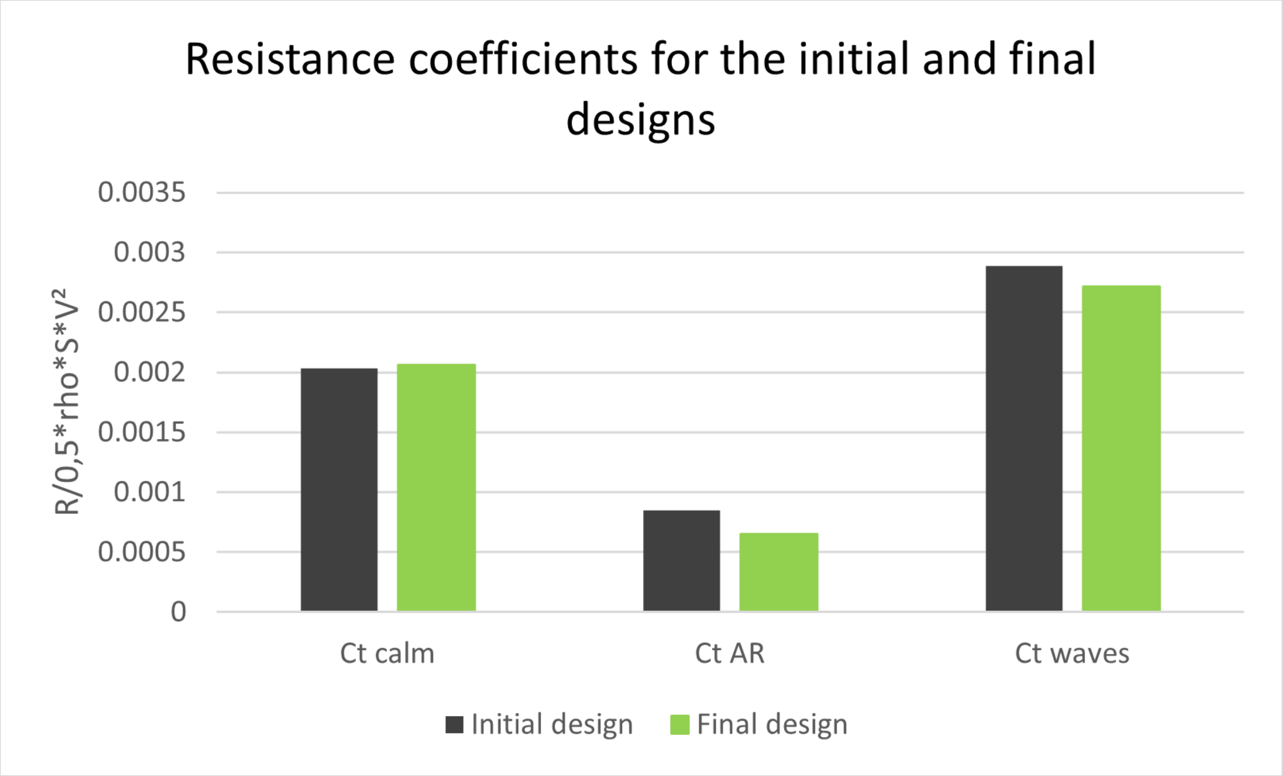

Figure 5.39: Resistance coefficients of the initial and final designs

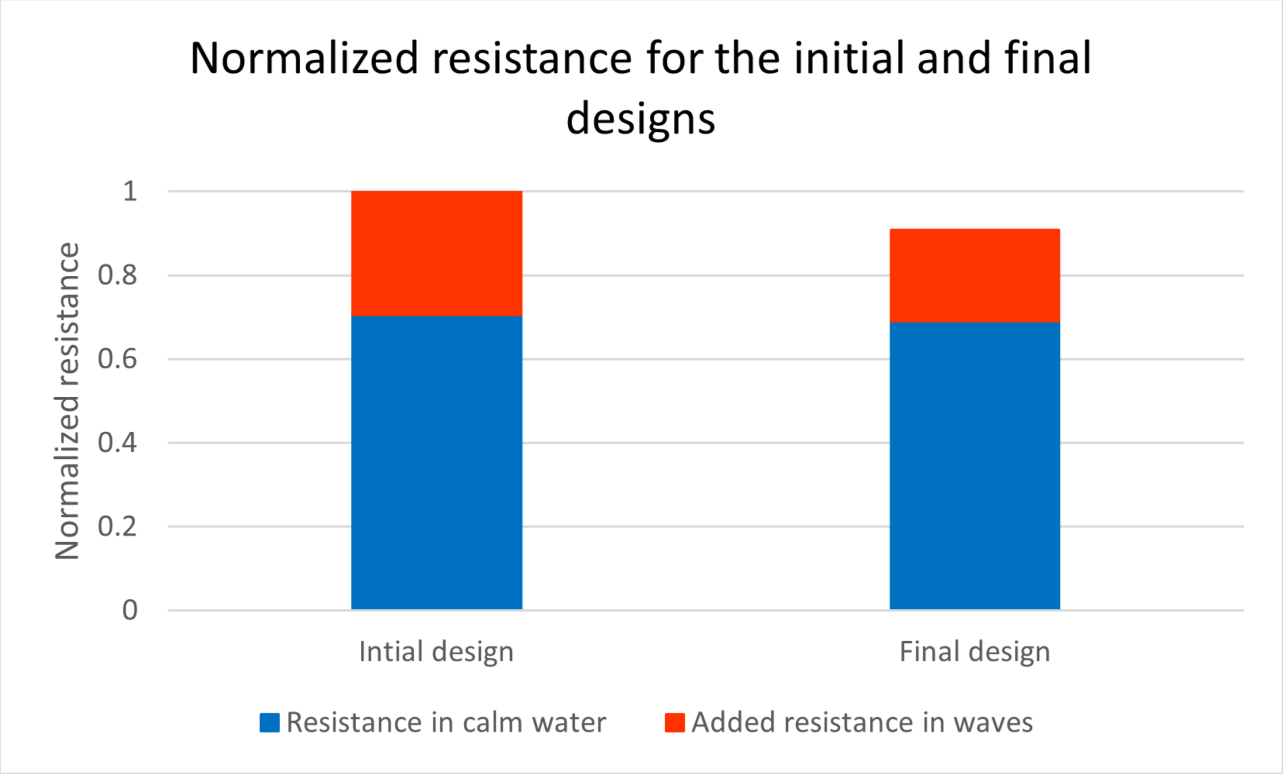

Figure 5.40: Normalized resistance of the initial and final designs

As one can notice, the two designs are quite equivalent in calm water but the final design presents a significant advantage in waves. The total resistance is then reduced by 9.14%.

Motions of the ship

The heave and pitch motions are shown respectively in the figures 5.41 and 5.43 and the figures 5.42 and 5.44 describe the standard deviation of the heave and pitch motions of the simulations. The table 5.5 compares the maximum amplitudes with the initial hull using the formula 5.1 as we done for the other cases.

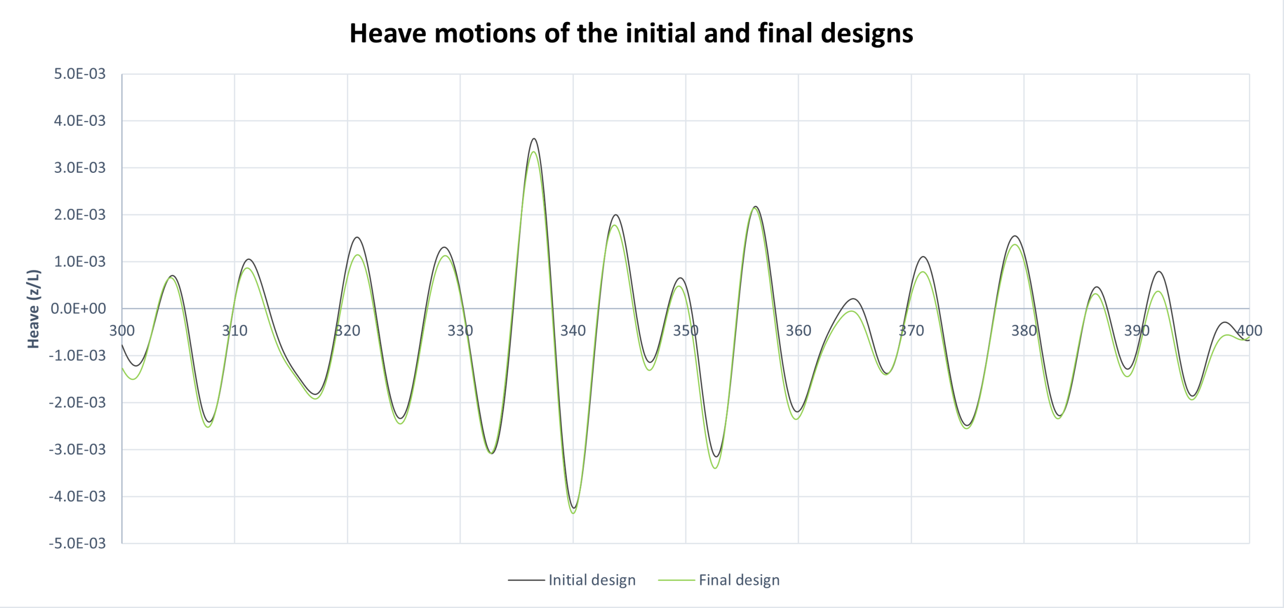

Figure 5.41: Heave motions coefficient of the initial and final designs

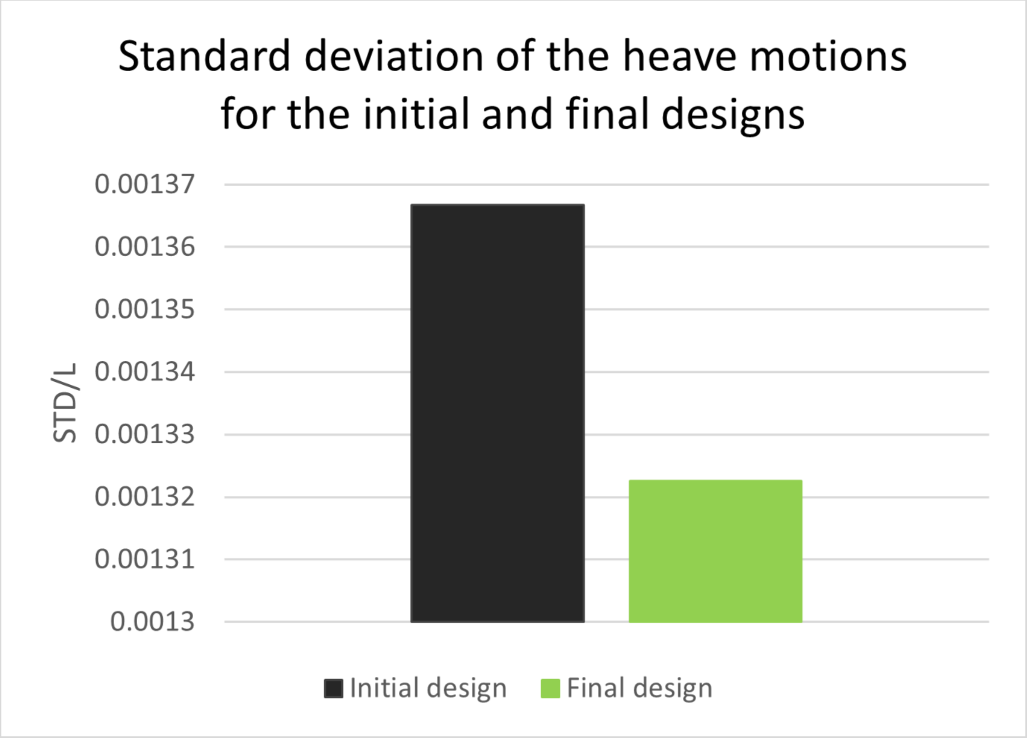

Figure 5.42: Standard deviation of heave motions coefficient for the initial and final designs

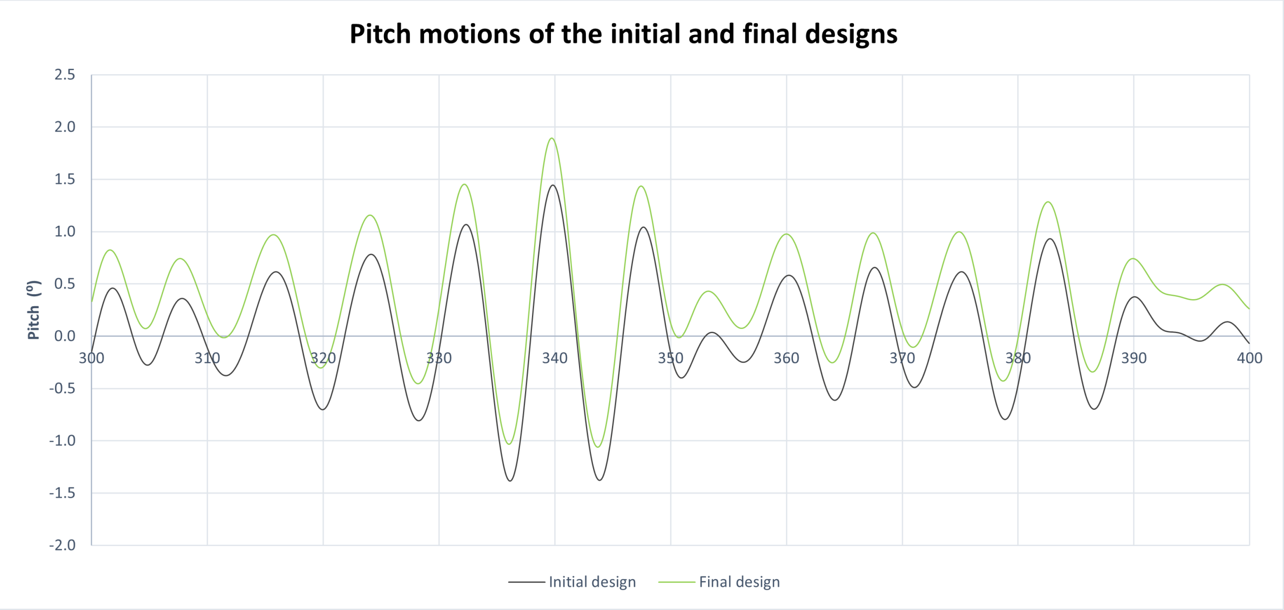

Figure 5.43: Pitch motions of the initial and final designs

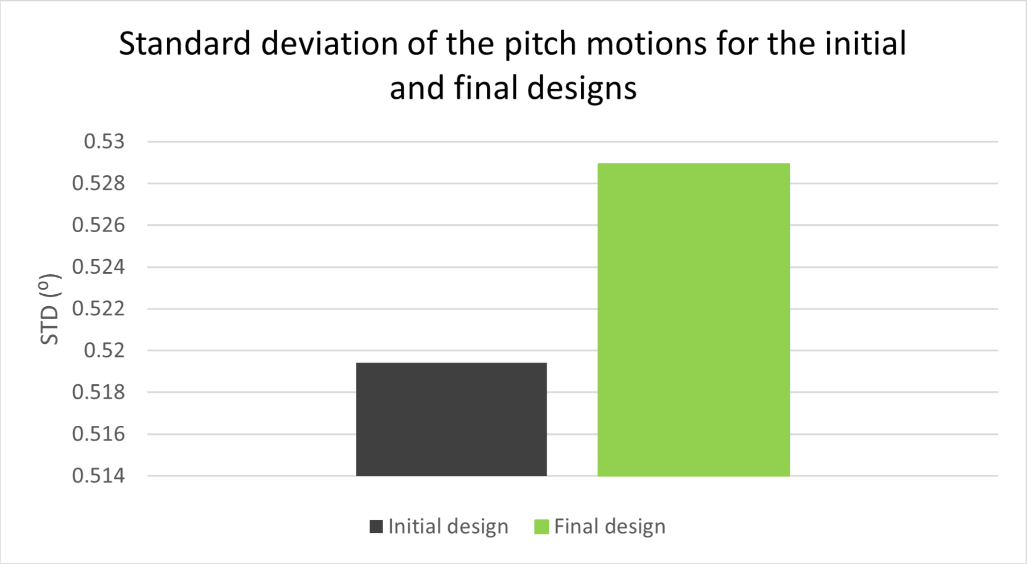

Figure 5.44: Standard deviation of pitch motions for the initial and final designs

Case	Heave relative amplitude (%)	Pitch relative amplitude (%)
Initial design	0	0
Final design	-2.96	4.53

Table 5.5: Relative motion amplitude comparison for the final design

The motions of the ship induced by the irregular waves are pretty similar from the initial design to the final one. The heave motion amplitudes are a bit lower for the final design but the pitch amplitudes are larger than for the initial design. This agree to the conclusion drawn in the previous summary: a more voluminous bow leads to less motions. Indeed the initial hull is more voluminous than the final design especially underwater even if some volume has been added above the waterline. The figure 5.43 highlights a steady trim angle different for the final design, explained by this difference in volume in the bow section.

Wave pattern and dynamic pressure distribution

In this section, the wave pattern of the final design is compared to the initial one in figure 5.45 and the dynamic pressure distribution is shown in figure 5.46.

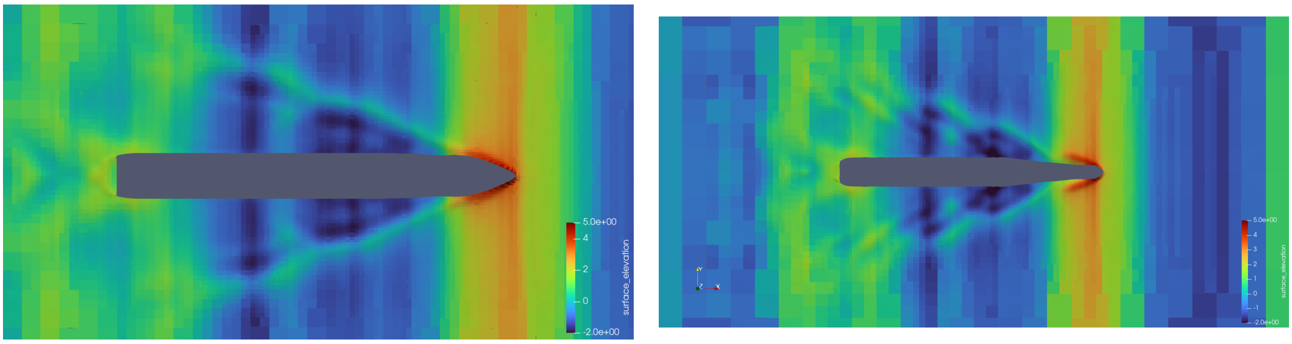

(a) Initial design (b) Final design

Figure 5.45: Global wave pattern of the initial hull and the final design

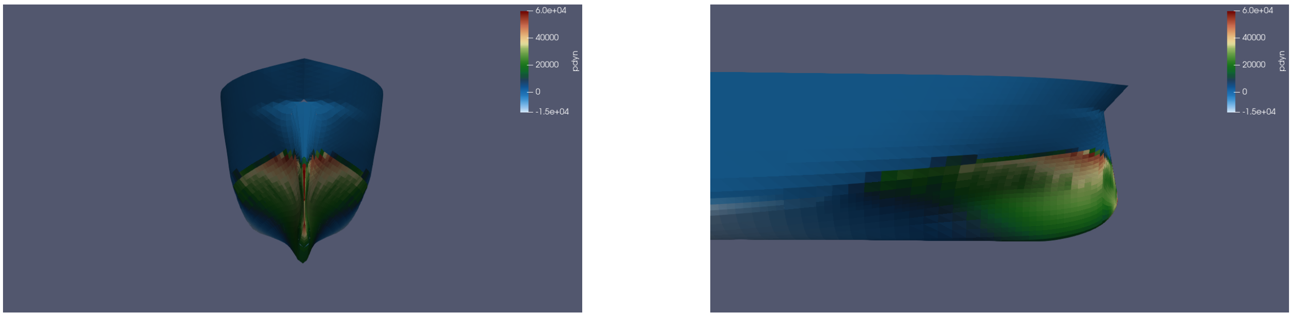

(a) Initial design face (b) Initial design profile

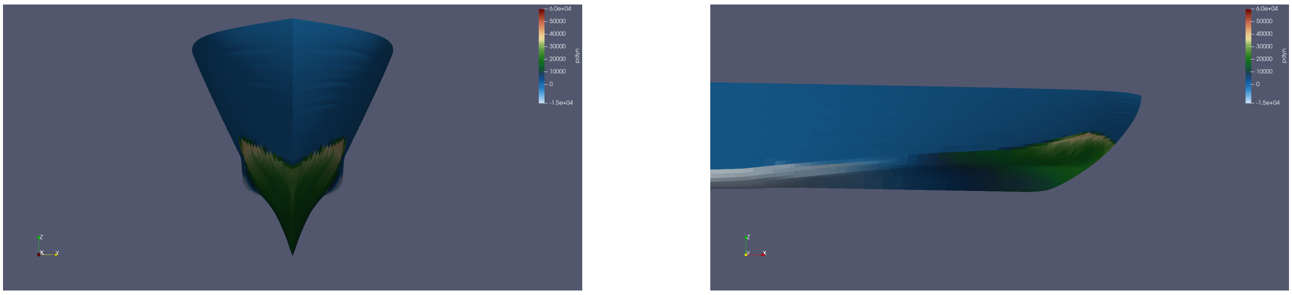

(c) Final design profile (d) Final design profile

Figure 5.46: Pressure distribution on the initial and final designs

It is interesting to see how the choice of each parameter can be found on those figures:
- The global wave pattern looks like the one of the case K (see figure 5.24) with a small second divergent wave coming from the first shoulder. By optimising the form of this first shoulder we might be able to reduce this wave and gain even more performances in resistance.
- The bow wave is comparable to the one we obtained for the cases H or I (see Appendix or figure A.2).
- The pressure distribution is as well close to the pressure distribution of the cases H and I (see Appendix or figure 5.18).

All those cases mentioned correspond closely to what was chosen for the final design. Even if this design needs further work to be well optimised, it is interesting to relate each part of the bow to their effects.

Chapter 6

Conclusion

6.1 Concluding remarks

Optimising bow designs to limit the added resistance and understand the effects of their different parameters was a challenging task.
Thanks to the use of CFD models validated with towing tank tests results we were able to study various different designs ans geometries with good accuracy. Even with long times of simulation, the CFD has shown its advantages compare to model tests in tanks by its ease to modify the geometries.
To highlight the effects of the different design parameters of the bow, they have been determined and studied one by one. In this thesis the focus was made on four main parameters: the waterline entrance angle, the flare angle, the first shoulder shape and the underwater form. Each parameter has undergone significant variations, leading sometimes to strange bow geometries, to create visible effects on the resistance, the motions of the ship and the water flow around the hull.
What we can conclude about this study and answer to the research question is:
RQ1: The motions and the resistance in irregular waves are not linked by some kind of rule.
RQ2: The design parameters studied do not have the same impact nor the same importance on resistance. Those effects can also be distinguished according to whether we look at the resistance in calm water or in waves. In waves we can state in order of importance on the added resistance : the flare angle, the first shoulder shape, the underwater form and finally the waterline entrance angle.
Generally speaking, more volume in the bow reduce the motions but can lead to a loss in resistance performances especially if the increase in volume is located under the free surface.
RQ3: By gathering the benefits of each design parameter, we can end up quickly with an efficient bow geometry which is a narrow but not too narrow bow at the waterline, with a larger volume above the waterline and a V-shape in the bottom part. Even without any optimisation process, the final design presented in this thesis allow to reduce the total resistance in waves by more than 9%.

6.2 Future work

In this thesis, even if three sea states with different ship speed have been simulated for validating the CFD model, we have focused on one medium sized sea state for the study of the different parameters. The effects of the different design parameters used here might be nuanced by a different sea state. It would be interesting in a future work to study various sea states not only by modifying the amplitude and length of the waves but also by looking at various steepness,

non heading waves and a wider range of ship speed.
It might also be relevant to implement a similar study with another CFD model such as a more accurate model like a RANSE model or carry out some model tests to validate the results and override the Shipflow wave breaking limitations.

Appendix A

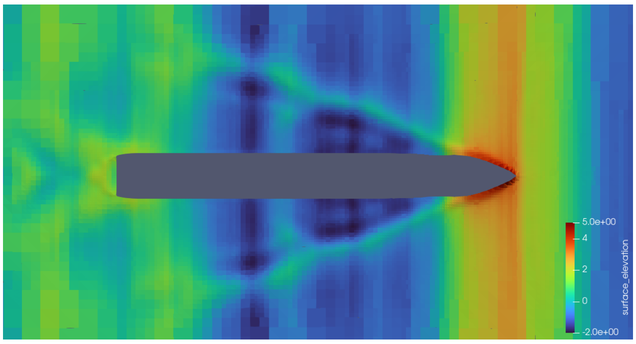

(a) Case A (initial)

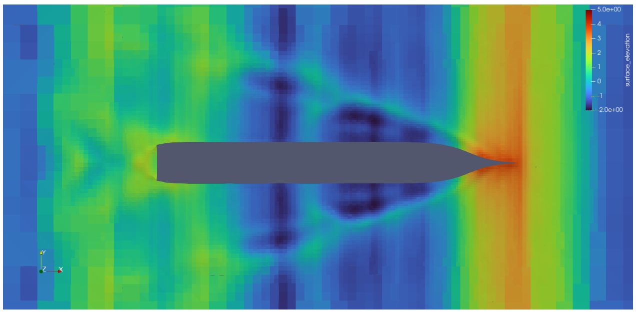

(b) Case E

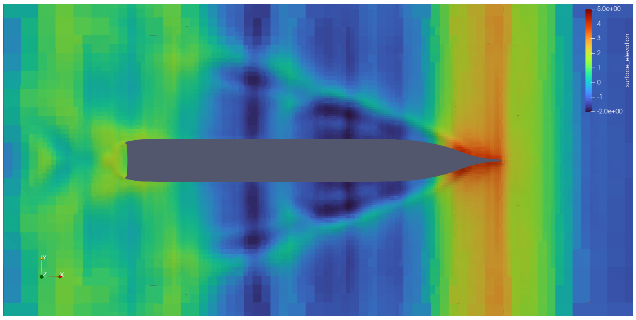

(c) Case F

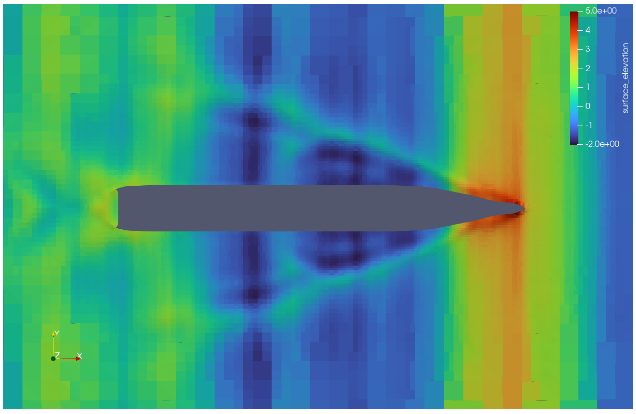

(d) Case G

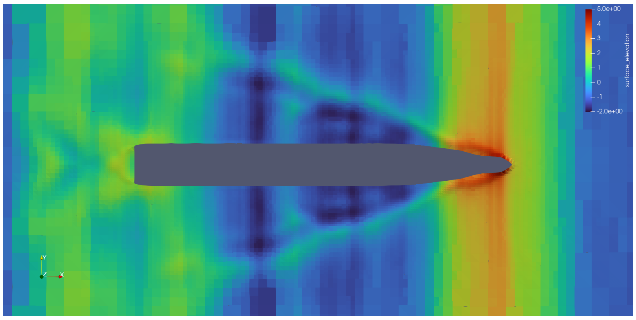

(e) Case H

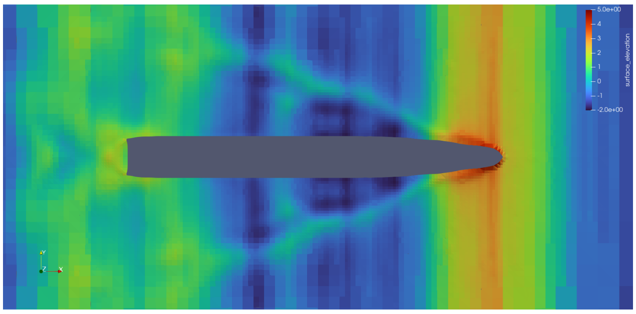

(f) Case I

Figure A.1: Global wave pattern of the different flare studied

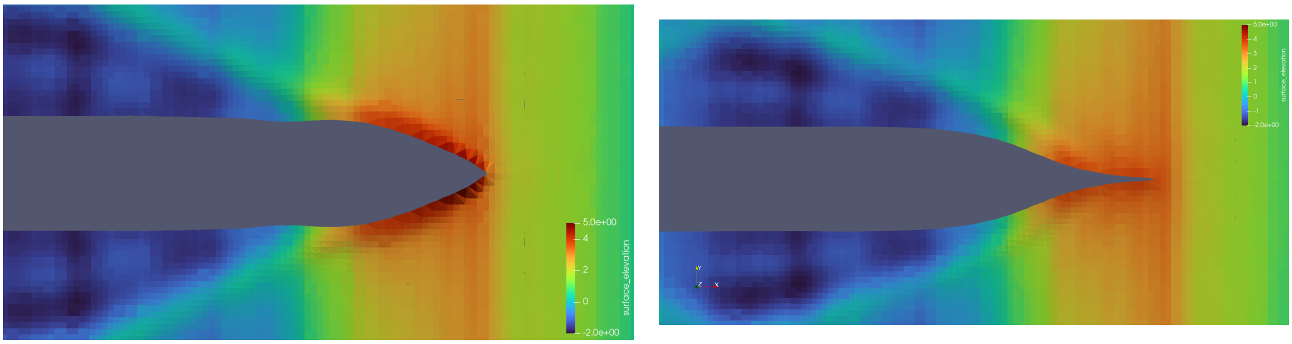

(a) Case A (initial)

(b) Case E

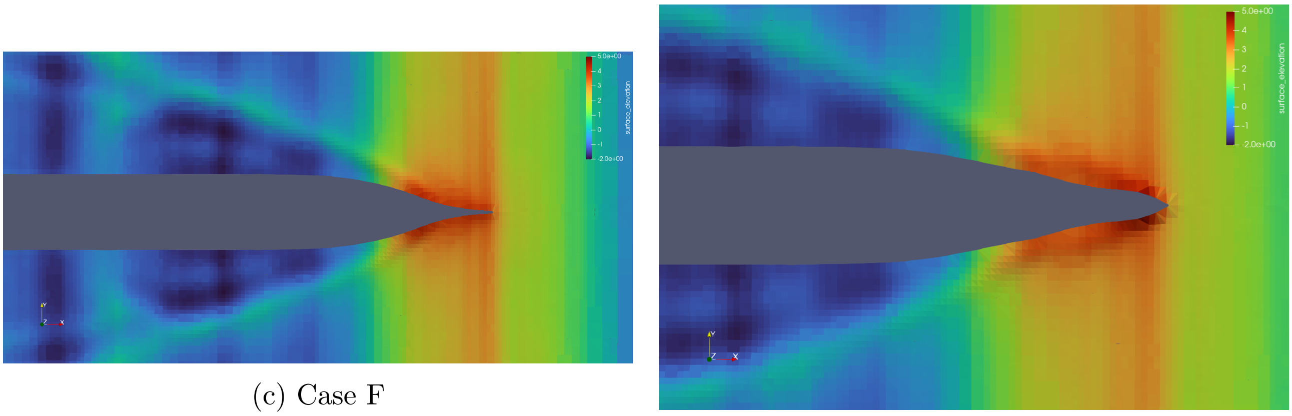

(c) Case F

(d) Case G

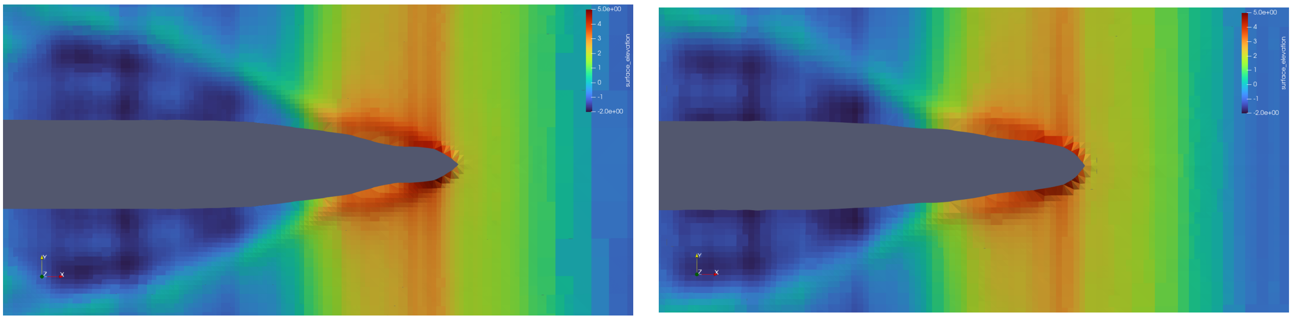

(e) Case H

(f) Case I

Figure A.2: Local wave pattern of the different flare studied

(a) Case A face (initial) (b) Case A profile (initial)

(c) Case E face (d) Case E profile

(e) Case F face (f) Case F profile

(g) Case G face (h) Case G profile

(i) Case H face (j) Case H profile

(k) Case I face (l) Case I profile

Figure A.3: Dynamic pressure distribution of the different flare studied

References

Ulstein (2023). *X-BOW*. n.d. URL: `https://ulstein.com/innovations/x-bow` (visited on 06/01/2023).

FLOWTECH (Dec. 2022). "Shipflow Motions 7.0 - User's Manual". In.

Newman, John Nicholas (1977). *Marine Hydrodynamics*. English. The Massachusetts Institue of Technology Press.

Hasselmann (1973). "Measurements of wind-wave growth and swell decay during the Joint North Sea Wave Project (JONSWAP)". In: *Ergnzungsheft zur Deutschen Hydrographischen Zeitschrift Reihe* Resistance Test.

Faltinsen, Odd Magnus (2005). *Hydrodynamics of High-Speed Marine Vehicles*. English. Cambridge University Press.

Beck, Robert F. et al. (1989). *Principles of Naval Architecture*. Edward V. Lewis. Vol. Volume III - Motions in Waves and Controllability.

Bolbot, Victor and Apostolos Papanikolaou (July 2016). "Optimization of ship's bow form for the added resistance in waves". In.

Söding, Heinrich and Vladimir Shigunov (Feb. 2015). "Added resistance of ships in waves". In: *Ship Technology Research* 62, pp. 2–13. DOI: `10.1179/0937725515Z.0000000001`.

Söding, Heinrich, Alexander Graefe, et al. (July 2012). "Rankine Source Method for Seakeeping Predictions". In: vol. 4. DOI: `10.1115/OMAE2012-83450`.

Park, Dong-Min et al. (2019). "Experimental and numerical studies on added resistance of ship in oblique sea conditions". In: *Ocean Engineering* 186, p. 106070. ISSN: 0029-8018. DOI: `https://doi.org/10.1016/j.oceaneng.2019.05.052`. URL: `https://www.sciencedirect.com/science/article/pii/S002980181831905X`.

Coslovich, Francesco et al. (2021). "Added resistance, heave and pitch for the KVLCC2 tanker using a fully nonlinear unsteady potential flow boundary element method". In: *Ocean Engineering* 229, p. 108935. ISSN: 0029-8018. DOI: `https://doi.org/10.1016/j.oceaneng.2021.108935`. URL: `https://www.sciencedirect.com/science/article/pii/S002980182100370X`.

Larsson, Lars and Hoyte C. Raven (2010). *The Principles of Naval Architecture Series*. English. J. Randolph Paulling. Vol. Ship Resistance and Flow.

Yang, Kyung-Kyu and Yonghwan Kim (June 2017). "Numerical analysis of added resistance on blunt ships with different bow shapes in short waves". In: *Journal of Marine Science and Technology* 22.2, pp. 245–258. ISSN: 1437-8213. DOI: `10.1007/s00773-016-0407-9`. URL: `https://doi.org/10.1007/s00773-016-0407-9`.

Chen, Shuling et al. (2022). "Comparative Study on Added Resistance and Seakeeping Performance of X-Bow and Wave-Piercing Monohull in Regular Head Waves". In: *Journal of Marine Science and Engineering* 10.6. ISSN: 2077-1312. DOI: `10.3390/jmse10060813`. URL: `https://www.mdpi.com/2077-1312/10/6/813`.

"ITTC - Recommended Procedures and Guidelines" (2011). In: *International Towing Tank Conference* Resistance Test, pp. 1–13.

NTNU
Norwegian University of
Science and Technology

VARD™
a **Fincantieri** company